CLONING, EXPRESSION AND STRUCTURAL CHARACTERIZATION OF HUMAN METAPNEUMOVIRUS FUSION GLYCOPROTEIN

By

Gabriella Cseke

Dissertation
Submitted to the Faculty of the
Graduate School of Vanderbilt University
in partial fulfillment of the requirements for
the degree of

DOCTOR OF PHILOSOPHY
in
Chemistry

December, 2006

Nashville, Tennessee

Approved:

Professor David W. Wright
Professor David E. Cliffel
Professor James E. Crowe
Professor Michael P. Stone
Professor John V. Williams

ACKNOWLEDGEMENTS

When I came to Vanderbilt to start my graduate studies in chemistry I had no idea what my research project would be. I wanted to do chemistry combined with molecular biology and I was looking for an advisor, who had similar research interests, so I asked Dr. David Wright if I could join his group. He accepted me without question and gave me an opportunity in a new project to do hMPV research in collaboration with Dr. Crowe and Dr. John Williams. I hope he did not regret his decision, because it turned out to be a great one (at least for me). He gave me the freedom to do my research in a way as I wanted, but always reminded me for my responsibilities (meetings, exams, course work, etc.). Although I didn't spend too much time doing my actual research in Dr. Wright's lab, I want to thank the Wright lab members for their help, especially Scott (now Dr. Miller) for his peptides and for his help with my presentations along with Elizabeth (Liddy). Clare (now Dr. Clare Kenny-Carney) and Alex, who helped me with the proteomics studies, and Sarah and Malgorzata, who helped me to locate or find Dr. Wright or Scott whenever I needed help.

I started my actual research in Dr. James Crowe's lab. The six months I spent there probably finalized my decision to do science, or at least try to do it in the way as the "Crowe lab" does. First, I want to thank Dr. Crowe for his help in my research, my committee meetings and lab meeting presentations, and of course Fran House, who is the soul of the Crowe lab and of course the "Lab-Mom". Many thanks to the past and present Crowe lab members: Nicole, Sean, Amber, Tom, Cuixia, Josh, Mike (Rock), Sandy, Mike (Lindquist), Chris, Sunny, Sujin, Sam, Emily, Kelly, Jungyun, Pat, Dr. Yu, Keipp

and Bryan. Here I also want to say thanks to Melissa from Dr. Dermody's lab, Dr. Jim Higginbotham and Dr. Kevin Weller for their help with flow cytometry, Dr. Amy Ham for her help with the disulfide-mapping and of course, Dr. Stone and Dr. Cliffel at the Chemistry Department, who gave me good advices on my committee meetings and qualifying exam.

After the six months in the Crowe lab I continued my research in Dr. John Williams's lab. Working in his group was the best experience that I had at Vanderbilt. John is an awesome mentor and a great person. I couldn't wish for a better one. He taught me everything, from the basic lab techniques (his famous 'sloppy' pipetting) to how to give presentations and how to work together with other labs. No matter what, John was always there to help me and answer my questions. He supported me for three and a half years continuously; thanks John, very much! And of course, Sharon Tollefson. What can I say? Sharon is the nicest, kindest person I have ever met. She works hard, she never raises her voice, but helps you whenever, wherever and whatever you need help in. I also want to say thanks to the Williams lab members: Amy, Rohith, Alex, Sarah and Kathryn.

And finally, I want to thank my family. Although they were far away, they supported me from home. My Grandma, who prayed for me, my Mom, who set an example how to be a good researcher, my Dad, who is a hard worker, a great teacher and the best Dad in the world, and my sister, Mariann, who is a fantastic sister. I couldn't do this without you.

And of course, more than anything, Tamas. He was there for me every day, all day, with his support and help. He was one reason, why I started my studies at Vanderbilt, and he was the one, why I could finish it. Thanks!

TABLE OF CONTENTS

Page

ACKNOWLEDGEMENTS ii

LIST OF TABLES vii

LIST OF FIGURES viii

LIST OF ABBREVIATIONS ix

Chapter

I. INTRODUCTION 1

1.1. Overview 1

1.2. Paramyxoviruses 3
Classification 3
Genome organization, virion structure and viral proteins 5
Viral replication 11

1.3. Human Metapneumovirus 13
Classification 13
Genome organization, viral proteins 14
Clinical manifestation and epidemiology 17

1.4. Fusion glycoprotein 19
Fusion process 19
F protein structure 22

II. CLONING, EXPRESSION AND PURIFICATION OF HUMAN METAPNEUMOVIRUS FUSION GLYCOPROTEIN 38

2.1. Introduction 38

2.2. Materials and Methods 43
Vaccinia virus expression system 43
Protein expression with pTracer vector 45
F expression with pcDNA3.1/myc-His vector 47

2.3. Results 50

2.4. Discussion 56

III. STRUCTURAL CHARACTERIZATION OF HMPV FUSION PROTEIN 59

3.1. Introduction 59
3.2. Circular dichroism spectroscopy, surface plasmon resonance 61
3.3. N-glycosylation, site-directed mutagenesis 68
3.4. Disulfide-mapping, computer models 75
3.5. Discussion 82

IV. F PROTEIN BINDING TO RGD-SPECIFIC ADHESION MOLECULES 85

4.1. Introduction 85
4.2. Materials and Methods 88
4.3. Results 91
4.4. Discussion 103

V. ANIMAL MODEL AND VACCINE DEVELOPMENT 105

5.1. Introduction 105
5.2. Materials and Methods 107
5.3. Results 109
5.4. Discussion 113

VI. CONCLUSION 116

Future work 118

REFERENCES 119

Appendix

A. FPLC PURIFICATION OF HMPV F ECTODOMAIN USING HISTRAP COLUMN AND ÄKTA-FPLC SYSTEM 125

B. SPR-BIACORE ANALYSIS OF HMPV F BINDING TO HMPV-SPECIFIC HUMAN MONOCLONAL ANTIBODY 128

LIST OF TABLES

Table Page

1. Classification of Paramyxoviridae virus family 4

2. PCR primers designed to generate N-glycosylation mutants. 70

3. Histopathological scoring of lung sections from immunized groups of cotton rats after hMPV challenge.. 113

4. Parameters for purification protocol of hMPV F ectodomain using ÄKTA-FPLC system and 5 ml HisTrap column. 127

LIST OF FIGURES

Figure Page

1. Genomic maps of the Paramyxoviridae virus family members 6

2. 3D structure of Pneumovirus.. 7

3. Schematic picture of membrane fusion..... 20

4. Fusion model for influenza virus 21

5. The conformations of influenza hemagglutinin. 23

6. Spring-loaded conformational change of influenza HA2. 24

7. Model for membrane deformation catalyzed by influenza HA 25

8. Diagrams of the N36/C34 complex. 27

9. Schematic diagram of RSV F protein. 29

10. Top and side views of SV5 F1 core trimer compared to other type I glycoproteins .. 31

11. Space-filling model of NDV F trimer. 32

12. Structure of the hPIV 3 F ectodomain. 34

13. Pre- and post-fusion F protein conformations. 36

14. Model for F-mediated membrane fusion. 37

15. Regulation of target gene expression in the absence (-) or presence (+) of inducer... 40

16. Schematic diagram of pTracer-EF/V5-His mammalian expression vector. 42

17. Schematic diagram of pcDNA3.1/*myc*-His expression vector. 43

18. HMPV FΔTM expression in LLC-MK2 cells using pTracer expression vector. 52

19 Purified FΔTM under denaturing, non-reducing conditions. 54

20. Purified FΔTM under native conditions. 55

21. FΔTM under denaturing conditions. 55

22. CD spectrum of hMPV F ectodomain shows predominant α-helical secondary structure..... 65

23. SPR-BIAcore kinetic analysis of anti-hMPV human monoclonal Fab binding to hMPV F ectodomain. 67

24. Western blot of hMPV FΔTM digested with N-glycosidase F. 72

25. Western blots of FΔTM and mutated proteins. 75

26. Coverage map of FΔTM digested with trypsin and chymotrypsin. 80

27. Hexameric fusion core of hMPV F model. 81

28. Effect of decreasing EDTA concentration on infectivity of hMPV and RSV. 92

29. Effect of decreasing GRGDSP linear peptide concentration on hMPV and RSV infectivity. 93

30. Effect of integrin-function blocking antibodies on hMPV and RSV infectivity. 95

31. Histograms of flow cytometric analysis of LLC-MK2 cells stained for cell surface binding of hMPV F protein. 97

32. Flow cytometric analysis of siRNA transfected LLC-MK2 cells..... 98

33. Infectivity of LLC-MK2 cells transfected with siRNA for αV and/or β1 integrins. .. 99

34. Histograms of flow cytometric analysis of integrin surface expression in transiently transfected CHO cells. 101

35. Effect of integrin function-blocking antibodies on infectivity of hMPV in integrin-transfected CHO cells. 102

36. Nasal and lung hMPV titer and reciprocal serum antibody titer in cotton rats..... 112

37. Representative sections demonstrating histopathology of hMPV infection in lungs of immunized cotton rats. 115

38. Kinetic analysis of hMPV F binding to anti-HMPV human monoclonal Fab..... 129

LIST OF ABBREVIATIONS

Amino acids (IUPAC, 1968):

Alanine	A (Ala)	Leucine	L (Leu)
Arginine	R (Arg)	Lysine	K (Lys)
Asparagine	N (Asn)	Methionine	M (Met)
Aspartic acid	D (Asp)	Phenylalanine	F (Phe)
Cysteine	C (Cys)	Proline	P (Pro)
Glutamic acid	E (Glu)	Serine	S (Ser)
Glutamine	Q (Gln)	Threonine	T (Thr)
Glycine	G (Gly)	Tryptophane	W (Trp)
Histidine	H (His)	Tyrosine	Y (Tyr)
Isoleucine	I (Ile)	Valine	V (Val)

BLAST	Basic Local Alignment Search Tool
BSA	bovine serum albumin
°C	degrees Celsius
CD	circular dichroism
cDNA	complementary DNA
E.coli	Escherichia coli
EDTA	ethylenediaminetetraaceticacid
ELISA	enzyme-linked immunosorbent assay
FBS	fetal bovine serum
FP	fusion peptide
F protein	fusion protein
G protein	attachment protein
h	hour
HA	hemagglutinin

hMPV	human metapneumovirus
HN	hemagglutinin-neuraminidase
HR	heptad repeat
hPIV	human parainfluenza virus
kDa	kilo Dalton
kb	kilobase
mg	milligram
µg	microgram
ml	milliliter
µl	microliter
MW	molecular weight
MWCO	molecular weight cut off
NDV	Newcastle disease virus
nm	nanometer
nt	nucleotide
OD	optical density
ORF	open reading frame
PBS	phosphate buffered saline
PBS-T	phosphate buffered saline with Tween 20
PCR	polymerase chain reaction
PNGase F	N-glycosidase F
RdRp	RNA-dependent RNA polymerase
rpm	revolutions per minute

RSV	respiratory syncytial virus
RT	room temperature
RT-PCR	reverse transcriptase-polymerase chain reaction
SDS	sodium dodecyl sulfate
SDS-PAGE	sodium dodecyl sulfate-polyacrylamide gel electrophoresis
TBS-T	Tris-buffered saline with Tween-20
TM	transmembrane
U	unit
V	Volt

CHAPTER I

INTRODUCTION

1.1. Overview

Human metapneumovirus (hMPV) is a recently discovered Paramyxovirus, which causes upper and lower respiratory tract infection in infants, young children, elderly and immunocompromized patients worldwide. This thesis concentrates on the structural characterization of the human metapneumovirus fusion (F) glycoprotein.

In Chapter I we show the taxonomy of the Paramyxoviridae virus family, list a couple of important viruses, which are human, mammalian, bird or rodent pathogens, and briefly overview the genome organization, virion structure and replication mechanism of Paramyxoviruses. In the following section we characterize the human metapneumovirus, specifically highlighting the similarities with other family members and showing details about the viral genome, structure and clinical manifestation of the infection. At the end of this chapter we describe the structural and functional characteristics of Paramyxovirus fusion proteins, their role in enveloped virus entry into the host cell, the important domains and structural units of the protein and the conformation change in the secondary and tertiary structure, which plays a key role in the viral entry process and membrane fusion.

In Chapter II we provide the theoretical background, experimental setups, materials, methods and results of cloning, expression and purification of hMPV F ectodomain. In this chapter we describe several different methods that we have tried to

express the fusion glycoprotein. The most successful method with pcDNA3.1 vector system is fully detailed at the end of this chapter. All of the procedures and steps were developed and optimized specifically for hMPV F protein expression and purification.

Chapter III contains the structural and biochemical characterization of hMPV F protein. We used several different techniques to determine the protein's secondary and tertiary structure. Besides the results of gel electrophoresis, IMAC chromatography and circular dichroism spectroscopy and SPR measurements we give a detailed description of the N-glycosylation/site-directed mutagenesis experiments and disulfide mapping of hMPV F protein.

In Chapter IV we will illustrate important biological features of the F protein. A group of specific cellular receptors called integrins bind proteins that contain RGD (Arg-Gly-Asp) motifs. We show that hMPV F protein, which contains the RGD sequence in the F1 subunit, binds to certain integrins and this binding can be inhibited by several ways. This fact might be a crucial point in the understanding of virus attachment and binding to host cells and the entry process.

Our hMPV F construct is a valuable vaccine candidate and the cotton rat is a good animal model for hMPV infection and vaccine studies. We showed that the hMPV F ectodomain is immunogenic and protective in cotton rats. Chapter V contains the detailed description and results of our vaccine development experiments.

Finally in Chapter VI we give a short discussion and conclusion of our results and future directions regarding further structural studies of hMPV F.

1.2. Paramyxoviruses

Classification

The *Paramyxoviridae* virus family contains many important human and animal pathogens. Some of them are the most infectious human pathogens (measles), some of them have major economic impact on poultry (Avian pneumovirus, Newcastle disease virus) and animal rearing (rinderpest virus, bovine respiratory virus), and there are a couple of newly discovered viruses also in this group (Human metapneumovirus, Hendra and Nipah viruses). The Paramyxoviruses are enveloped, negative-sense, single-stranded RNA viruses. The virus family has been reclassified in 2000 into two subfamilies: the *Paramyxovirinae* and the *Pneumovirinae*. The newest classification is based on the genomic organization, the virion structure, the biological role of the viral proteins and the sequence relationship of the encoded proteins[1]. Paramyxovirinae subfamily has five genera: Avulavirus, Henipavirus, Rubulavirus, Respirovirus and Morbillivirus, Pneumovirinae subfamily contains two genera: Pneumovirus and Metapneumovirus (**Table 1**)[2]. Pneumoviruses can be distinguished from the Paramyxovirinae morphologically because Pneumovirinae have narrower nucleocapsids and their attachment protein is very different from that of the Paramyxovirinae. However, all of the Paramyxoviruses have a protein (F), which mediates viral and host cell membrane fusion at neutral pH. This makes an important difference from the *Orthomyxoviridae* virus family, where the viral-cell membrane fusion occurs at low pH in endosomal compartments.

Table 1. Classification of Paramyxoviridae virus family

Family: *Paramyxoviridae*
Subfamily: *Paramyxovirinae*
Genus: Avulavirus
Newcastle disease virus (NDV)
Genus: Henipavirus
Hendra virus
Nipah virus
Genus: Respirovirus
Sendai virus
Human parainfluenza virus types 1 and 3 (hPIV 1 and 3)
Bovine parainfluenza virus type 3
Genus: Rubulavirus
Mumps virus
Simian parainfluenza virus type 5
Human parainfluenza virus types 2 and 4 (hPIV 2 and 4)
Genus: Morbillivirus
Measles virus
Dolphin morbillivirus
Canine distemper virus
Phocine distemper virus
Rinderpest virus
Subfamily*: Pneumovirinae*
Genus: Pneumovirus
Human respiratory syncytial virus (hRSV)
Bovine respiratory syncytial virus (bRSV)
Pneumonia virus of mice
Genus: Metapneumovirus
Human metapneumovirus (hMPV)
Avian pneumovirus

Genome organization, virion structure and viral proteins

The Paramyxovirus genome is a single strand of non-segmented RNA genome with negative polarity. It is 15 to 19 kb in length and contains six to ten tandemly linked genes (seven for some rubulaviruses and eight to ten in pneumoviruses)[1, 2]. The genome also contains an approximately 50 nucleotide long 3' extracistronic leader region and a 50 to 161 nt long 5' trailer sequence, which are essential in the transcription and replication processes[1] (**Figure 1**).

The Paramyxovirus virion is generally irregular spherical and 150 to 350 nm in diameter, but pleiomorphic and filamentous forms can be observed too. The virion is surrounded by a lipid bilayer, which derives from the host cell plasma membrane during budding. In the lipid envelope two surface glycoproteins are inserted (F and G or HN or H) and they extend about 8-12 nm from the surface of the membrane. Inside the envelope is the nucleocapsid core, which contains the single negative-stranded RNA genome, the nucleocapsidprotein (N), the phosphoprotein (P) and the large (L) protein. Between the envelope and the nucleocapsid is the matrix (M) protein. This protein is very important in virion architecture. In addition to the structural genes Paramyxoviruses also contain "accessory' genes, which are transcriptional units or their function is still unknown. **Figure 2** shows the 3D structure of Pneumoviruses with the lipid membrane, the nucleocapsid, the matrix, fusion and attachment proteins.

Figure 1. Genomic maps of the Paramyxoviridae virus family members. Figure is adapted from Easton et al.[2]

The nucleocapsid (N) protein encapsidates the RNA genome and makes it resistant to RNases. It associates with the P and L proteins during the transcription/replication process and also interacts with the M protein. The intracellular concentration of the free nucleocapsid protein is important in replication, because it is thought to control the switch from transcription to viral replication. The N protein contains 390-553 amino acids with a molecular weight of 53,167 to 57,896.

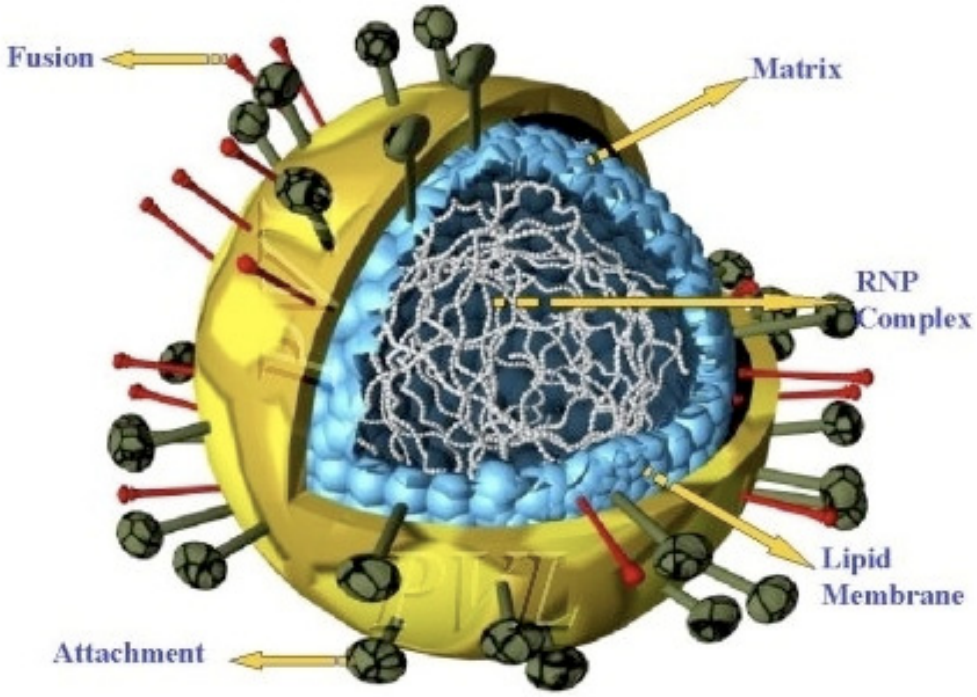

Figure 2. 3D structure of Pneumovirus. Adapted from Pneumovirus Laboratory, University of Warwick, UK.

The P gene of the *Paramyxovirinae* subfamily contains several overlapping reading frames on a single mRNA transcript, but in the *Pneumovirinae* it encodes for the P or phosphoprotein, which is essential for viral RNA synthesis. The catalytic domain of the viral RNA-dependent RNA polymerase in the L protein binds to the N-RNA complex

via the P protein, so the carboxy terminus of the phosphoprotein represents the polymerase (pol) cofactor module. In hRSV the P protein is smaller than that of the *Paramyxovirinae* subfamily; it is 241 amino acids long and forms the major phosphorylated complex in the virion.

The L or large protein is the viral RNA-dependent RNA polymerase; it is the largest protein in the virion. Its gene is at the most distal position from the promoter in the transcriptional map, so it is the last to be transcribed and the protein is less abundant. In hRSV a putative nucleotide-binding domain involved in capping mRNA was identified, which further suggests that the L protein contains polymerase motifs.

The matrix (M) protein is the most abundant protein in Paramyxoviruses. An electron-dense layer under the lipid bilayer represents this protein in the virion. The M protein is non-glycosylated and based on the nucleotide sequence of the M gene in Paramyxoviruses this protein has a net basic charge and contains hydrophobic domains. It is also associated with the peripheral viral membranes. In genetically engineered recombinant measles virus and SV5 the M protein has a major role in particle assembly and budding. It is considered as the central organizer of viral morphogenesis for these viruses, since it is associated with the cytoplasmic tails of the surface glycoproteins, the nucleocapsid and the lipid bilayer.

Paramyxoviruses encode for two integral glycoproteins: the attachment (HN, H or G) and the fusion (F) proteins, some rubulaviruses and pneumoviruses also have a third surface glycoprotein (SH). The attachment protein in respiroviruses and rubulaviruses binds to sialic acid-containing receptors on the cell surface. Because of the low affinity but high avidity of the binding, these viruses cause hemagglutination meaning they

agglutinate erythrocytes. The attachment protein of these paramyxoviruses also has neuraminidase activity (enzymatic cleavage of sialic acid from the surface of infected cells and virions), so the protein of respiro- and rubulaviruses is called hemagglutinin-neuraminidase (HN). Besides the hemagglutinin and neuraminidase activity, in most paramyxoviruses HN protein also has fusion-promoting activity, since co-expression of F and HN protein is needed for successful virus-cell or cell-cell membrane fusion. The attachment protein of Morbilliviruses, like measles, binds to CD46 and CDw150/SLAM surface receptors and the protein causes hemagglutination but it has no neuraminidase or esterase activity, so it is designated as H protein. The attachment protein of Pneumoviruses, like hRSV or hMPV, does not have neuraminidase or hemagglutinating activity and it is called the G protein. In RSV G protein binds to heparan sulfate and G-specific antibodies inhibit virus binding to cultured cells. The G protein is a type II glycoprotein and in Pneumoviruses it is heavily glycosylated (N-linked and O-linked glycosylation). Studies showed that recombinant RSV and hMPV strains that lack G protein were attenuated, but replicated efficiently in Vero cells and in hamsters, so G protein is not essential *in vitro* and *in vivo*. These findings also mean that the fusion (F) protein might have some binding activity too.

The fusion (F) glycoprotein is a type I transmembrane protein, which mediates viral envelope and cell membrane fusion at neutral pH during viral entry and cell-cell membrane fusion during syncytia formation in infected cells. The F protein is synthesized as an inactive F0 precursor and cleaved into the disulfide-linked F1 and F2 subunits by host cell proteases. The protein assembles into homotrimers, the N-terminal hydrophobic fusion peptide in the F1 subunit inserts into the target membrane, and a conformational

change in the protein structure brings the viral and cellular membrane into close proximity resulting membrane fusion (for more details see 1.4.). SV5, measles or RSV F cDNAs expressed in mammalian cells induced syncytia formation without co-expression of the attachment protein, which means that F protein has some attachment activity. However, for many other paramyxoviruses, like hPIV-2, hPIV-3, NDV, CDV and mumps virus co-expression of the attachment protein is necessary for multinucleated syncytium formation. It is important to mention that F and G proteins induce neutralizing antibodies. In hRSV monoclonal antibodies raised against the RSV F protein neutralize infectivity and inhibit fusion. For some of them the antigenic epitopes are conformation-dependent, so in these cases monoclonal and polyclonal antibodies don't react with denatured protein. By comparison, antibodies against G protein recognize denatured protein, indicating no structural dependence. Individual monoclonal antibodies raised against hRSV G protein don't neutralize infectivity efficiently, although a mixture of MAbs give more complete neutralization. In hMPV, however, the F protein appears to be the only neutralizing and protective antigen and vectors expressing the G protein were poorly immunogenic and protective in rodents.

Pneumoviruses, rubulaviruses, SV5 and mumps virus encode for a small hydrophobic protein (SH), which represents the third envelope protein in these viruses. The SH protein is a type II membrane glycoprotein and its function in the virus life cycle is still unknown. Deletion of the SH gene from recombinant RSV resulted no alterations in viral growth *in vitro* or *in vivo*, and it has also been found that the gene can be deleted spontaneously in viruses passaged extensively *in vitro*.

In pneumoviruses the M2 gene contains two overlapping open reading frames: M2-1 and M2-2. The translation of the M2-2 gene is not clear, but it involves a ribosomal stop-restart mechanism. In RSV the M2-1 protein is an essential transcriptional elongation factor and the non-essential M2-2 is thought to be involved in the transcription and RNA replication process.

In RSV there are two non-structural proteins at the beginning of the genomic map designated as NS1 and NS2, which are missing from hMPV and other paramyxoviruses. The function of these proteins is still unknown, but they seem to be non-essential as deletion of NS1 and NS2 genes resulted viable viruses with a slower viral growth rate.

Viral replication

After viral adsorption to the host cell surface receptors the viral membrane fuses with the host cell plasma membrane at neutral pH and the viral nucleocapsid is released into the cytoplasm, where all steps of the paramyxovirus replication take place. A single growth cycle takes usually 14-30 hours in cell culture, but for some strains it can be as short as 10 hours[1]. Paramyxoviruses are single, linear negative-sense RNA viruses and the RNA genome is transcribed exclusively in the cytoplasm by viral RNA-dependent RNA polymerase (RdRp) and the primary viral transcription begins shortly after viral infection. The genomic RNA is tightly wrapped with N protein, which makes it resistant to RNases and this N-RNA complex serves as a template for RdRp, which would not recognize a viral RNA lacking the N protein. The viral polymerase functions in two distinct modes: transcription and replication. In the transcription mode, it copies the viral genome to produce mRNAs corresponding to each gene by a stop-restart mechanism[3].

The transcription starts at the 3' end to generate the (+) leader RNA and then the 5'-capped and 3'-polyadenylated mRNAs by stopping and restarting at each junction. The transcription process exhibits polarity, which means that the genes most proximal to the promoter at the 3' end are transcribed most abundantly. This is also reflected in the relative abundance of the corresponding viral proteins[3, 4]. The viral mRNA is translated to viral proteins by host cell translation machinery. Transcription and translation generate more N protein, which wraps the newly transcribed RNA, and also more L protein boosting the transcription further. Once the primary transcripts generated enough viral proteins transcription is switched to replication. During replication the RdRp ignores the intergenic stop signals at the junctions and synthesizes a full-length positive-sense (mRNA sense) complementary strand of the viral genome called the antigenome. The antigenome is also wrapped with N protein, no mRNAs are transcribed from it and serves as a template for genomic replication to produce more full-length negative-sense viral genome.

At the end of the viral life cycle virus particles assemble by packaging the newly formed, encapsidated genome and viral proteins together, and the virion particles bud from the apical surface of the host cell in form of filament structures. It is thought that the accumulation of the M protein is the trigger to initiate the assembly of virions[2].

1.3. Human Metapneumovirus

Classification

In 2001 van den Hoogen et al. in the Netherlands reported the isolation of human metapneumovirus (hMPV) from nasopharyngeal aspirate samples taken from young children[5]. The newly discovered virus showed a high percentage of sequence identity with avian pneumovirus (APV) serotype C, the avian pneumovirus primarily found in turkeys and chickens in the United States[6]. The overall percentage of amino acid sequence identity between APV and hMPV N, P, M, F, M2-1, M2-2 and L ORFs was 56 to 88%[7]. Until the discovery of hMPV, APV was the sole member of the *Metapneumovirus* genus in the *Pneumovirinae* subfamily of the *Paramyxoviridae* virus family. But because of the similar genomic organization, the high percentage of sequence identity and the evidence provided by phylogenetic analyses the human metapneumovirus became the first mammalian member of the Metapneumovirus genus. The Pneumovirinae subfamily also contains the Pneumovirus genus with important mammalian respiratory pathogens (human, ovine, bovine RSV).

The sequence variations between different virus isolates of hMPV in the N, M, F and L genes revealed the existence of two different genotypes, genotype A and B. Based on further small differences in the sequences each of the two major subgroups has 2 minor groups: A1, A2, B1 and B2.

Genome organization, viral proteins

The hMPV genome is a single strand of negative-sense RNA that ranges in length from 13,280 to 13,335 nucleotides (nt) for the available sequences. The genome contains eight genes and encodes for nine proteins[7, 8]. The gene constellations of pneumoviruses and metapneumoviruses are different; metapneumoviruses lack the non-structural proteins NS1 and NS2. Comparing the genomic organization of human respiratory syncytial virus (3'-NS1-NS2-N-P-M-SH-G-F-M2-L-5') and hMPV (3'-N-P-M-F-M2-SH-G-L-5') we can see a difference not only in the numbers of the encoded proteins but in the relative positions of F, G and SH proteins[2]. By analogy to the hRSV the hMPV proteins are the following: N, nucleoprotein; P, phosphoprotein; M, matrix protein; F, fusion glycoprotein; M2-1, putative transcription factor; M2-2, RNA synthesis regulatory factor; SH, small hydrophobic protein of unknown function; G, attachment glycoprotein and L, viral polymerase.

The first gene in the genomic map of hMPV encodes for the 394 amino acid long nucleoprotein (N). Its length is identical to the N protein of APV-C and shows 88% sequence identity with it[7]. This is the most abundant protein translated from mRNA. The N protein binds the entire length of the viral genomic and antigenomic RNA.

The second open reading frame in the genomic map is the phosphoprotein (P). Its length is 294 aa and it shares 66% sequence identity with APV-C P protein, but only 22% with the P protein of RSV. The phosphoprotein is associated with the nucleocapsid and also serves as a polymerase cofactor. In Paramyxoviruses it forms a soluble complex with the free monomeric N protein.

The matrix (M) protein is the third in the hMPV genomic map; it is 254 aa long. It builds up the inner surface of the viral envelope and it is very important in virion morphogenesis. The sequence identity with APV-C M is 76-87%, and with RSV M it is 37-38%.

The position of the gene encoding for the fusion (F) protein is right after the M gene in metapneumoviruses, in RSV it is after the SH and G genes, The hMPV F protein is 539 aa long, sequence analysis revealed 67% sequence identity with APV-C fusion protein and only 10-18% with other pneumovirus F proteins. The fusion glycoprotein is a type I transmembrane surface protein with important role in viral penetration and syncytium formation. It is synthesized as F0 precursor, which will be cleaved into the fusion active F1 and F2 subunits by host cell proteases. The three N-linked glycosylation sites present in the F of hMPV are conserved in all of the isolates worldwide, but none of these sites are shared with RSV. However, some of the 14 cysteine residues (12 in F1 and 2 in F2) are conserved among all paramyxoviruses.

The M2 gene is unique to the members of the Pneumovirinae subfamily. Two ORFs have been observed in all pneumoviruses. The first ORF represents the M2-1 protein, which enhances the processivity of the viral polymerase and it is called putative transcription factor. This protein is 187 aa long and it shows the highest sequence identity to the APV-C M2-1 protein. Its N-terminal half has 100% identity with APV-C in the first 80 aa residues of the protein.

The second ORF (M2-2) overlaps with the M2-1 ORF in all pneumoviruses. The M2-2 protein is thought to be involved in the control of the switch between virus RNA replication and transcription and it is called the RNA synthesis regulatory factor. This

protein doesn't show as high similarity to APV or RSV proteins as M2-1. Sequence comparison revealed only 56% sequence identity between hMPV and APV-C M2-2.

The gene of small hydrophobic protein (SH) encodes for a 183 aa long protein and it is located next to the M2 ORF. The amino acid composition of SH is relatively similar to that of APV and RSV, but the numbers of cysteine residues and N-glycosylation sites are different in case of APV and RSV. The SH protein is transmembrane surface glycoprotein with N-linked sugars and polylactosaminoglycans. Its function is unknown and deletion of the SH gene results viable but slightly attenuated viruses in case of RSV.

The gene of the major attachment (G) glycoprotein encodes for a heavily N- and O-glycosylated, 236 aa long protein. Basic Local Alignment Search Tool (BLAST) analyses revealed no discernible sequence identity at the nucleotide or amino acid sequence level with other known virus genes or gene products. Low percentage sequence identity found with other G proteins, such as those of APV-A and B (38%) and RSV-A and B (53%). In RSV deletion of the gene results viable but attenuated virus.

The last open reading frame of the hMPV genome is the gene of the RNA-dependent RNA polymerase component of the replication and transcription complexes. The L gene encodes for a 2005 aa protein, which shares 64% sequence identity with APV-A, 44% with RSV and 13-15% with other paramyxoviruses L proteins. The L protein contains the catalytic domains of the RNA dependent RNA polymerase and it is associated with the nucleocapsid.

The non-coding regions between the ORFs of pneumoviruses contain gene end signals, intergenic regions and gene start signals and they vary in size and sequence. The

non-coding regions between the hMPV ORFs range in size from 23 to 209 nt and don't show significant sequence similarity with APV or RSV.

Clinical manifestation and epidemiology

The clinical symptoms of hMPV are similar to the respiratory illnesses caused by human respiratory syncytial virus, which can range from mild respiratory problems to more severe illnesses. The clinical manifestations of hMPV infection in young children include bronchiolitis, croup, pneumonia, wheezing and asthma exacerbations. In infants hMPV is also associated with a substantial number of upper respiratory infections (URI) and with acute otitis media (AOM)[9]. The incidence of hMPV-associated lower respiratory infections (LRI) in young children is in the range from 5 to 15%, and it varies with geographical locations and time of the year. In older children and in adults, especially in the elderly hMPV causes upper respiratory tract infection, croup, laryngitis, bronchitis, asthma exacerbation and pneumonia. The peak age of hospitalization with hMPV occurs during 6 to 12 months of age. By the age of 5 most of the people appear to experience primary hMPV infection and reinfection is common[5, 10].

At Vanderbilt University Medical Center Williams et al.[10] tested nasal wash specimens for human metapneumovirus obtained from otherwise healthy children presenting with acute respiratory tract illness. The Vanderbilt Vaccine Clinic in Nashville followed 2009 infants and children over a 25-year period from 1976 to 2001 and in 249 children with lower respiratory tract infection no virus was identified previously. In this study they found that 20% of the specimens from children with lower respiratory tract illness contained human metapneumovirus RNA by RT-PCR or viable virus by the

presence of CPE in cell cultures. These samples were previously determined as virus-negative samples for all other respiratory viruses. By looking at all of the lower respiratory tract infections, 12% were due to hMPV in this cohort. It was also found that 15% of upper respiratory tract infections were caused by human metapneumovirus. The mean age of children with hMPV was 11.6 months and 78% of the human metapneumovirus infections occurred between December and April.

The hMPV season overlaps with those of RSV and influenza virus. HMPV infections occur during the late winter and early spring months, but the peak incidence of hMPV is usually one or two month later than the peak of RSV. Because the seasonal distribution of hMPV and RSV overlap, the potential for dual infection exists. Several studies found a coinfection rate of <10 %, but one report from the United Kingdom showed that 70% of the RSV-infected children, who required intensive care in Liverpool, were coinfected with hMPV[8].

1.4. Fusion glycoprotein

Fusion process

Membrane fusion is necessary for a large number of diverse biological processes for instance protein trafficking, endo- and exocytosis, protein secretion, synaptic transmissions, fertilization, myoblast fusion and viral infections. Without the specific proteins that mediate membrane fusion, formation of a single lipid bilayer from distinct membranes would be very slow. When two juxtaposed membrane begin to fuse the contacting monolayers (called 'cis' leaflets) have merged, but the distal layers (the 'trans' leaflets) remain intact. This formation is often referred as the 'stalk'. The hemifusion intermediate results from the juxtaposition of the trans monolayers, which evolves to the fusion pore, the next intermediate that allows mixing of the aqueous content of the fusing membranes. The schematic picture of membrane fusion is shown in **Figure 3**[11]. Infection of eukaryotic cells by enveloped viruses requires the fusion of the viral and the plasma or endosomal membranes. In case of influenza virus, which belongs to the Orthomyxoviridae virus family, the viral entry and membrane fusion is a pH-dependent process. Fusion of the endosomal and plasma membrane requires low pH (pH = 5) [12, 13].

The membrane fusion process directed by Paramyxovirus glycoproteins is of particular interest, because it is pH-independent and because it requires two separately synthesized glycoproteins, the attachment (G, H or HN) and the fusion (F) glycoproteins[14]. Paramyxoviruses initiate infection by attaching to cell surface receptors allowing fusion of the viral membrane with the host cell plasma membrane. Surface receptors have been identified for a number of paramyxoviruses, for example SV5 binds to sialic acid, RSV to heparan sulfate, Hendra and Nipah virus G proteins bind to Ephrin

B2 and for measles CD46 and CDw150/SLAM were identified as cellular surface receptors[15].

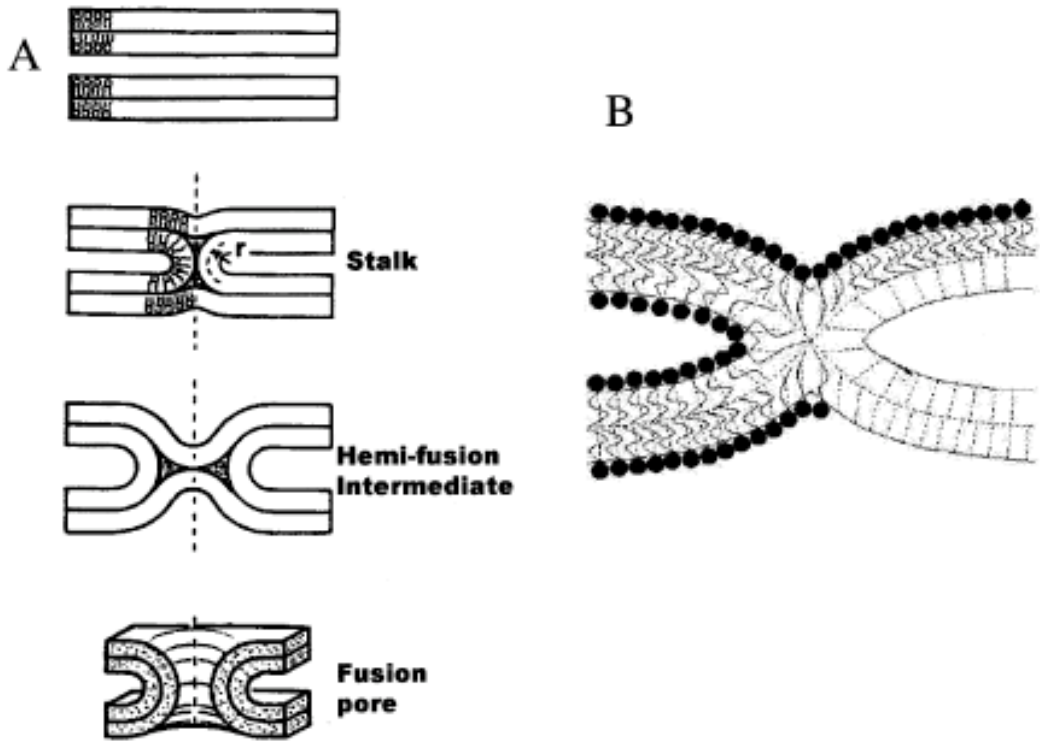

Figure 3. Schematic picture of membrane fusion. A) Intermediate steps from intact membranes to fusion pore formation. B) Packing voids, the space left between cis and trans monolayers are filled by phospholipid chains. Adapted from Blumenthal et al.[11]

Membrane fusion generally proceeds in a series of specific steps: (1) viral attachment to the surface of the host cell, (2) F protein activation and conformational change, (3) approach of the viral and host cell membranes, (4) pore formation, (5) pore expansion and (6) membrane fusion (**Figure 4**)[11, 13]. The current accepted hypothesis postulates that, at one stage of the fusion process, the viral fusion proteins interact simultaneously with both the viral and cell membranes, therefore bridging the gap between them[12]. The paramyxovirus fusion is pH-independent, meaning the infection

does not require the acidic pH of the endosomes, so it can occur at the plasma membranes. As a result of the acid independence infected cells expressing the viral attachment and fusion glycoproteins can fuse with the adjacent cells resulting in syncytia (giant cell with multiple nuclei) formation, a hallmark of paramyxovirus infection[14].

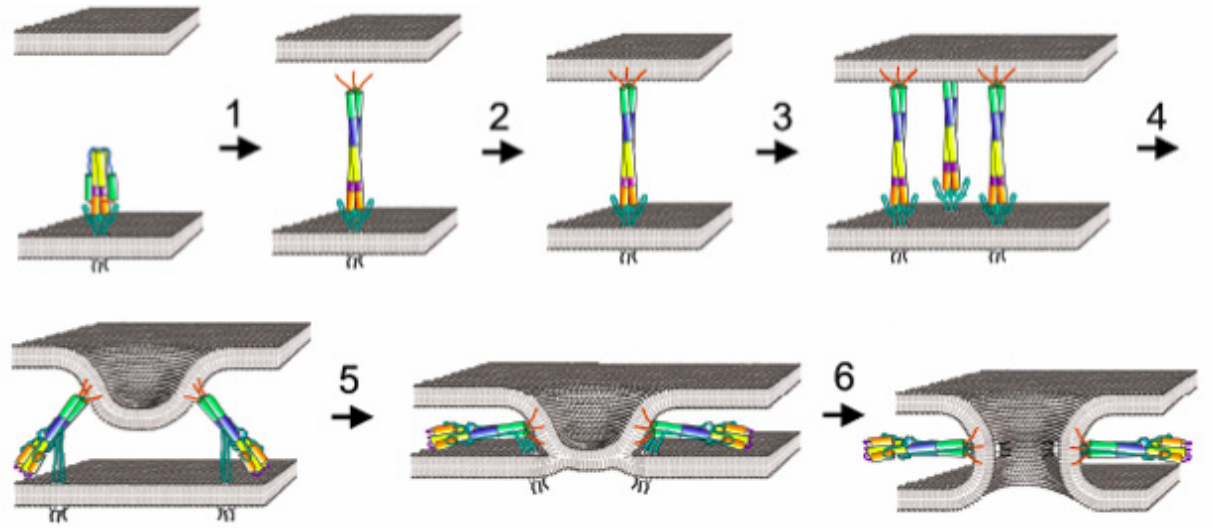

Figure 4. Fusion model for influenza virus[13]

The detailed thermodynamic analysis of influenza hemagglutinin binding to the lipid bilayer was published by Li et al. [16]. The interaction of the fusion peptides with lipid bilayers is driven by a negative value of enthalpy but opposed by negative entropy. The calculated total driving force after the enthalpy gains and entropy losses comes from two sources: 1) from the energy of conformational changes during fusion protein folding and 2) from the energy and entropy due to the insertion of fusion peptide into the lipid bilayer. The structures of fusion proteins of different viruses, the protein folding and conformational changes are described in the next chapter.

F protein structure

Influenza Hemagglutinin. Influenza virus infects cells by binding to sialic acid residues on cell surface molecules and, following transfer into the endosomes by receptor-mediated endocytosis, the viral membrane and the endosomal membrane fuse together releasing the viral genome into the host cell. Sialic acid binding and viral and host cell membrane fusion is mediated by the influenza virus hemagglutinin (HA), which is a trimeric integral glycoprotein. HA is probably the most extensively studied viral glycoprotein. The 3-dimensional crystal structures of the native protein at neutral pH, the fusion active low-pH form and also the uncleaved protein precursor are known (**Figure 5**)[17] and it serves as a model of viral fusion[11] for enveloped viruses.

HA is a trimer and each HA monomer is composed of two disulfide-linked subunits: the receptor binding HA1, which also represents the major antigenic sites of the protein and the fusion active HA2 subunits, which contains the N-terminal hydrophobic fusion peptide and the C-terminal transmembrane domain[13, 18]. HA is synthesized as an uncleaved HA0 precursor and cleavage primes HA from the native metastable state to the fusion active, stabilized low-pH state. In the native form HA2 trimerizes through the formation of a parallel coiled coil. At the N-terminus of the native coiled coil a loop region connects to a second α-helix, which runs anti-parallel to the first. This second α-helix contains the transmembrane region at the C-terminus, which anchors the protein to the viral membrane.

At the N-terminus of the first helix is the hydrophobic fusion peptide, which is buried in the center of the native trimer (**Figure 6**). The three sialic acid-biding HA1 subunits assemble on the top of the HA2 three-stranded stem and they serve as a clamp.

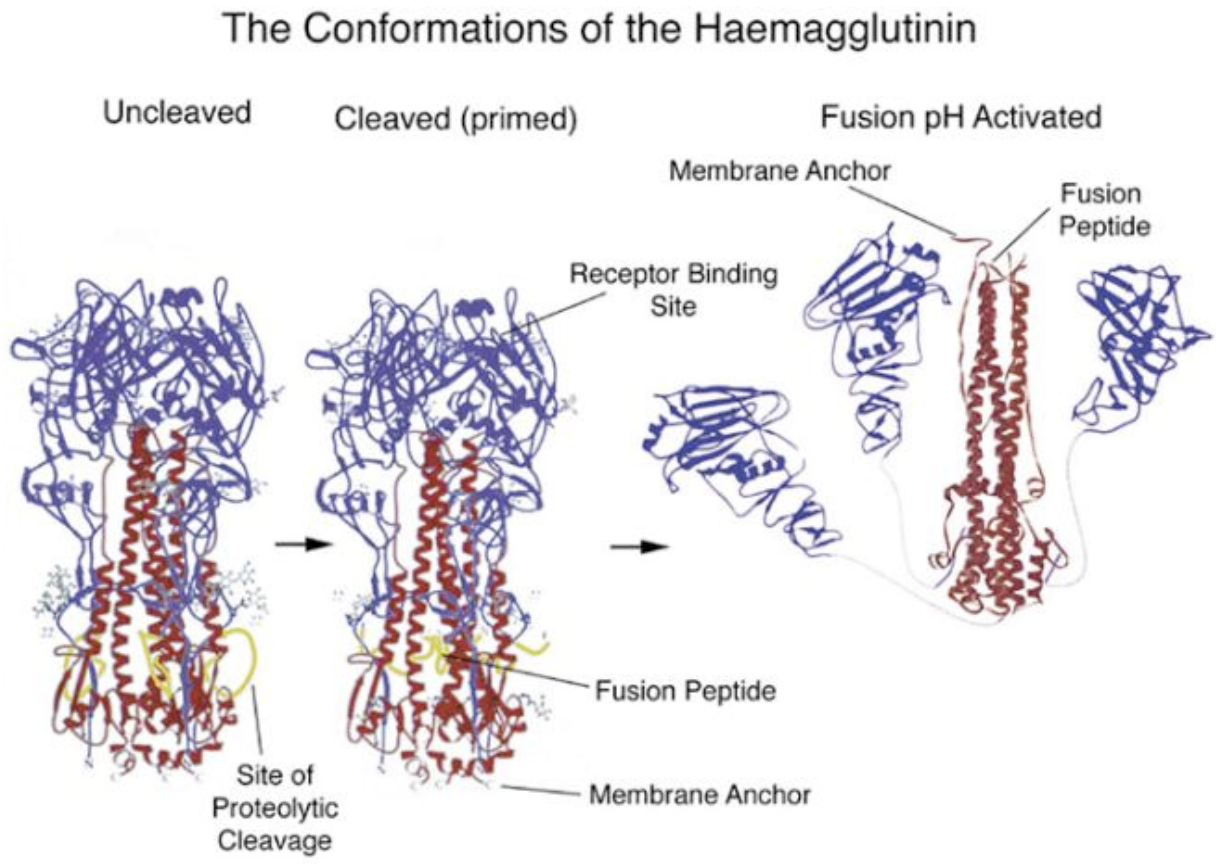

Figure 5. The conformations of influenza hemagglutinin. Adapted from Skehel et al.[17]

In the low-pH state, however, a conformation change happens, which is often referred as the spring-loaded conformational change[13, 19]. In acidic environment the loop region of HA2 refolds into an α-helix connecting the original helices into one extended coiled coil. Now the N–terminal fusion peptide is relocated toward the target membrane to promote fusion. (**Figure 5**)[19].

This dramatic change in the secondary structure has been confirmed by CD spectroscopy results, which revealed a change in the α-helical signal of the loop region between pH=5 and pH=7. The formation of the extended coiled coil can also be induced by elevated temperature at neutral pH.

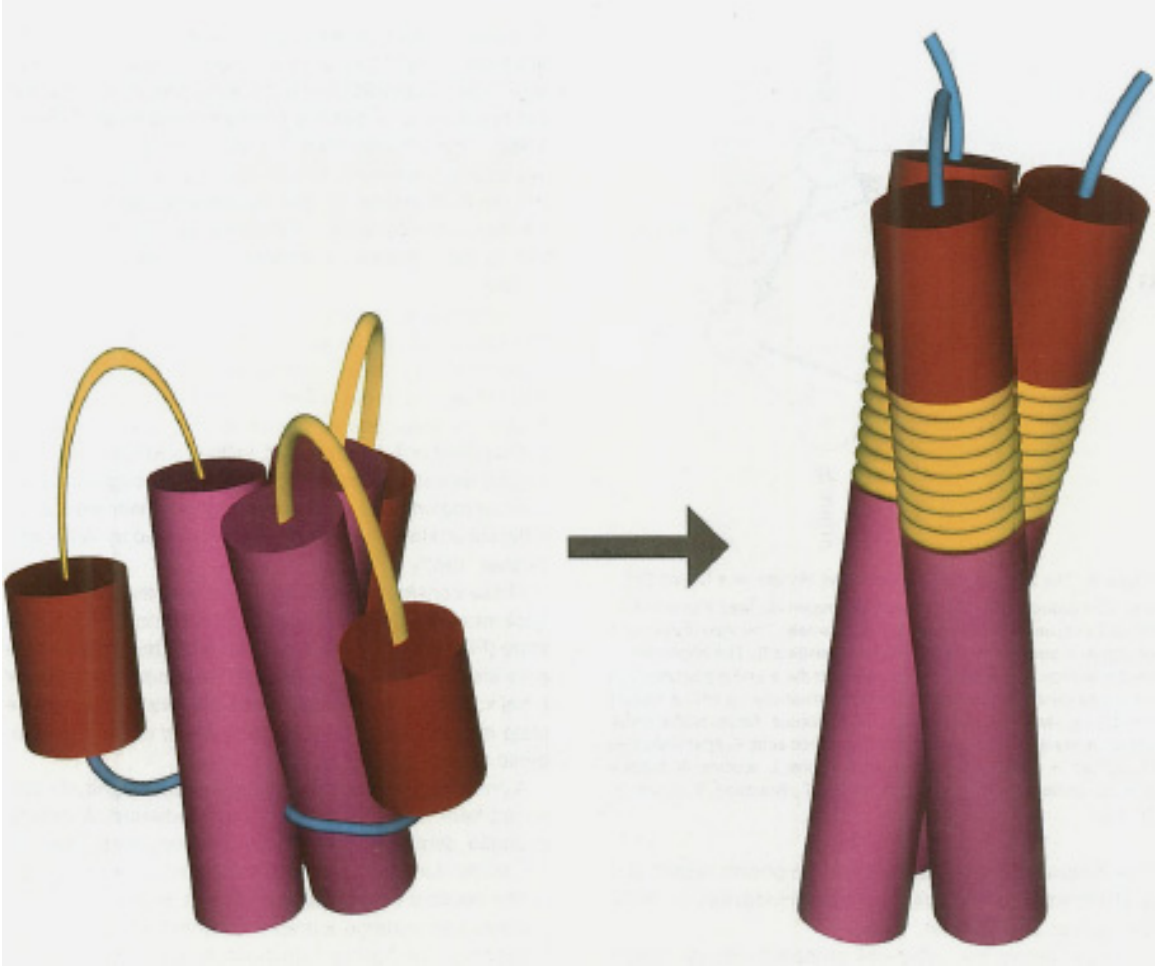

Figure 6. Spring-loaded conformational change of influenza HA2. From Carr et al.[19]

The coiled coil structure is not a unique motif, it is found in many other proteins, including the leucine zipper domain of some transcription factors. In general the coiled coil motifs consist of α-helices that wrapped around each other with a left-handed superhelical twist. Coiled coil sequences contain hydrophobic and hydrophilic amino acid

residues in a repeating pattern. These regions are called the heptad repeat regions (denoted positions from a through g), where the hydrophobic residues occur at the first (a) and fourth (d) positions of the repeating pattern and the helices are held together by hydrophobic interactions between these amino acids. The heptad repeat is also known as the 4-3 hydrophobic repeat and it is the hallmark of coiled coil formation[19].

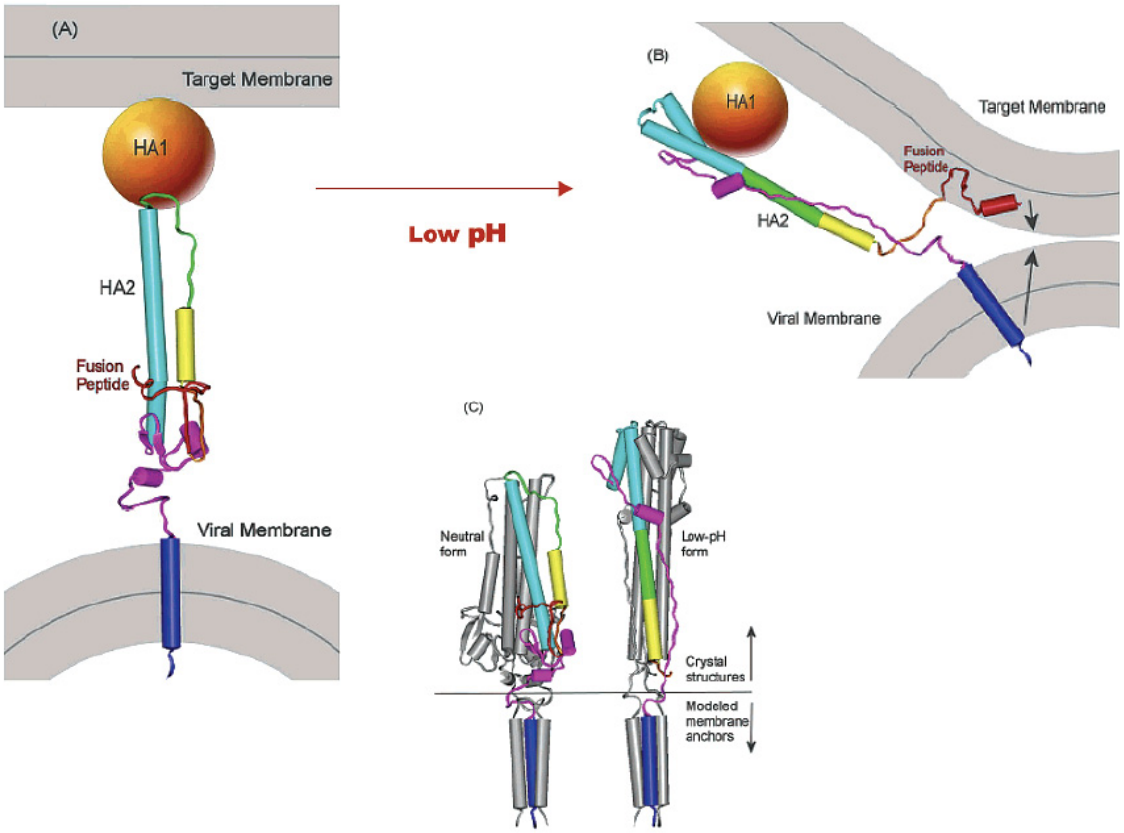

Figure 7. Model for membrane deformation catalyzed by influenza HA. Adapted from Blumenthal et al.[11]

The conformation change in the HA2 region is coupled to deformation of the target and viral membranes through the fusion peptide and the transmembrane (TM) domain, respectively. The second α-helix in HA2, which contains the TM domain at its

C-terminus, is in anti-parallel position to the extended coiled coil, so the fusion peptide and the TM anchor is on the same side pulling the viral and target membrane close to each other for fusion (**Figure 7**).

HIV gp-160. The structure of the envelope glycoprotein of Human Immunodeficiency Virus Type 1 (HIV-1) shows striking similarity to the low pH-induced conformation of influenza hemagglutinin. The gp-160 glycoprotein precursor consists of a complex of gp-120 and gp41 glycoproteins that are generated by proteolytic cleavage of the precursor polypeptide chain. The gp120 is the highly glycosylated receptor-binding subunit, it directs target cell recognition and viral tropism through interaction with the cell-surface receptor CD4 and with chemokine co-receptors CCR5 and CXCR4. Sequence analysis of HIV isolates revealed that gp120 can be organized into variable (V1-V5) and conserved (C1-C5) regions. Its primary role is to attach HIV to the target cell and bring the virus close to the membrane of these target cells. Once this is achieved, the transmembrane protein gp41 mediates the fusion of the viral and target membranes to enable genetic information of the virus flow into the target cell. Gp41 is relatively well conserved and most of its surface is hidden from antibody recognition before attachment and fusion[20]. Binding to CD4 surface receptors induces conformational changes both in the gp120 and gp41 structures. These conformational changes are thought to expose the hydrophobic, glycine-rich fusion peptide region of gp41 that is essential for membrane-fusion activity. Previous studies identified an α-helical region in gp41, which consists of a trimer of two interacting peptides (N36 and C34). Crystal structure of this complex showed that three peptides N36 form the interior, parallel coiled-coil trimer and three

C34 helices are packed into the hydrophobic outside grooves of the inner trimer in anti-parallel fashion (**Figure 8**)[21].

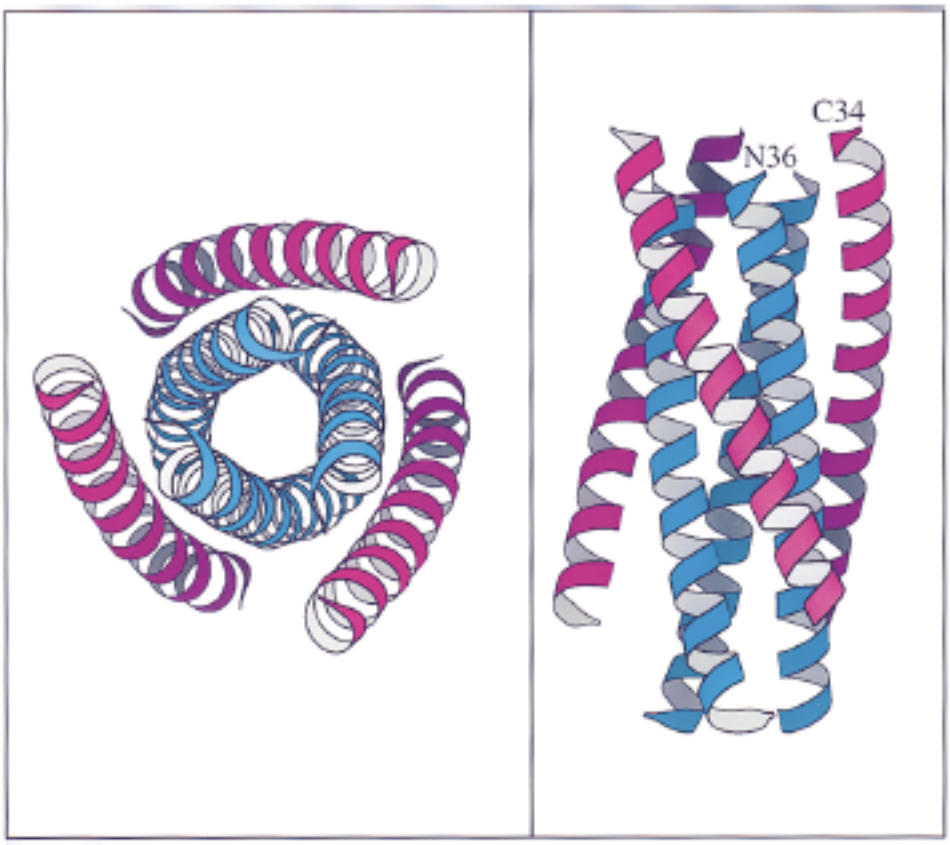

Figure 8. Diagrams of the N36/C34 complex. The left panel shows an end-on view of the N36/C34 complex looking down the three-fold axis of the trimer. The right panel shows a side view of the complex. The N36 helices (blue) form the inner trimer and their amino-termini point toward the top of the page. The C34 peptides (purple), located in the surface grooves, form the anti-parallel outer helices. Adapted from Chan et al.[21]

Sequence analysis of the gp41 ectodomain also revealed the 4-3 heptad repeat pattern with hydrophobic residues at the first (a) and fourth (d) positions of N36 and C34 peptide regions. However, the generation of stable gp41 trimers for structural and immunological studies is very difficult because of the lability of these glycoprotein

complexes. Both the intersubunit interactions that promote trimer formation and also the association between gp120 and gp41 are labile. Soluble forms of HIV-1 envelope glycoprotein have been produced by deletion of the transmembrane region and cytoplasmic domain of gp41 and as well as modification of the proteolytic cleavage site between gp120 and gp41. These attempts resulted unstable heterogeneous dimers and tetramers instead of stable glycoprotein trimers. Other approaches, including introduction of cysteine residues[22] that form intersubunit disulfide bonds, addition of trimerization domains (GCN4[23, 24] or T4 bacteriophage fibritin[25]) to the gp41 ectodomain or generation of chimeric proteins of HIV-1 gp120 and influenza HA1/HA2[26] resulted more stable constructs with patterns of neutralizing and non-neutralizing antibody binding, but further studies are needed to clarify the conformational state of the stabilized HIV-1 envelope glycoprotein trimer.

Paramyxovirus F protein. The most straightforward way to better understand the mechanism of fusion in paramyxoviruses would be solving the structure of the fusion protein by crystallization. To date, the best data that come from crystallized paramyxovirus fusion proteins are the partially proteolyzed structure of Newcastle disease virus F protein[27] and the pre- and post-fusion structures of an uncleaved human parainfluenza virus F ectodomain expressed in insect cells[15, 28]. These models give some insight to the structures of paramyxovirus F proteins, but further studies with other viral fusion proteins are needed to elucidate the fusion mechanism.

The Paramyxovirus F genes encode 540 to 580 residues. All Paramyxovirus fusion (F) proteins are type I integral membrane glycoproteins, which spam the viral

membrane once and contain a signal sequence at their N-terminus. The signal sequence directs the growing polypeptide chain to the ER, where glycosylation and post-translational modifications take place. At the C-terminus the hydrophobic transmembrane (TM) domain anchors the protein to the membrane leaving a short (20-40 residues) cytoplasmic tail. F proteins are synthesized as single-chain inactive precursors (F0), which are subsequently cleaved into the fusion active, disulfide linked F1 and F2 subunits by host cell proteases (**Figure 9**)[29]. Based on the cleavage site paramyxoviruses can be divided into two groups: those that have multiple basic residues at their cleavage site, and the ones with only a single basic residue at the cleavage site[1, 14]. Cleavage of the proteins with multiple basic cleavage site occurs in the *trans*-Golgi, the enzyme that is responsible for the cleavage is furin, a subtilisin-like endoprotease, which recognizes a specific sequence (R-X-K/R-R). Since furin is a cellular protease in the *trans*-Golgi network, F proteins of the viruses (RSV, NDV virulent strain, measles, SV5, mumps) that have multiple basic sites are cleaved intracellularly and delivered to the plasma membrane as cleaved and potentially active F proteins.

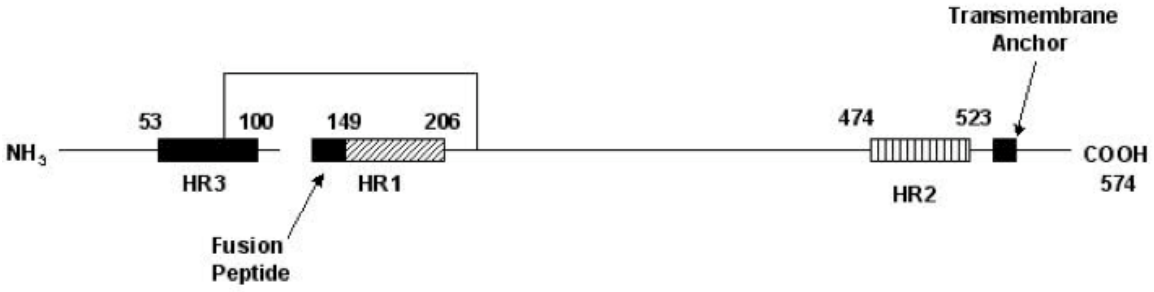

Figure 9. Schematic diagram of RSV F protein. The fusion peptide, heptad repeat regions (HR1-3) and transmembrane anchor is shown. Adapted from Lawless-Delmedico et al.[29]

Paramyxoviruses (e.g. Sendai virus) with a single basic residue at the cleavage site between F1 and F2 subunits tend to be restricted in the respiratory tract, where the necessary protease can be found. The protease, which is responsible for activating paramyxoviruses in the respiratory tract, is secreted from Clara cells in the bronchial epithelium. The fusion protein is delivered to the plasma membrane as an inactive, uncleaved form and cleavage by the extracellular host cell protease activates the fusion protein. It has been shown that RSV F protein has two cleavage sites; one at the F1-F2 junction and the other is in the F2 subunit. For membrane fusion activity RSV F needs to be cleaved at both furin cleavage sites[30].

Besides the signal sequence and transmembrane region paramyxovirus fusion proteins have several conserved domains that have crucial roles in viral fusion. Right after the proteolytic cleavage site at the N-terminus of the F1 subunit is the hydrophobic fusion peptide. Similarly to influenza HA and HIV-1 gp41, the fusion peptide is thought to be inserted into the target membrane to initiate fusion. Between the fusion peptide and transmembrane domain are the 4-3 heptad repeat regions with hydrophobic amino acid residues in every *a* and *d* position. In paramyxoviruses there are at least two heptad repeat domains, but in some cases (e.g. RSV, Sendai, measles, parainfluenza, rinderpest, SV5 or NDV) a third heptad repeat region (HR3 or HRC) can be found in the F2 subunit[31]. The role of HR3 has yet to be identified, but it is thought that this domain probably does not form helix in the crystal structure of F protein. Crystal structures of many paramyxovirus HR cores have been solved previously and all revealed a trimeric coiled coil formation beginning near the C-terminal end of the fusion peptide[15, 28, 29, 31, 32]. The structure of paramyxovirus heptad repeat coiled coils also show similarities to other type I viral

fusion proteins, such as low-pH induced influenza HA, gp41, Ebola Gp2 or MMLV Env-TM protein (**Figure 10.**)[32, 33]

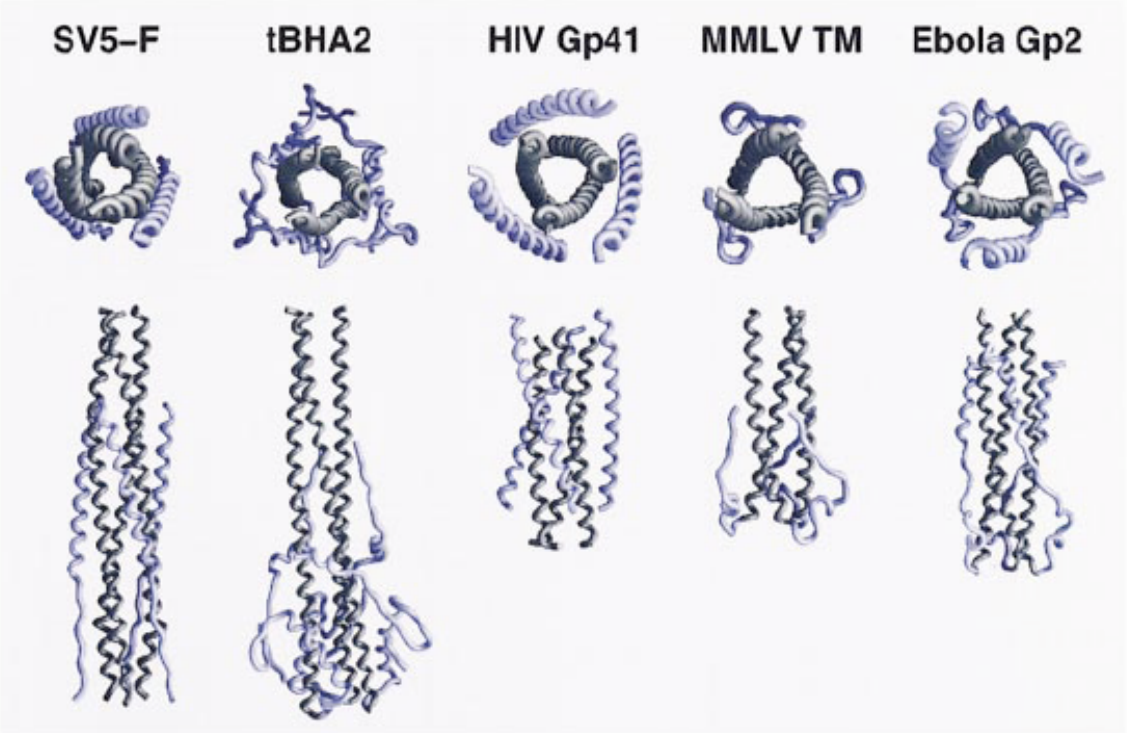

Figure 10. Top and side views of SV5 F1 core trimer compared to other type I glycoproteins, such as the low pH-induced influenza HA (tBHA2), HIV-1 gp41, MMLV Env-TM and Ebola Gp2 protein. Interior trimers are shown in grey, exterior helices in blue. Adapted from Baker et al.[33]

The first solved crystal structure of a paramyxovirus F protein was determined by Chen et al.[27, 34] with an uncleaved F protein from an avirulent strain of Newcastle disease virus. It crystallized as a trimer with distinct regions of head, neck and stalk shown in **Figure 11**. The head and neck regions contained sequences from both the F1 and F2 subunits, the stalk region was a long coiled coil trimer from residues 171 to 221.

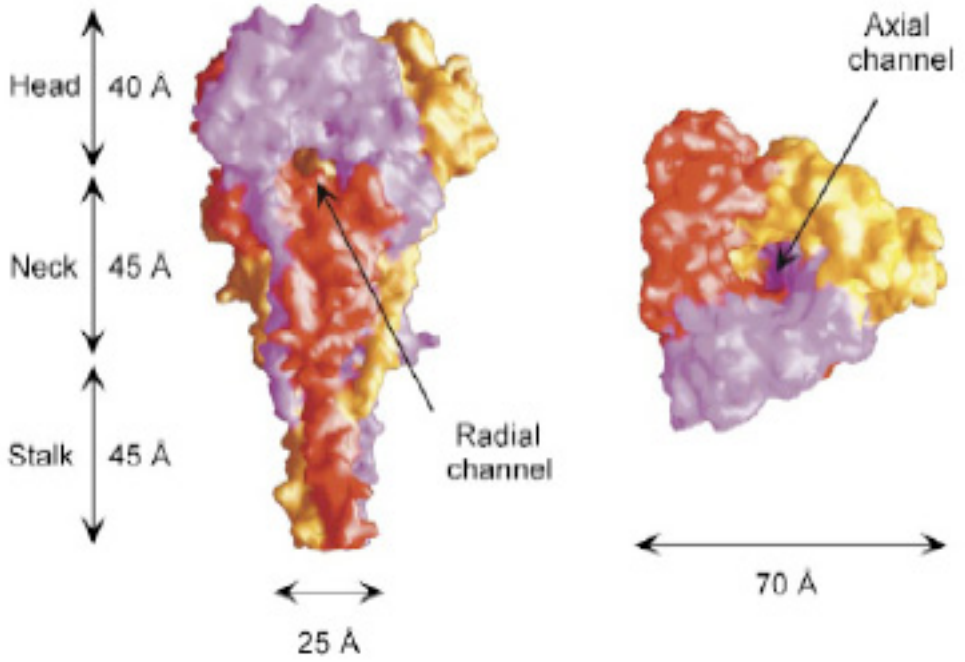

Figure 11. Space-filling model of NDV F trimer. The left panel shows the side view of the trimer with monomers colored differently. Head, neck and stalk regions labeled on the left. The right panel shows a top view of the trimer looking down the three-fold axis. Adapted from Chen et al.[27]

The structure is missing several crucial domains that would be important to understand the fusion mechanism. First, the entire transmembrane domain and cytoplasmic tail was eliminated from the structure in order to allow secretion of the mutated F protein from the cells. This may be important, since expression of a mutant NDV F protein missing the cytoplasmic region resulted in decreased efficiency of cleavage and surface expression. The region from amino acid residues 106 to 170 is also missing from the construct. This important region contains the cleavage site, the fusion peptide and the amino terminal half of the HR1 region. Another missing region from

residues 455 to 499 includes the entire HR2 domain, which might be the result of protein degradation. These missing domains complicated consideration of the structure of the pre- and post-fusion conformation of the NDV F protein and raised many questions about the conformational changes required for fusion activation[14].

The crystal structure of the uncleaved human parainfluenza virus 3 F protein ectodomain (hPIV 3) was determined in 2005 by Yin et al.[28, 32]. The construct was truncated right before the membrane anchor domain and protein was expressed in insect cells by using the baculovirus expression system. The crystal structure of hPIV3 F showed a trimer with the head, neck and stalk regions previously determined in NDV F, and it also contains the complete six-helical bundle coiled coil core, which was not observed in NDV F (**Figure 12**). The only part that was missing from this structure was the cleavage site between F1 and F2 and probably because of that the fusion peptide could not be located in the structure. Although the fusion peptide was not at the appropriate end of the heptad-repeat coiled coil and the polypeptide chain was intact, the trimeric hPIV 3 F structure was thought to be the post-fusion conformation of the protein. However, the crystal structure of the hPIV 3 F also raised further questions. First, it was not known, what the pre-fusion conformation of the paramyxovirus F protein was and how stable this formation was. Second, it was also not clear how membrane fusion could be achieved by the post-fusion state, because the cleavage site was disrupted in the construct and according to fusion models this proteolytic cleavage would allow repositioning of the fusion peptide toward the target membrane. And third, since the transmembrane region was missing, the role of the TM domain in the stability of the pre-

fusion state and in the conformational change during the transition between the pre-and post-fusion forms also remained unsolved.

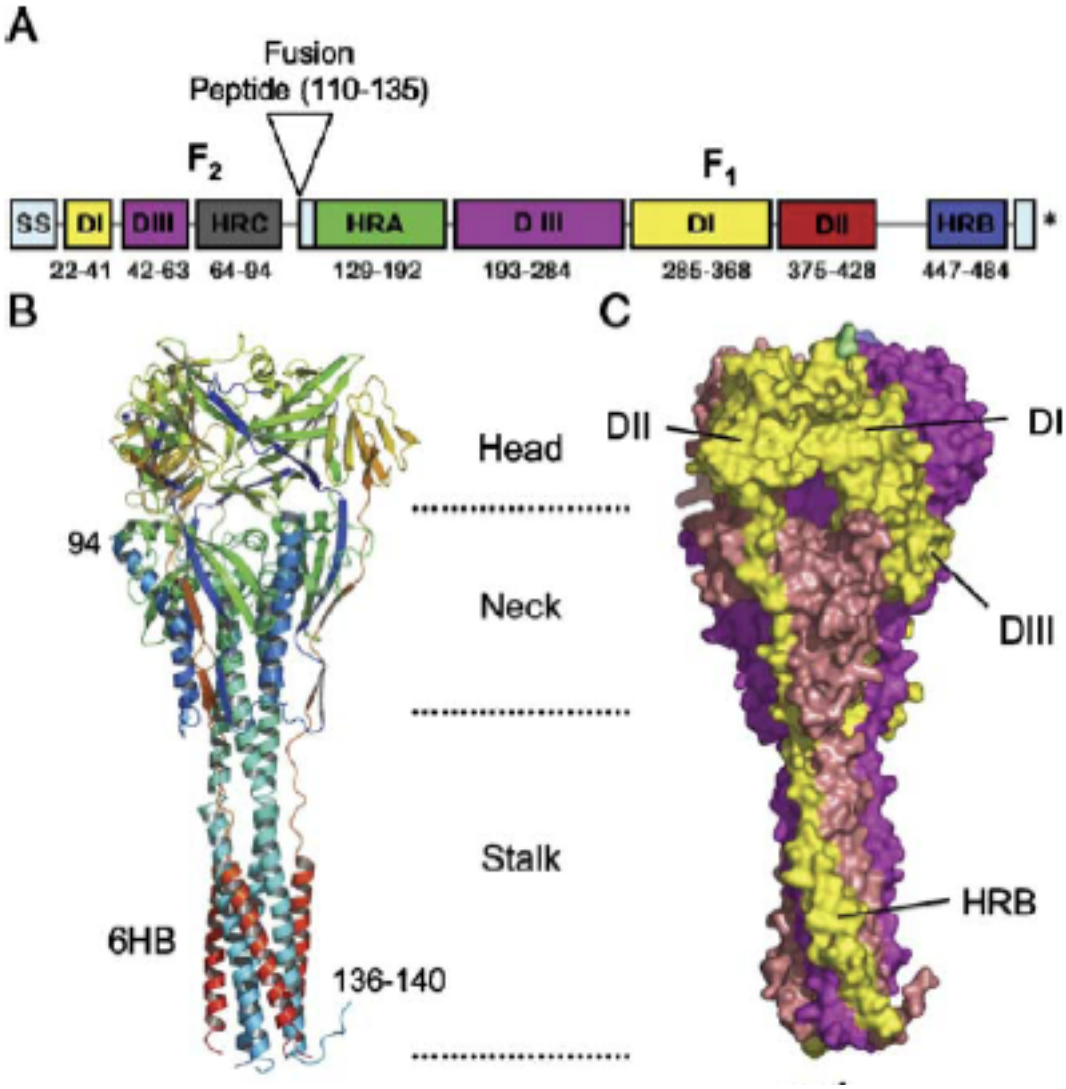

Figure 12. Structure of the hPIV 3 F ectodomain. A) Schematic of the domain structure of hPIV 3 F. Colors correspond to those used in Figure 12. B. B) Ribbon diagram of hPIV F trimer. The six-helix bundle of the heptad repeats is labeled as 6HR C) Surface representation of hPIV 3 F trimer. Monomers are colored differently. Head, neck and stalk regions are shown in the middle. Adapted from Yin et al.[28]

In 2006 Yin et al. published another paramyxovirus F protein crystal structure. They published the structure of the parainfluenza virus 5 (previously known as SV5) F protein in its pre-fusion conformation. Since the soluble SV5 F ectodomain did not trimerize efficiently a trimerization domain (GCNt) was engineered C-terminal to the HRB region. Trimerization domains have been successfully attached to influenza HA and HIV gp41 to help the formation of stable trimers and the SV5 F-GCNt construct indeed formed stable trimers. Comparison of the pre-fusion SV5 and the post-fusion hPIV 3 F protein structures shows striking differences (**Figure 13**). The first obvious differences are the position of the stalk region relative to the head and the size of the head regions. In the post-fusion orientation the head is more compact and the stalk is flipped to the other side of the head turning the whole structure upside-down. The second striking difference is the conformation of the HRA region in pre-and post-fusion states. In the pre-fusion form HRA is folded around the DIII core (**Figure 13.c**) containing short helical and β-sheet segments. In the post-fusion form HRA folds into a single strand of a long helix, pulling HRB to the other side of the head and forming six-helical bundle coiled coil core. It is interesting that in this structure the HRB heptad-repeat residues form the three helical bundle stalk region in the pre-fusion state along with the GCNt trimerization motifs, however, isolated HRB peptides alone don't form stable trimers in aqueous solutions. This suggests that the GCNt domain, or the transmembrane region and cytoplasmic tail in the natural protein stabilize the HRB stalk as well as the prefusion conformation state.

Based on the pre-fusion and post-fusion crystal structures Yin et al. proposed an F protein-mediated fusion model for paramyxoviruses (**Figure 14**)[35].

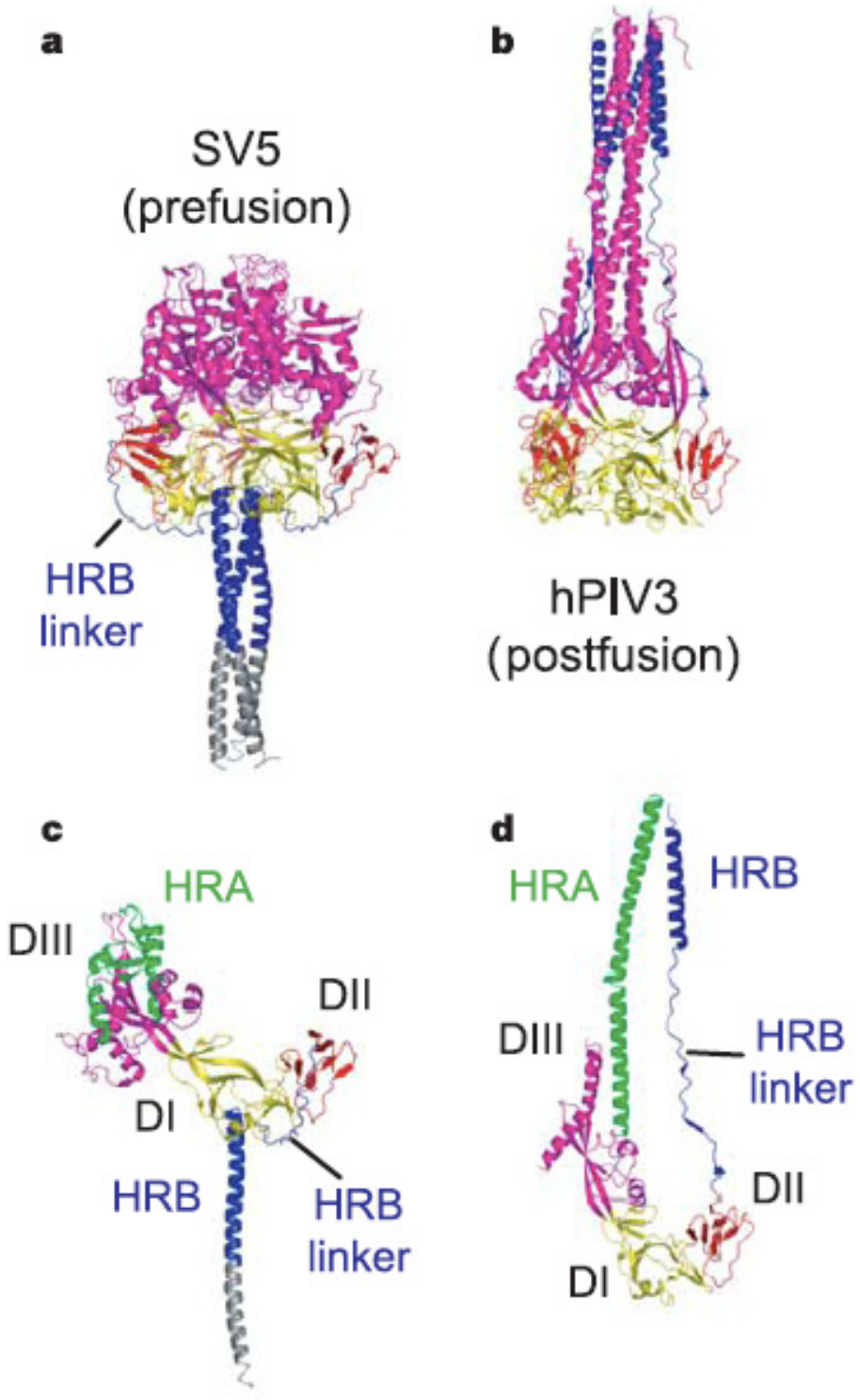

Figure 13. Pre- and post-fusion F protein conformations. **a**. Ribbon diagram of SV5 F-GCNt trimer (pre-fusion). **b**. Ribbon diagram of hPIV 3 F trimer (post-fusion). **c**. and **d**. Ribbon diagrams of single monomers of SV5 F and hPIV 3 F, respectively. Adapted from Yin et al.[35]

In this model starting from the pre-fusion state (**Figure 14 a**), the first step is when the HRB helices break the interactions with the head region and form the 'open stalk' intermediate (**b**). The HRA region is still in its pre-fusion conformation; no coiled coil is formed yet. In the next step (pre-hairpin intermediate, **c**) the HRA region is flipped over the head and forms coiled coil helices relocating the fusion peptide toward the target membrane. Refolding of the HRB region into an α-helical structure (**d**) and the six-helical bundle formation pulls the target membrane close to the viral membrane resulting pore formation and the post-fusion protein structure (**e**).

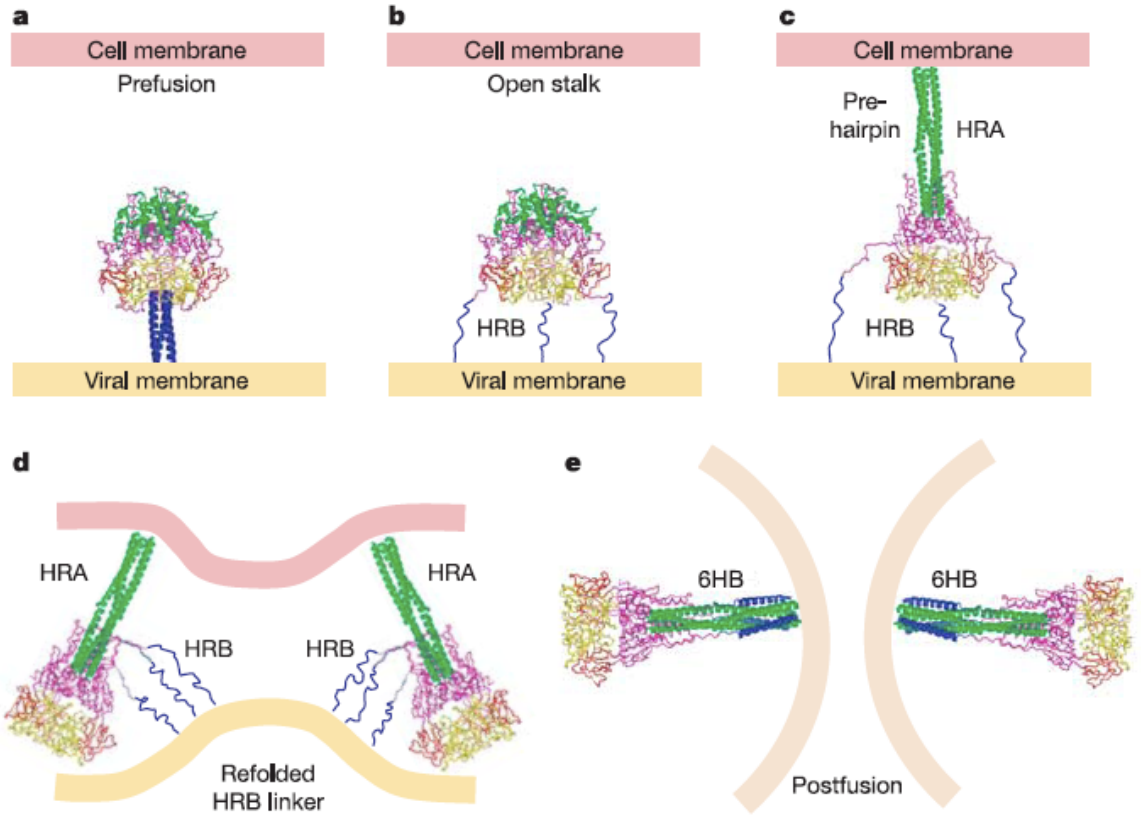

Figure 14. Model for F-mediated membrane fusion. See explanation in the text above. Adapted from Yin et al.[35]

CHAPTER II

CLONING, EXPRESSION AND PURIFICATION OF HUMAN METAPNEUMOVIRUS FUSION GLYCOPROTEIN

2.1. Introduction

Sequence analysis of hMPV F clearly showed homologous regions to other paramyxovirus fusion proteins and we hypothesized that these regions might have similar functions. Based on the hMPV F sequences we predicted that the hMPV fusion protein monomer is approximately 58 kDa in size. There is a potential single basic cleavage site between F1 and F2 subunits, which is homologous to that in hPIV-1 and Sendai virus. Further, we found that the fusion peptide region right after the cleavage site shows high sequence homology to that of hPIV-1, Sendai and hRSV. Using secondary structure predicting algorithms (such as LearnCoil-VMF, MultiCoil, ParaCoil), which are specifically designed to predict the propensity of a protein sequence to form coiled coil, we identified HR1 and HR2 heptad repeat regions in the amino acid sequence. Now we had strong evidence, based on the predicted amino acid sequences that significant homology exists between hMPV F and other paramyxovirus fusion glycoproteins. To study the structural and biochemical properties of hMPV fusion protein, we needed a stock of purified hMPV F protein expressed in mammalian cells. We wanted to use mammalian cell lines (instead of expression in bacteria or insect cells) to make sure that our protein is glycosylated and folded correctly or close to its native conformation.

For protein expression we tried several approaches, the first strategy was to use an inducible T7 vaccinia virus expression system. For that approach, cDNA of hMPV F protein was generated by RT-PCR from isolate TN/92-4 (A2 strain) and cloned into pET-11KC[36] vector, in order to add C-terminal 6xHistidine tag and BirA biotinylation site. The hMPV F insert with the fused His-tag and BirA site was excised from pET-11KC by restriction sites flanking the cloning sites and the whole construct was subcloned into pVOTE.1 vaccinia virus vector[37] (**Figure 15**). A recombinant vaccinia virus was generated, using standard infection/transfection protocols (see section 2.2. *Generating recombinant vaccinia virus stock*), by homologous recombination of the vector, which contains vaccinia virus sequence flanking the inserted F gene and the infecting vaccinia virus strain. The pVOTE.1 vector contains the *gpt* gene, which encodes for mycophenolic acid (MPA) resistance, allowing selection for recombinant vaccinia virus by using MPA-containing selective medium.

The vector also encodes for a bacteriophage T7 polymerase gene. T7 is a single subunit RNA polymerase that recognizes a highly conserved promoter sequence, so synthesis of T7 RNA polymerase by a recombinant vaccinia system allows high-level expressions of genes placed next to the T7 promoter within a transfected plasmid. Previously an inducible expression of a reporter gene under T7 promoter control has been generated when incorporated into a recombinant vaccinia virus, vT7lacOI, which contains the *E. coli lac* repressor (*lacI*) gene, regulated by the vaccinia virus early/late promoter and the bacteriophage T7 RNA polymerase gene (*gene 1*) regulated by a modified perfect palindromic *E. coli lac* operator (*lacO*) placed several nucleotide downstream of vaccinia virus late promoter[37] (**Figure 15**).

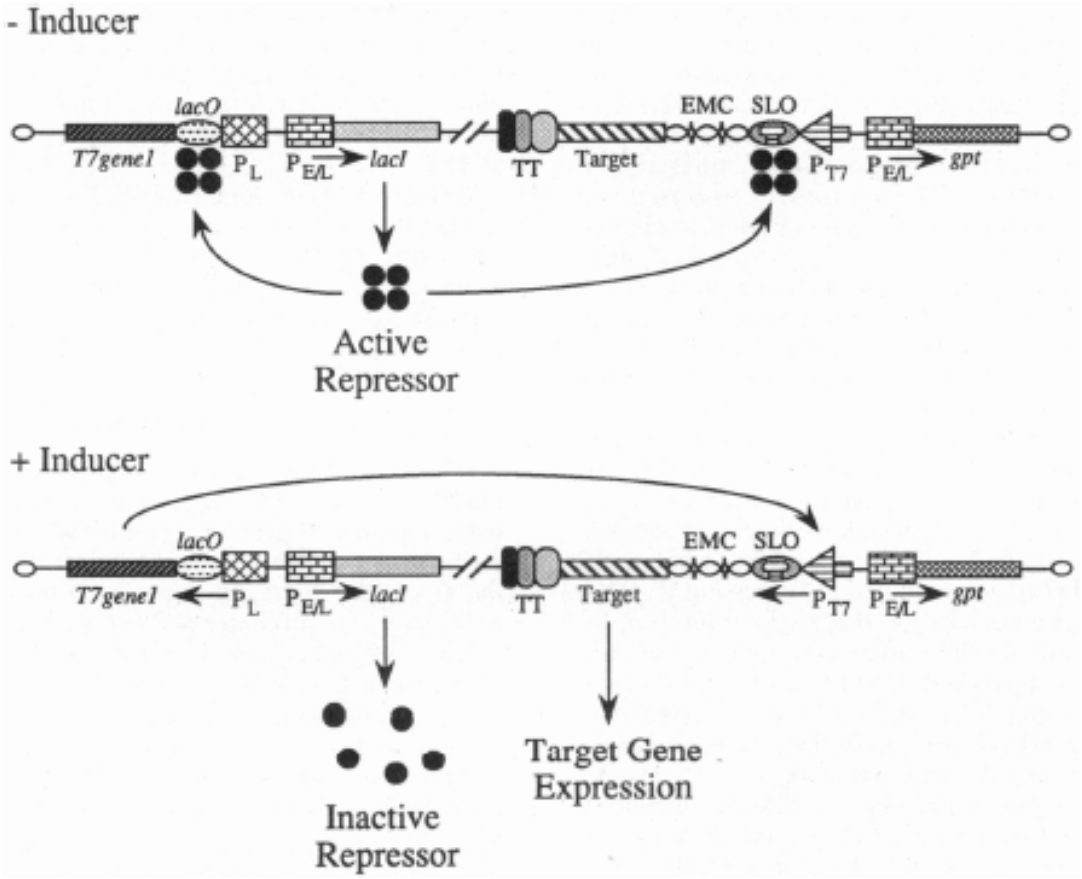

Figure 15. Regulation of target gene expression in the absence (-) or presence (+) of inducer. $P_{E/L}$ is the vaccinia virus early/late promoter, *T7 gene I* is the bacteriophage T7 polymerase gene, SLO is the modified lac operon and P_{T7} is the T7 promoter. From Ward et al.[37]

In our expression system hMPV F gene expression was induced by the addition of isopropyl β-D-thiogalactopyranoside (IPTG) (see section 2.2. *IPTG-induced protein expression*).

The second method that we tried for recombinant hMPV F protein expression is using codon optimized F sequence for cloning and a mammalian expression vector system designed for visual detection of transfected mammalian cells. Codon optimization

is a method for replacing one or more codon that is rarely used in the host with one that is more frequently used. Elimination of codon that would be read as termination signals, *cis*-acting negative regulatory elements or different amino acids in the host is essential to improve protein expression, especially in case of viral proteins. Codon optimization also increases the stability of mRNA, optimizes the RNA secondary structure and DNA GC content, eliminates common restriction enzyme sites and repetitive elements from the sequences. These all enhances the expression level of the recombinant protein. To produce a soluble form of hMPV F protein (FΔTM), the codon-optimized full-length F gene was PCR amplified using primers that amplified the sequence without the predicted hydrophobic transmembrane region and cytoplasmic domain. So, we had two sets of optimized F gene, one for membrane bound full-length F expression, and another to produce soluble truncated hMPV F (FΔTM). For expression vector we chose pTracer-EF/V5-His (Invitrogen) with a human elongation factor (hEF) and human cytomegalovirus immediate/early (CMV) promoter, a C-terminal improved Green Fluorescent Protein (GFP) gene and V5 epitope and 6xHistidine tag. Detection of transfected cells is possible because of the GFP expression and 6xHistidine tag is for metal ion affinity purification purposes (**Figure 16**). With that we were able to detect expressed full-length F protein bound to the transfected cell membrane, and also soluble FΔTM expressed in the culture media. Although protein expression level was moderate, this was the first successful attempt to produce and purify hMPV F protein.

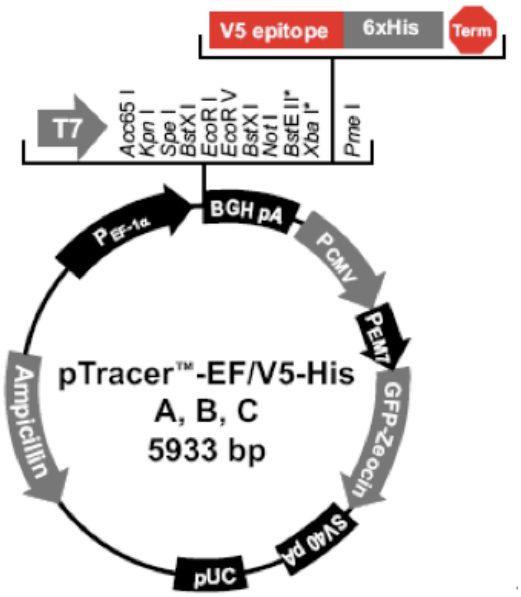

Figure 16. Schematic diagram of pTracer-EF/V5-His mammalian expression vector. (Invitrogen)

The best method for protein expression was the third one, when we changed the cell line and also chose a different expression vector. Instead of using adherent mammalian cells (e.g. HEp-2 or LLC-MK2) we used a suspension adapted mammalian cell line, FreeStyle 293-F from Invitrogen, which grows in serum-free culture medium, and allows high level of protein expression. The optimized full-length F and FΔTM gene was cloned into pcDNA3.1/*myc*-His expression vector (Invitrogen) with C-terminal *c-myc* epitope and 6xHistidine tag (**Figure 17**). We found that the peak of expressed FΔTM protein production was 96 h post-transfection and protein was detected mostly in the culture media and smaller amount in the cell lysate. For structural and biochemical analyses this F protein construct has been studied and all experiments detailed in the following sections used FΔTM protein expressed with the pcDNA3.1-FreeStyle 293-F expression system.

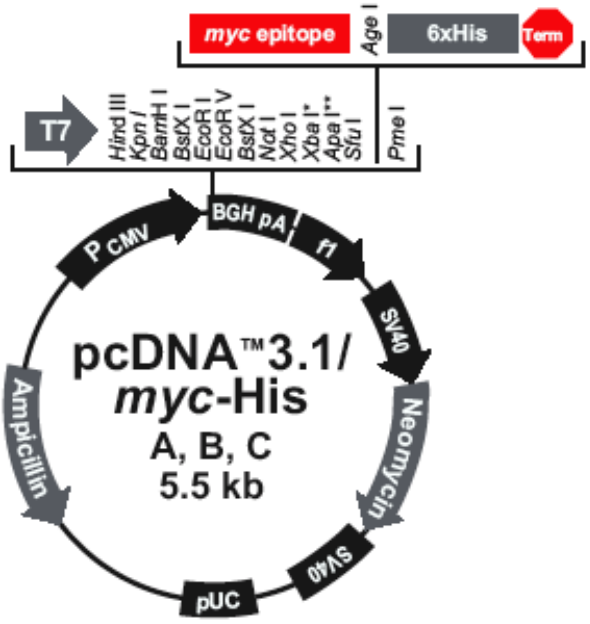

Figure 17. Schematic diagram of pcDNA3.1/*myc*-His expression vector. (Invitrogen)

Since the FreeStyle 293-F expression medium is a serum-free medium, purification of the expressed FΔTM protein was done from the culture media by using immobilized metal ion affinity chromatography. The 6xHistidine tag at the C-terminus of the construct has high affinity to nickel (Ni^{2+}) ions immobilized on a Sepharose column. We used HisTrap 1ml or 5ml Nickel-Sepharose columns (GE Healthcare) operated either with syringe or with ÄKTAdesign automated FPLC system.

2.2. Materials and Methods

Vaccinia virus expression system

Cells, viruses, expression vector. BSC-40 cells were maintained at 37 °C and 5% CO_2 in Eagle's MEM medium supplemented with 10% fetal bovine serum. Vaccinia virus (vT7lacOI) was obtained from Dr. Crowe's lab (Vanderbilt University), pVOTE.1

vaccinia vector was obtained from MedImmune Inc., Gaithersburg, MD, and PCR primers were ordered from Invitrogen.

Cloning hMPV F gene into pVOTE.1 vector. The full-length F sequence from isolate TN/92-4 was cut out from pET-11KC vector and ligated with T4 DNA ligase into pVOTE.1 vector between *Nco* I and *BamH* I multiple cloning sites. Ligation reaction was transformed into E.coli DH5α strain, bacteria were plated on LB/Ampicillin plates and colonies were picked, plasmid DNA was purified with QIAprep Miniprep Kit (QIAGEN). DNA sequencing by Vanderbilt DNA Sequencing Core Facility confirmed successful ligation.

Generating recombinant vaccinia virus stock. BSC-40 cell monolayer in T75 culture flask was infected with trypsinized vT7lavOI vaccinia virus ($1.5x10^5$ pfu/ml) and incubated for 2 h at 37 °C and 5% CO_2. Medium was removed, cells were washed with phosphate buffered saline (PBS, Gibco) and cell were transfected with pVOTE.1-F plasmid DNA using Effectene transfection reagent (Qiagen). Infected/transfected BSC-40 cells were incubated for 2 days at 37 °C and 5% CO_2.

Plaque purification of recombinant virus. 2 days post-infection cells were removed from culture flask by scraping and centrifuged at 1800 rpm for 5 min. Old media was discarded and cells were resuspended in 1.0 ml fresh medium. 500 µl infected cells were mixed with 500 µl 0.025 mg/ml trypsin and incubated in water bath at 37 °C for 30 min and vortexed every 5-10 min. Recombinant virus stock was sonicated for 30 sec twice on ice. BSC-40 cell monolayer was infected with recombinant virus stock in 10 fold dilutions for 2 h then overlayed with 2% low melting agarose/selective medium containing: mycophenolic acid (MPA), xanthin, hypoxanthin. Agarose was let stand to

solidify and plates were incubated for 2 days at 37 °C and 5% CO_2. Second agarose layer with 1% neutral red (from 10mg/ml neutral red stock) was overlayed and plates were incubated overnight. Recombinant vaccinia virus plaques were picked on the next day. Cells were trypsinized, sonicated (see above) and plaque purification was repeated two more times with selective medium. Final recombinant virus titer was determined by plaque assay.

IPTG-induced protein expression. BSC-40 cell monolayer was infected with recombinant vaccinia virus containing hMPV F gene in the presence of 2.0 mM IPTG to induce F protein expression. Cell were incubated for 2 days then harvested and lysed. Cell lysate was run on SDS PAGE gel for Coomassie staining and Western blot to test for F protein expression.

Protein expression with pTracer vector

Cells, expression vector, PCR primers, restriction enzymes. LLC-MK2, HEp-2 and 293-T cells were maintained in Opti-MEM medium with 2% FBS at 37 °C and 5% CO_2. Expression vector pTracer-EF/V5-His was purchased from Invitrogen. Restriction enzymes *Kpn* I and *Not* I were purchased from New England Biolabs (NEB). PCR primers were ordered from Invitrogen.

Cloning hMPV F and FΔTM into pTracer vector. Full length F sequence was obtained from isolate TN/92-4 by RT-PCR and sequence optimized by a commercial source (Aptagen). Optimized hMPV F sequence was amplified with forward and reverse PCR primers to introduce *Kpn* I and *Not* I restriction enzyme sites at 5' and 3' ends, respectively. Vector and PRC-amplified F sequence was digested by restriction enzymes

and ligated together using T4 DNA ligase. Ligation reaction was transformed into DH5α E.coli strain, bacteria were plated on LB/Ampicillin plates, colonies containing the pTracer-F plasmid were picked, and plasmid was purified with QIAprep Miniprep Kit (QIAGEN). DNA sequencing at Vanderbilt DNA Sequencing Core Facility confirmed that plasmids contained the F insert and it has been cloned in frame.

Detection of hMPV F and FΔTM. LLC-MK2, HEp-2 and 293-T cells were transfected with the pTracer-F of pTracer-FΔTM constructs using Effectene Transfection Reagent (QIAGEN) as recommended by the manufacturer. 24-48 h post-transfection cells were fixed with 80% methanol and stained with anti-hMPV polyclonal guinea pig serum and Alexa Fluor 568-conjugated goat anti-guinea pig secondary antibodies. Stained cells were examined on a Nikon Diaphot inverted microscope. To detect GFP expression in transfected cells, fixed cell monolayer was irradiated with 400 nm light and cells were analyzed on a Nikon Diaphot microscope and photographed with a Nikon D1000 digital camera For Western blot detection transfected cells were harvested by scraping, centrifuged and supernatant was removed for gel electrophoretic analysis. Cell pellet was resuspended in lysis buffer (50 mM Tris-Cl, 140 mM NaCl, 1.5 mM $MgCl_2$, 0.5% NP-40 and PMSF) and lysed on ice for 15 min. Cells were centrifuged again for 15 min and cell lysate was removed and analyzed with Western blot technique. Mouse anti-polyHistidine monoclonal antibodies and anti-hMPV polyclonal guinea pig serum were used as primary antibodies for Western blot detection.

F expression with pcDNA3.1/myc-His vector

Cells, expression vectors, PCR primers, restriction enzymes. Freestyle 293-F cells were purchased from Invitrogen, and maintained in Freestyle 293 Expression medium at 37 °C and 5% CO_2 in suspension. Cells were continuously rotated on an orbital shaker platform at 125 rpm. pcDNA3.1/*myc*-His B vector was ordered from Invitrogen. PCR primers were ordered from Invitrogen and reconstituted in our laboratory by preparing a 20 μM stock. *Kpn* I, *Not* I, *BamH* I restriction enzymes were ordered from New England Biolabs, *Apa* I from Promega.

Cloning of hMPV F full-length and hMPV F ectodomain. We used RT-PCR to amplify a full-length F sequence from isolate TN/92-4, a prototype A2 lineage strain according to the proposed nomenclature. The forward and reverse primers that were used for PCR amplification are the following: 5'-CAAGAACGGGACAAATAAAAATG-3' and 5'-CTAATTATGTGGTATGAAGCC-3'. The full TN/92-4 F sequence was sequence-optimized by a commercial source (Aptagen) to alter suboptimal codon usage for mammalian tRNA bias, improve secondary mRNA structure and remove AT-rich regions, increasing mRNA stability. The optimized full-length F sequence was cloned into the mammalian expression vector pcDNA3.1 (Invitrogen) to generate the construct pcDNA3.1-F. To generate the hMPV F ectodomain construct (pcDNA3.1-FΔTM) the optimized full-length cDNA of the F gene was PCR amplified with primers 5'-GGAGGTACCATGAGCTGGAAG-3' and 5'-GAAGCGGCCGCTGCCCTTCTC-3' and PCR product was digested and ligated into the KpnI/NotI sites (restriction sites underlined in primer sequences) of vector pcDNA3.1/*myc*-His B (Invitrogen). Ligations were transformed into E.coli strain DH5α competent cells, and plasmids were purified

with the QIAprep Miniprep Kit (QIAGEN). All plasmid constructs were sequenced on an ABI 3730xl DNA Analyzer in the Vanderbilt DNA Sequencing Core Facility to confirm in frame cloning with the C-terminal *c-myc* epitope and polyhistidine (6xHis) tag of the expression vector.

HMPV F ectodomain expression in mammalian cells. The pcDNA3.1-FΔTM recombinant plasmid was transfected into suspension 293-F cells as recommended by the manufacturer (Freestyle 293 Expression System, Invitrogen). Both the cell fraction and the supernatant were assayed by SDS-PAGE and Western blot for FΔTM protein at 24, 48, 72 and 96 hours. At indicated time points post-transfection, cells were centrifuged for 5 min at 100 x g at room temperature and the supernatant and cells harvested separately. Supernatant was additionally filtered through 0.2 μm filters before purification. Cells were lysed in lysis buffer consisting of 50 mM Tris-Cl, 140 mM NaCl, 1.5 mM $MgCl_2$, 0.5% NP-40 and PMSF protease inhibitor cocktail (Sigma).

Purification of 6xHis-tagged F ectodomain. Protein purification was performed on an ÄKTA FPLC system controlled by UNICORN 4.12 software (GE Healthcare). The His-tagged F ectodomain FΔTM was purified by immobilized metal ion affinity chromatography using pre-packed HisTrap Ni-Sepharose columns (GE Healthcare). Sample was diluted with concentrated binding buffer stock to adjust pH, salt and imidazole concentration before purification. Protein was loaded on a 5 ml HisTrap column with a loading flow rate of 5.0 ml/min, and the binding buffer contained 20 mM sodium phosphate, 0.5 M NaCl, 30 mM imidazole (pH 7.4). Wash and elution protocols were extensively optimized for imidazole concentration and wash/elution column volumes (data not shown). Unrelated proteins were eluted in Elution Step 1 using 4

column volumes of 6% elution buffer, and the 6xHistidine-tagged F protein was eluted in Elution Step 2 with 4 column volumes of 25% elution buffer. The elution buffer contained 20 mM sodium phosphate, 0.5 M NaCl, 500 mM imidazole (pH 7.4). Purified protein was concentrated and dialyzed against PBS (Invitrogen) through Amicon Ultra centrifugal filters with 30,000 MWCO (Millipore).

Gel electrophoresis, Coomassie staining and Western blot. Purified protein fractions were loaded on NuPAGE 4-12% Bis-Tris Gel (Invitrogen) and run at 200 V constant voltage in MES-SDS running buffer (Invitrogen). Under native conditions protein was loaded on 4-12% Tris-Glycine gel and gel was run at 85 V constant voltage at 4°C. Gels were stained with Simply Blue SafeStain (Invitrogen) or Silver Stain Plus (Bio-Rad) to visualize protein bands. For Western blot analysis, separated protein bands were transferred to Invitrolon PVDF membrane (Invitrogen) at 30 V for 1 h. After blocking with 5% milk in Tris-buffered saline with 0.05% Tween-20 (TBS-T), membranes were incubated with anti-polyhistidine mouse monoclonal antibody (Sigma) and anti-hMPV polyclonal guinea pig serum at a 1:500 dilution. Anti-hMPV guinea pig serum was generated in our laboratory as described by Williams et al[38]. Membranes were washed with TBS-T and incubated with horseradish peroxidase-conjugated goat anti-mouse or goat anti-guinea pig secondary antibodies (Southern Biotech). Membranes were again washed with TBS-T and developed with TMB Membrane Peroxidase Substrate (KPL).

Immunofluorescent detection of expressed F protein. LLC-MK2 cell monolayers were transfected with pcDNA3.1-F recombinant plasmid by using TransFectin Lipid Reagent (Bio-Rad). At 24 h after transfection cells were fixed with 80% methanol,

washed with PBS-T then incubated with anti-hMPV polyclonal guinea pig serum in PBS-T/milk (1:500 dilution) for 1 h at 37 °C. After washing with PBS-T, cells were stained with AlexaFluor568-conjugated goat anti-guinea pig Ig or AlexaFluor568-conjugated goat anti-rat Ig antibody (Molecular Probes) in PBS-T/milk for 1 h at 37 °C. Monolayers were examined on an inverted Nikon Diaphot microscope and images captured with a Nikon D1000 digital camera.

2.3. Results

We generated recombinant vaccinia virus stock and passaged plaque-to-plaque three times to ensure clonality. Infected cell lysate was analyzed by Western blot technique using anti-hMPV polyclonal guinea pig serum as primary antibody. hMPV F expression was minimal in infected BSC-40 cells even at the highest (2.0 mM) IPTG concentration, as detected by Western blot (data not shown). Cell viability was low in MPA-containing selective medium, which may have been one reason for low protein expression.

The sequence optimization strategy was undertaken to enhance expression of hMPV F in mammalian cells. The codon-optimized F sequence was expressed in moderate amounts when cloned into pTracer plasmid and transfected into adherent mammalian cells (293-T, HEp-2, LLC-MK2). We successfully detected it with anti-hMPV guinea pig serum by immunofluorescence (**Figure 18 B)** or Western blot (data not shown). Transfection efficiency has been monitored by GFP expression in transfected cells upon irradiation with 400nm light, as shown in **Figure 18 A**. While the full-length F protein was localized in the cell membrane, FΔTM ectodomain was detected mostly in the membranes of cellular compartments (ER, Golgi) in the cytoplasm.

In contrast, the sequence-optimized construct in pcDNA3.1 vector was expressed at high levels when transfected into LLC-MK2 cells. Furthermore, full length F protein was detected by immunofluorescence in a membrane distribution similar to that observed in hMPV-infected cells. The predicted molecular weight of the full-length hMPV F protein based on the nucleotide sequence is 58 kDa, the F ectodomain, without the transmembrane and cytoplasmic regions, is 56 kDa. The supernatant of transfected 293-F cells has been purified in 2 steps with different imidazole concentrations in the elution buffer. In the first elution step unrelated proteins have been eluted off the column, using 30mM imidazole concentration. In the second step hMPV FΔTM has been eluted with 125mM imidazole concentration in the binding buffer.

SDS-PAGE and immunoblot analysis of pcDNA3.1-FΔTM–transfected 293-F cells showed that the hMPV F ectodomain (FΔTM) was present in the medium rather than the cell lysate. After affinity purification with HisTrap column FΔTM protein was highly pure as determined by Coomassie blue and silver staining of SDS-PAGE gels (**Figure 19 A**). Denaturing, non-reducing SDS-PAGE and immunoblot analysis of transfected cells showed that the majority of the hMPV F protein was detected as a monomer (**Figure 19 B, C**), and both mouse anti-polyHistidine monoclonal antibody (Sigma) and our anti-hMPV polyclonal guinea pig serum detected the protein on Western blot. Under native, non-denaturing conditions F protein has been detected as trimer or higher size oligomers (**Figure 20**) and under reducing conditions (**Figure 21**) it has been detected as a monomer, which is cleaved into F1 (approx. 45 kDa) and F2 (11 kDa) subunits.

A)

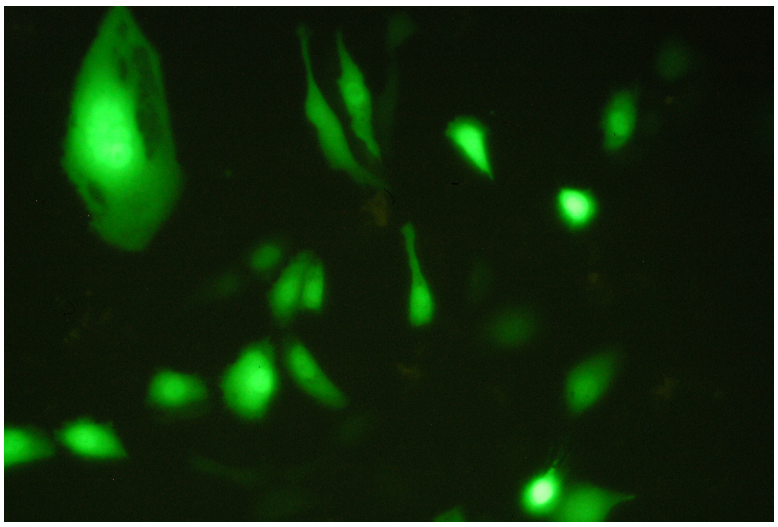

B)

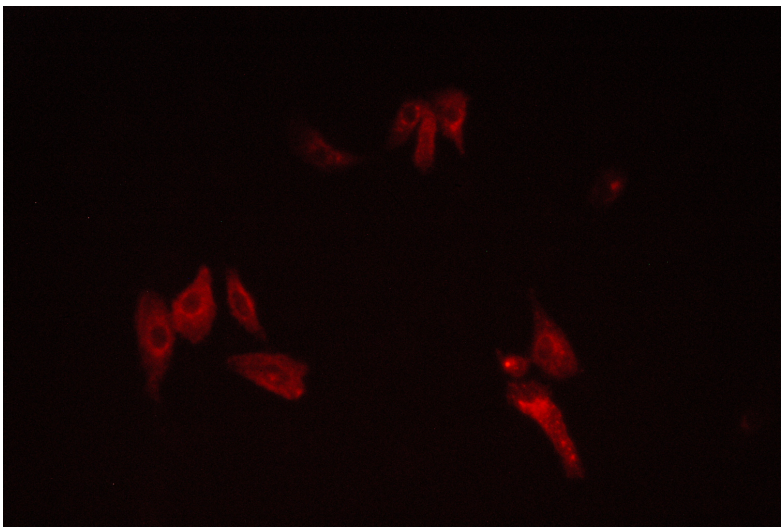

Figure 18. HMPV FΔTM expression in LLC-MK2 cells using pTracer expression vector. A) Transfection efficiency was monitored by Green Fluorescent Protein (GFP) expression. B) Immunofluorescence detection of hMPV FΔTM. LLC-MK2 cells are stained with polyclonal anti-HMPV guinea pig serum. Pictures were taken on an inverted Nikon Diaphot microscope with a Nikon D1000 digital camera.

Figure 21 shows a picture of hMPV FΔTM on a Coomassie blue stained 4-12% SDS gel. The picture has been taken at Oak Ridge National Laboratory (ORNL) before and after a Small Angle X-ray Scattering (SAXS) experiment. F1 and F2 subunits can be detected under reducing conditions (lanes 2 and 4). In lane 4 (after SAXS) a fragment with 38 kDa size appeared on the gel, possibly the result of protein degradation during the experiment. The antiserum we used to detect recombinant F protein in both immunofluorescent and immunoblot assays was generated previously by infecting guinea pigs with live hMPV. F protein was also detected with both immunofluorescent and immunoblot assays by human serum with an hMPV-neutralizing titer of 1:640 (data not shown).

Appendix A shows a sample chromatogram and method section of the two-step purification process with the UV absorbance of the loaded sample, wash and eluted fractions. We used 1ml or 5 ml HisTrap columns depending on the original sample volume with 1.0ml/min or 5.0ml/min sample loading flow rate, respectively. After the supernatant containing F protein has been loaded on the column (X1-X6 fractions), unbound sample was washed off with 2-column volume binding buffer (20mM imidazole). Then 4-column volume of elution buffer with 30mM imidazole was used to elute unrelated protein in fractions A1-A2 (first elution step). Another 4-column volume of elution buffer with 125 mM imidazole content eluted hMPV F corresponding to an increase in the UV signal in fractions A3-A4 (second elution step).

A)

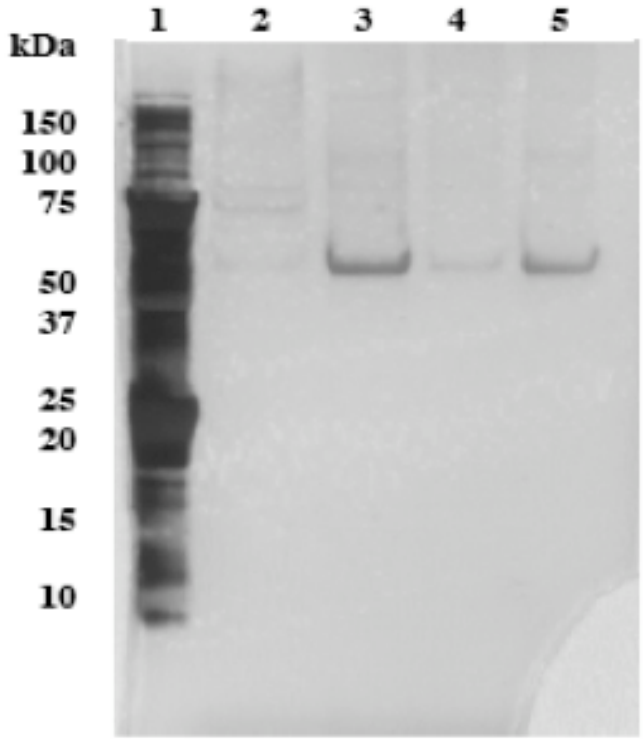

B)

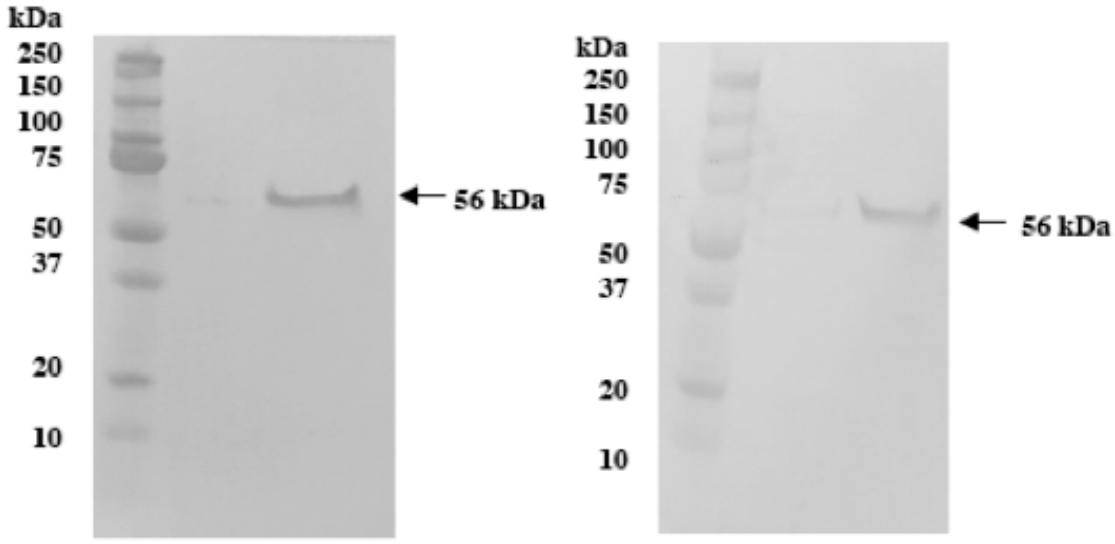

Figure 19 Purified FΔTM under denaturing, non-reducing conditions. F protein band is a monomer with 56 kDa MW. A) Silver stained Bis-Tris 4-12% SDS gel, Lane 1: MW marker, lane 2: original supernatant, lane 3: purified protein fraction, lane 4: flow-through after filtration with a 50 kDa MWCO filter, lane 5: final protein fraction. B) Western blots of FΔTM with anti-polyHistidine and anti-hMPV antibodies, respectively.

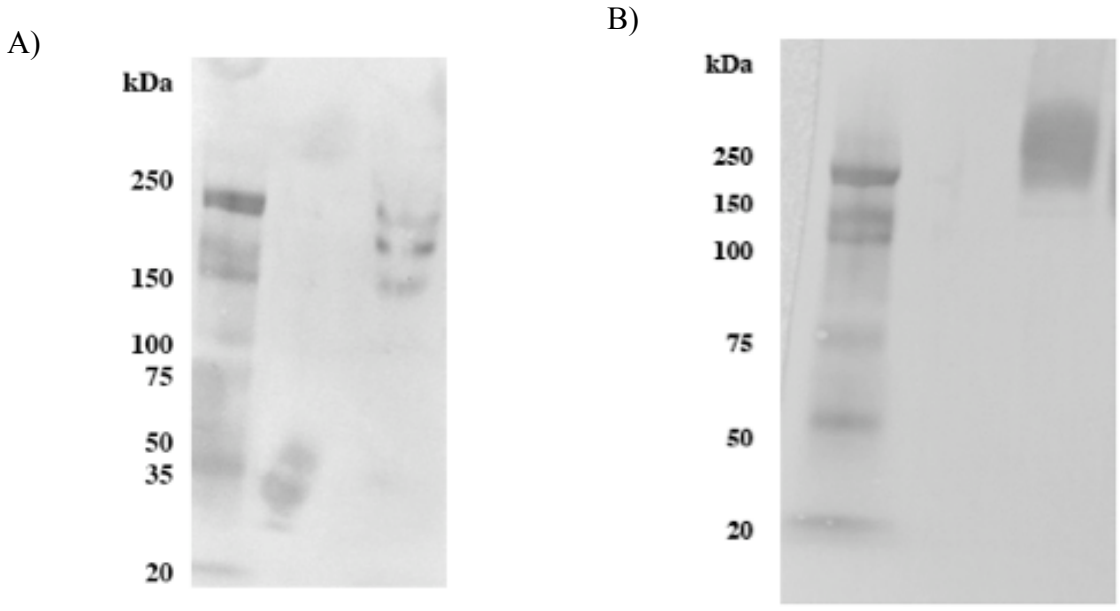

Figure 20. Purified FΔTM under native conditions. A) Diluted and B) undiluted purified protein loaded on Tris-Glycine gel. Diluted protein has multiple bands in the range of 120 kDa-250 kDa suggesting different oligomeric forms. Undiluted protein band shows a 250 kDa highly aggregated state. No monomer was detected. Anti-polyHistidine monoclonal antibody has been used for Western blot detection.

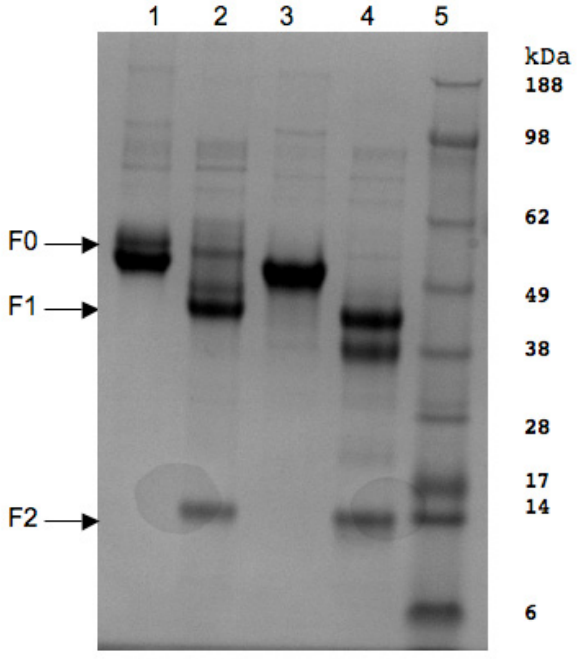

Figure 21. FΔTM under denaturing conditions. Lanes 1 and 3: denaturing, non-reducing, Lanes 2 and 4: denaturing, reducing conditions (F1 and F2 subunits). Picture was taken by Kevin L. Weiss (ORNL) before (Lanes 1, 2) and after (3, 4) SAXS experiment.

2.4. Discussion

We tried several different strategies to produce hMPV F glycoprotein in mammalian cells. Other paramyxovirus recombinant fusion proteins (e.g. hPIV-3 or SV5 F protein) were previously expressed in insect cells using the baculovirus expression system[28, 35] or the IPTG-induced vaccinia virus system.

For us the most successful method was when the codon-optimized sequence of hMPV F ectodomain was cloned in pcDNA3.1/*myc*-His expression vector and expressed in 293-F suspension adapted mammalian cells. FΔTM was secreted in a soluble state and could be detected as a 56 kDa monomer under denaturing conditions. The protein was cleaved and F1 and F2 subunits were detected under reducing conditions, as it was expected based on the position of the predicted putative cleavage site and the sequence homology with other paramyxovirus F proteins. Successful fusion of the paramyxovirus membrane with the host cell requires cleavage activation of the F protein[1, 28]. Following activation, the hexameric core is formed through conformation changes and the fusion peptide is inserted into the target membrane. The cleavage activation in the hMPV F construct makes all these changes possible, and suggests that our protein is capable for the conformation change necessary for fusion.

It is likely that the truncated ectodomain does not form a completely stable trimer and the results of our purification optimization strategy support this hypothesis. Gel electrophoresis results showed that under native, non-denaturing conditions multiple bands could be detected, which suggests that the protein is expressed as a mixture of multiple oligomers. The predicted molecular weight of an FΔTM trimer is 168 kDa, yet the majority of the purified protein could be passed through a 100,000 molecular weight

cut-off membrane with little retention (data not shown). These results suggest that while FΔTM is capable of forming trimers, trimerization may be a concentration-dependent equilibrium, where a highly concentrated protein stock would form more trimers and less dimers or other oligomers. Optimizing salt and detergent concentration or choosing different protein storage buffer that may reduce protein aggregation and promote trimer formation could be another strategy to produce stable trimers.

Also, the transmembrane domain and cytoplasmic tail might have a stabilizing effect on trimer formation, but since they were removed in order to generate a soluble protein, FΔTM might be unable to trimerize without the TM region. The same problem was reported in case of HIV gp41[22-25], SV5 F[35] or hPIV-3 F[28] ectodomains. To solve this issue a variety of trimerization domains were introduced in the fusion protein ectodomain constructs to help trimer formation. In further studies an hMPV FΔTM construct fused with a trimerization domain (e.g. GCNt or T4 bacteriophage Fibritin)[24, 25] might form more stable trimers.

The overall quality, yield and purity of our hMPV F construct were comparable to the previously reported recombinant paramyxovirus fusion protein constructs. The yield of protein expression was similar to the yield that could be achieved with baculovirus expression. Affinity purification using the 6xHistidine tag gave us reasonably pure protein stock, although further purification techniques (e.g. size exclusion or ion exchange chromatography) could be use to improve protein purity. We could also utilize the *c*-myc-epitope attached to the C-terminal end of our construct for purification or protein detection purposes.

The hMPV F ectodomain was detected by immunofluorescence and immunoblots using guinea pig antiserum generated by infection with live virus, and by human convalescent serum. These results suggest that FΔTM may be conformationally intact or it retains at least some of the epitopes that are present in the native viral protein and are important for antigen-recognition by hMPV-specific antibodies. The current hMPV FΔTM construct could be a good subject for epitope mapping experiments and/or to generate neutralizing or non-neutralizing anti-hMPV monoclonal antibodies. Furthermore, because of the antigenic epitopes presented on FΔTM, it is a valuable reagent for serological testing, such as enzyme-linked immunosorbent assay (ELISA) to detect hMPV infection sensitively and specifically.

The same overall strategy of recombinant protein expression that we developed for hMPV F and similar affinity purification methods can be applied to produce other transmembrane proteins. In our lab we also successfully expressed and purified RSV F, hMPV G protein and influenza HA ectodomain, but the cloning, expression and purification steps have been optimized for each protein specifically.

CHAPTER III

STRUCTURAL CHARACTERIZATION OF HMPV FUSION PROTEIN

3.1. Introduction

Sequence analysis of hMPV F using algorithms such as LearnCoil-VMF, MultiCoil or PairCoil gave some insight to the predicted secondary structure of the fusion protein. Based on the predicted helices, homology models and scoring matrix results, which aligned and compared F protein sequences from 12 paramyxoviruses to the hMPV F sequence, Scott Miller[39] at the Department of Chemistry at Vanderbilt University identified the heptad repeat fusion core in hMPV F and synthesized 21-mer short, overlapping peptides from the 43-mer (residues 130-172) HR-1 and 33-mer (454-486 residues) HR-2 regions. CD spectrum of HR-1 peptides in PBS showed a lack of helical structure, which was surprising, since HR-1 peptides from other viral fusion proteins had significant α-helical content. Adding trifluoroethanol (TFE) to the original phosphate buffer to induce helix formation resulted a strong signal in the helical spectrum. HR-2 peptides displayed little secondary structure by CD spectroscopy, which was consistent with previous reports from other viral fusion cores. However, CD spectrum of an equimolar mixture of HR-1 and HR-2 peptides following a freeze/thaw cycle revealed a significant increase in the α-helical content suggesting that HR-1 and HR-2 peptides indeed form the putative coiled coil secondary structure. Thermal stability and melting experiments of the synthetic heptad repeat fusion core gave a T_m ~ 90 °C, which is consistent with the previously reported T_m of RSV hexameric core (88 °C). It has been

previously shown that peptides synthesized from other viral fusion protein heptad repeat cores have potent inhibitory effects on viral propagation and fusion. Miller showed that HR-2 peptides inhibit viral growth with an EC_{50} ~ 165 nM. Surprisingly, HR-1 peptides also showed inhibitory effect and it was at least 1000 times more potent (EC_{50} ~ 46 nM) than the previously reported HR-1 peptides from other paramyxoviruses.

Gel electrophoretic results and Western blots of the purified F ectodomain showed that hMPV F protein forms oligomers under native, non-denaturing conditions, which fall apart into monomers in denaturing gel. We also found out that the protein is cleaved, and F1 and F2 subunits are present in the structure. However, we had no information (other than the synthetic HR-1/HR-2 peptide results) about the protein secondary structure, the presence and positions of α-helices and coiled coils. Based on the amino acid sequence we found 14 cysteines in the protein, but we did not know if they all form disulfide bonds and what the bonding pattern looks like. N-glycosylation site-predicting algorithms (e.g. NetNGlyc 1.0 Server by CBS) found 3 potential N-glycosylation sites based on the Asn-Xaa-Ser/Thr triplet. Furthermore, guinea pig and human anti-hMPV polyclonal serum recognized the F ectodomain by immunofluorescence and on immunoblots, but we needed information about hMPV-specific monoclonal antibody affinity to F and the kinetics of antibody-antigen binding.

In this chapter we show several methods and results that help to understand the structure of hMPV F protein. For all experiments we used our purified hMPV F ectodomain expressed in 293-F mammalian cells. To determine the secondary structure of the protein and α-helical content we used circular dichroism (CD) spectroscopy. Surface plasmon resonance (SPR) method was used to analyze monoclonal antibody-

hMPV F binding and kinetics. N-glycosylation sites were identified by enzymatic digestion and site-directed mutagenesis studies. Cysteines and disulfide bonding pattern was analyzed by labeling the cysteine residues with different alkylating agents, enzymatic digestion with trypsin and chymotrypsin were performed and the bonding pattern was analyzed by Dr. Amy Ham at the Mass Spectrometry Research Center at Vanderbilt University. Some of these results are not complete, and further studies are necessary to get closer to understand the structure of hMPV F protein.

3.2. Circular dichroism spectroscopy, surface plasmon resonance

The far-UV protein spectrum (190-240 nm) measured by circular dichroism (CD) spectroscopy is sensitive to the overall secondary structure of the protein. It measures the absorbance difference by the sample between the right-handed and left-handed circularly polarized light. The method is sensitive to chirality and asymmetry around the chromophores in the sample. By spectral fitting one can estimate the percentage of α-helix, β-sheet and random coil in the sample. The near-UV (240-340 nm) CD spectrum doesn't have direct structural interpretation; it is sensitive to the local tertiary structure around aromatic residues and disulfide bonds. To characterize the hMPV F secondary structure we measured the far-UV absorbance of the sample by CD spectroscopy and analyzed the thermal stability of the protein.

Surface plasmon resonance is a label-free technology to study biomolecular interactions and binding events. In BIAcore systems (BIAcore, Uppsala, Sweden), SPR is used to monitor interactions occurring in a biospecific surface, on a gold-coated sensor chip, where the surface is modified with a carboxymethylated dextran layer. The protein

(or other molecule) of interest is immobilized on the dextran surface and constant concentration of analyte(s) pass(es) over the sensor surface in a controlled, pulse-free flow. Binding events, association and dissociation rates are determined by detection of mass changes in the aqueous layer close to the sensor chip surface by measuring the changes in the refractive index. Since SPR provides quantitative information in real time on specificity of binding, kinetics and affinity, we used this method to study hMPV-specific monoclonal antibody binding to purified hMPV F ectodomain.

Materials and Methods

CD spectroscopy. Purified hMPV F ectodomain stock was diluted to a 150 µg/ml concentration in phosphate buffered saline (PBS, Gibco) at pH=7.4, and CD spectra were collected on an Aviv 215 CD spectrophotometer over the wavelength range of 190 and 260 nm at 25 °C with a resolution of 0.5 nm and bandwidth of 1.0 nm. For thermal stability the spectrum was measured at the same wavelength range with variable temperature control at every 5°C in the temperature range of from 25 to 100 °C. Sample was analyzed in a 300 µl stain-free quartz cuvette with 1 cm path length.

SPR-BIAcore. The interaction between hMPV-specific monoclonal antibodies with hMPV F protein was monitored using surface plasmon resonance on a BIAcore 2000. HMPV-specific human monoclonal Fab generated by combinatorial phage display technology was obtained from R. Anthony Williamson (Scripps Research Institute, La Jolla, CA); hamster monoclonal IgG was kindly provided by Nancy D. Ulbrandt (MedImmune, Gaithersburg, MD); Purified RSV F ectodomain and anti-RSV monoclonal antibody (Palivizumab) was obtained from Chris Keefer in Dr. Crowe's lab

at Vanderbilt. Purified recombinant hMPV F and RSV F protein were diluted to 30 μg/ml in 10mM sodium acetate, pH 4.5, and covalently immobilized at 5 μl/min by amine coupling to the dextran matrix of a CM5 sensor chip (BIAcore) with an aimed RU density of 1200. Unreacted active ester groups were blocked with 1 M ethanolamine. For use as a reference, a blank surface, containing no protein, was prepared under identical immobilization conditions. Purified hMPV F antibodies and RSV-specific monoclonal antibody (Palivizumab), were injected over the immobilized hMPV F protein, RSV F protein, and reference cell surfaces at concentrations ranging from 5 to 500 nM in HBS/Tween 20 buffer (BIAcore). Antibody binding was measured at a flow rate of 30 μl/min for 180 seconds and dissociation was monitored for an additional 360 seconds. Residual bound antibody was removed from the sensor chip by pulsing 50 mM HCl at 100 μl/min for 30 seconds. Ka, kd, and KD was determined by globally fitting the binding curves to fit a 1:1 Langmuir binding model using the BIAevaluation software.

Results

The CD spectrum of purified F ectodomain indicated a predominant α-helical secondary structure. (**Figure 22**) This was not surprising, since it has been shown previously that the mixture of synthetic HR-1 and HR-2 peptides had similar curve with negative ellipticity (with double minima at 208 and 222 nm) characteristic of the α-helical content. The protein concentration was 150 μg/ml; protein stock with higher concentration gave inconsistent results, probably because of protein aggregation. Although these data suggest that the protein is folded correctly and it contains the coiled

coil fusion core with dominant α-helices formed by HR-1 and HR-2 regions, it is still not known whether the protein is in its pre- or post-fusion state, in an intermediate form between the pre-and post-fusion state or in an artificial (but α-helical) conformation that was the result of our expression method and purification process.

The thermal stability curve of the protein, however, did not give an exact melting temperature (T_m); the protein has been melted continuously in the temperature range of 50-100 °C resulting an almost linear melting curve (data not shown). This was unexpected based on the previous HR-1/HR-2 synthetic peptide results, since they showed a very high, distinct melting point at about 90-95 °C. Our different melting data might be the result of the complexity of the whole protein, the instability of the trimers and the effects of the side chains, subunits, folding and storage buffer.

SPR-BIAcore studies indicated that hMPV-specific Fab and hamster monoclonal IgG both bind to hMPV F ectodomain, but RSV-specific Palivizumab does not. **Figure 23 A** shows the binding curve of anti-hMPV Fabs to hMPV F (The original measurements and fitted curves are shown in **Appendix B**). The binding curves at different antibody concentrations were fitted with a 1:1 Langmuir binding model. The BIAevaluation software determined the values of ka, kd and KD. In contrast, **Figure 23 A** shows that Palivizumab, which is an anti-RSV monoclonal antibody did not bind to hMPV F at all, not even at 100 nM concentration. We tested the binding ability of Palivizumab to RSV-F (data not shown), and it exhibited strong, specific binding, so the lack of binding to hMPV F was the result of specificity and related to the quality of the antibody.

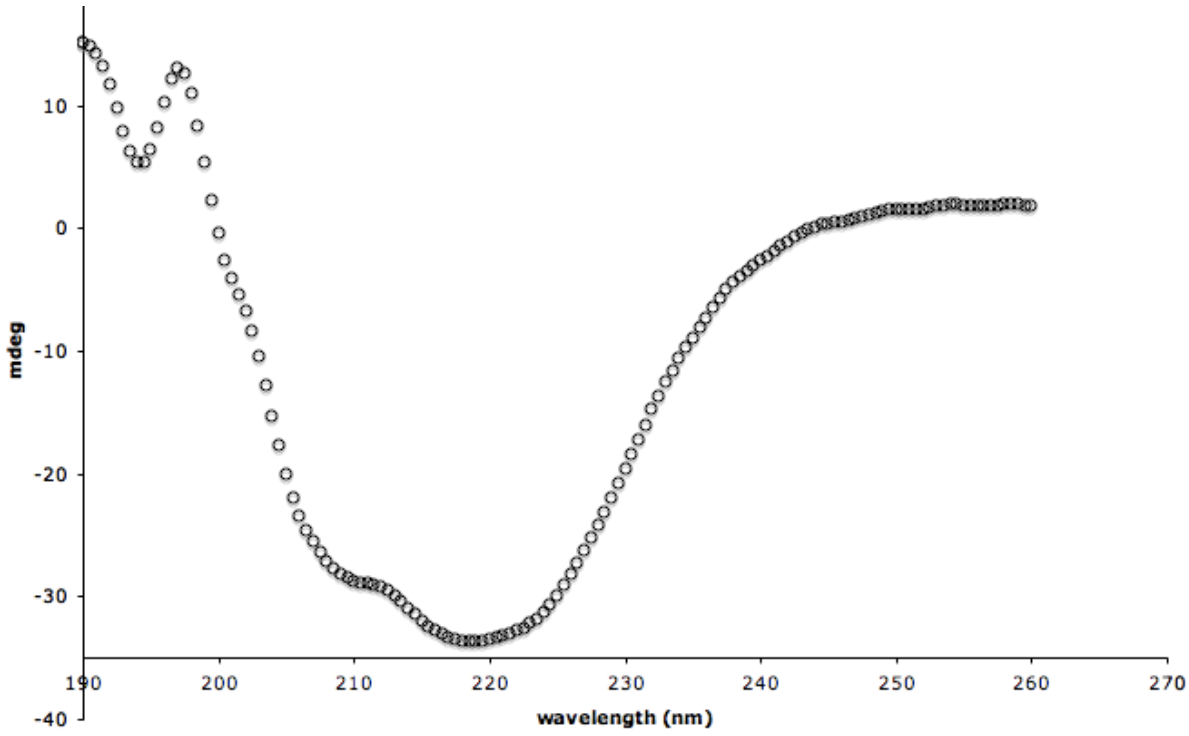

Figure 22. CD spectrum of hMPV F ectodomain shows predominant α-helical secondary structure. Spectrum was collected from a 150 µg/ml protein stock in PBS at 25 °C.

Our anti-hMPV human monoclonal Fabs had specific affinity to hMPV F as indicated on **Figure 23 B**. It shows that the Fab at 50 nM concentration binds to hMPV F, but it has no affinity to RSV F protein. Values of ka, kd and KD were calculated by the fitted curves based on the association and dissociation rates. For the anti-hMPV human monoclonal Fab ka = $3.54e^{5}$ (1/s), kd = $3.48e^{-4}$ (1/s) and KD = $9.84e^{-10}$ (M). These values suggest a strong, specific antibody-antigen binding, and we got similar results for the full-length hamster monoclonal antibodies with a ka = $1.01e^{5}$, kd = $8.65e^{-4}$ and KD = $8.56e^{-9}$ (M). For the human Fab we also found that it had significant neutralizing activity, with a neutralizing concentration of 1.1 µg/ml. So, this antibody specifically binds to a

neutralizing epitope on the protein surface. The hamster IgG did not have high neutralizing activity, but the strength of antibody-antigen binding was similar to that of the Fab.

The antibodies were generated with different techniques and we received them from two distinct sources, and both showed specific binding to hMPV F ectodomain, which proves that our antigen retains at least some of the antigenic epitopes that are important in antigen-antibody recognition, binding and for some, virus neutralization. By detailed epitope mapping studies using the SPR-BIAcore method we could further test these antibodies (and others) in a pair-wise/competitive manner to see if they bind to the same epitope or to independent antigenic sites on the protein surface. This technique can also give some insight to the surface topology and steric interactions on the surface of the antigen, which comes from the secondary structure of the protein and the conformation of surface residues.

The strong binding of these antibodies to hMPV F offers another approach for us to determine the protein structure. Since purification and crystallization of Fab fragments are relatively easy and substantial improvements in the methodologies helped to crystallize and determine Fab structures and also the structure of Fab-antigen complexes, we could use the strong binding of human Fabs to hMPV F to co-crystallize the antibody-antigen complex. Fab might help stabilizing the crystals and we could get structural information not only about the protein itself, but the detailed structure of the epitope that serves as a place for specific, neutralizing antibody binding.

A)

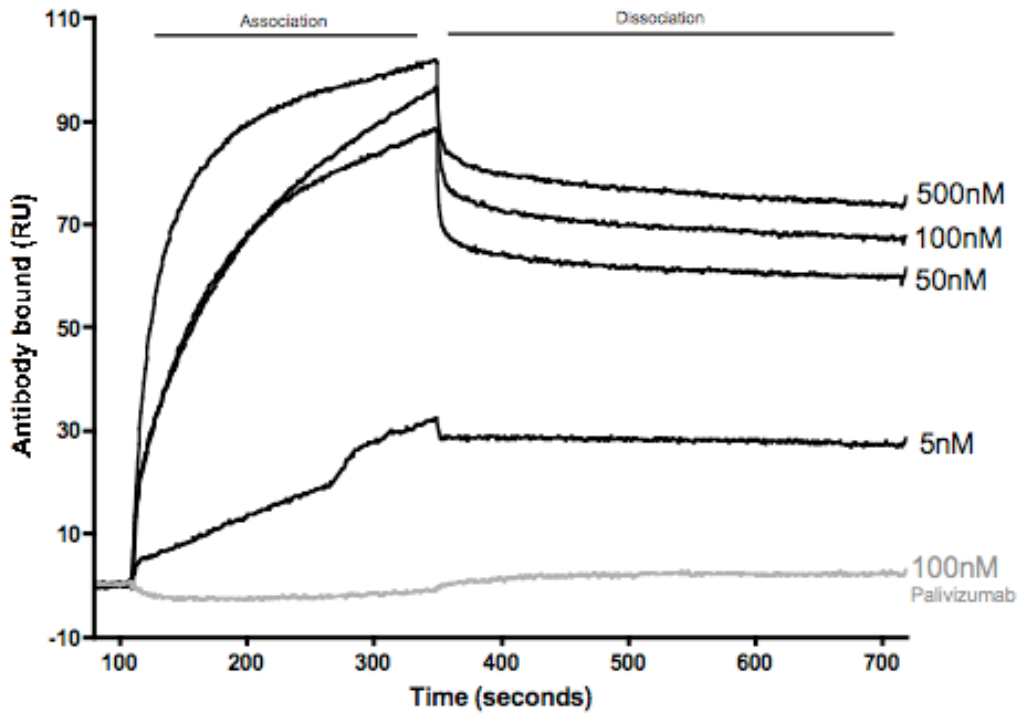

B)

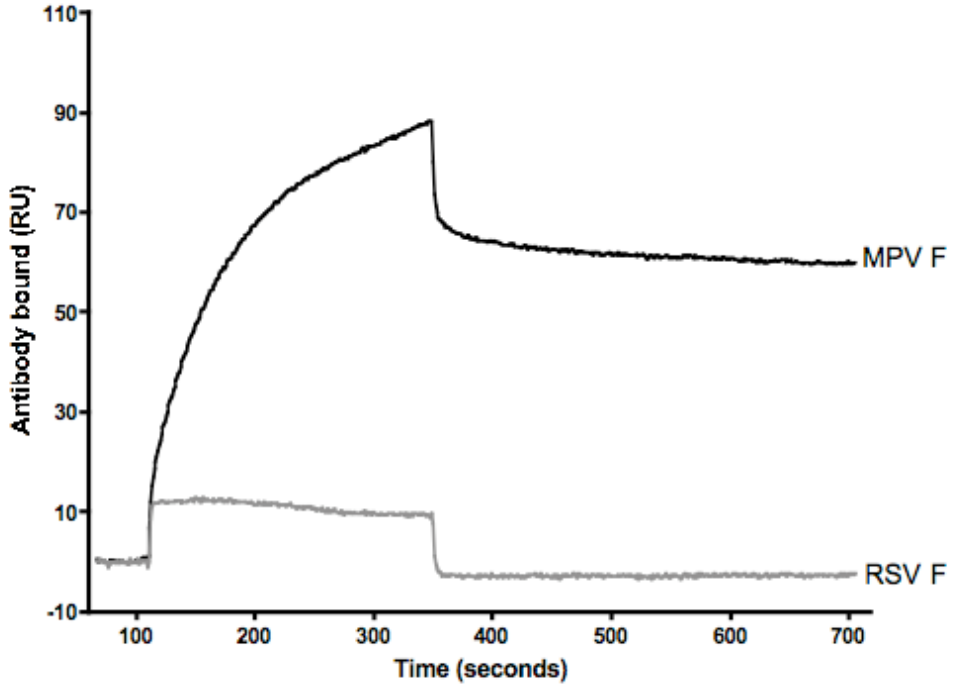

Figure 23. SPR-BIAcore kinetic analysis of anti-hMPV human monoclonal Fab binding to hMPV F ectodomain. **A)** HMPV-specific Fab (5-500 nM) binds to hMPV F ectodomain immobilized on CM5 sensor chip. 100 nM Palivizumab did not show binding. **B**) Anti-hMPV Fab (50 nM) binds specifically to hMPV F, but not to RSV F.

3.3. N-glycosylation, site-directed mutagenesis

Glycosylation is a post-translational modification by carbohydrates that are attached to different amino acid side chains. O-glycosylated proteins have oligosaccharides at Thr and Ser residues, C-glycosylation means sugar chains are attached on Trp residues and N-glycosylated proteins are modified at the Asn residue of the consensus sequence Asn-Xaa-Ser/Thr (where Xaa can be any amino acid except Pro)[40]. The translation of mRNAs of membrane-bound or secretory proteins is initiated on membrane-bound ribosomes. The growing polypeptide chain is co-translationally translocated across the ER membrane via Sec61 translocon complex. During the process of translocation, the glycosylation sites on the nascent polypeptide chain are glycosylated in the lumen of the ER by a multi-subunit membrane protein complex called oligosaccharyl transferase (OT), so the processes of translocation and N-glycosylation are expected to be coupled events. N-glycans not only determine the folding, transport and translocation[41] of the protein inside the cell, but they also modulate their immunogenicity and antigenic activity. Glycans can shield large portions of the protein surface, providing protection from proteases and masking epitopes. It has been shown that removal of carbohydrates from the protein surface can result a shift in the conformation of the polypeptide backbone, altering the recognition of immunogenic epitope[42, 43]. The role of N-glycosylation in protein function and immune recognition is not very well understood, but several studies have been performed to investigate N-glycans in paramyxoviruses[42-45] and in case of other viruses[46].

The NetNGlyc 1.0 algorithm predicted that hMPV fusion (F) protein has three potential N-glycosylation sites at the positions of N57, N172 and N353. These

asparagines represent conserved residues in all of the hMPV isolates worldwide. To determine N-glycans that are attached to the asparagine residues at these positions we used enzymatic digestion with N-glycosidase F and site-directed mutagenesis to modify the asparagine residues to glutamine. Single, double and triple mutants were generated by changing N to Q either individually or in combinations. All of the mutated plasmid constructs were successfully transfected in 293-F mammalian suspension cell line and mutated proteins were expressed in the culture medium.

Materials and Methods

Site-directed mutagenesis of N-glycosylation sites. N-glycosylation mutants were generated by replacing asparagine (N) residues with glutamine (Q) at positions N57, N172 and N353. Single, double and triple mutants were made by changing only one (N57Q, N172Q, N353Q), two (N57/172Q, N57/353Q, N172/353Q) or all three (N57/172/353Q) N-glycosylation sites, respectively. Combinations of two and three sites were performed in a stepwise manner. QuikChange Site-Directed Mutagenesis Kit (Stratagene, La Jolla, CA) was used to make point mutations at potential glycosylation sites. Sense and antisense PCR primer pairs designed for mutations are listed in **Table 2**. Triplet AAC encoding for asparagine was changed for CAA, which encodes for glutamine in the codon-optimized sequence (changes underlined in the primer sequences). All mutated plasmid constructs were sequenced by the Vanderbilt DNA Sequencing Facility to confirm nucleotide changes.

Table 2. PCR primers designed to generate N-glycosylation mutants.

N57Q	(sense) 5'-GTGGGCGACGTGGAGCAACTGACCTGCAGCGAC-3'
	(antisense) 5'- GTCGCTGCAGGTCAGTTGCTCCACGTCGCCCAC-3'
N172Q	(sense) 5'-AAGGACTTCGTGAGCAAGCAACTGACCAGAGCCATCAAC-3'
	(antisense) 5'- GTTGATGGCTCTGGTCAGTTGCTTGCTCACGAAGTCCTT-3'
N353Q	(sense) 5'- GTGCAACATCCAAATCAGCACAACCAACTACCCC-3'
	(antisense) 5'- GGGGTAGTTGGTTGTGCTGATTTGGATGTTGCAC-3'

HMPV F ectodomain and the N-glycosylation site-mutated protein expression in transfected mammalian cells. The pcDNA3.1-FΔTM recombinant plasmid and mutated plasmid constructs were transfected into suspension 293-F cells as recommended by the manufacturer (Freestyle 293 Expression System, Invitrogen). $1x10^7$ number of cells and 30 μg plasmid were used for each transfection, so the rate of protein expression is comparable. Four days post-transfection cells were centrifuged for 5 min at 100 x g at room temperature, supernatant containing the expressed, soluble protein was removed for purification and further analysis.

Gel electrophoresis, Coomassie staining and Western blot. Procedure was followed as written in 2.2 in Chapter II.

Deglycosylation with N-glycosidase F. To determine the N-glycans that are attached to asparagine residues at the potential glycosylation sites protein was treated with N-glycosidase F (Calbiochem, San Diego, CA). 30 μl of purified protein was heat

denatured at 95 °C for 10 min in denaturation buffer (Calbiochem). After cooling 2.5 µl of NP-40 and 2 µl of N-glycosidase F were added and protein was digested at 37 °C overnight. Migration of protein bands was analyzed on SDS-PAGE gels.

Staining cells on Bartels identification slides. 293-F and transfected cells were centrifuged for 15 seconds, supernatant was removed and cells were resuspended in PBS. One drop of suspended cells were placed on the wells of identification slides, dried and fixed in acetone at -20°C. Slide was placed in humidified chamber and stained with anti-hMPV polyclonal guinea pig serum at 1:200 dilution in phosphate buffered saline with 1% Tween (PBS-T) for 30 min. Slides were incubated in PBS-T for 6 min in a Copeland jar, then dried and stained for 30 min with secondary goat anti-guinea pig antibodies conjugated with Alexa Fluor 568. Washing step in PBS-T was repeated and the slide was finally washed with water. Stained cells were examined in a Nikon Diaphot inverted microscope.

Results

We digested the purified hMPV FΔTM with N-glycosidase F in order to see if the expressed, purified protein contains carbohydrate chains at the potential N-glycosylation sites. Digested protein was loaded on 4-12% SDS gel and run under denaturing, non-reducing conditions (for enzymatic digest the protein already had to be in denatured form, so we couldn't use native conditions). Coomassie blue stained gel, Western blots with anti-*poly*Histidine mouse monoclonal primary antibodies and with anti-hMPV polyclonal guinea pig serum were used to analyze protein digestion. **Figure 24 A, B** shows the Western blot results following N-glycosidase F digestion of FΔTM.

A)

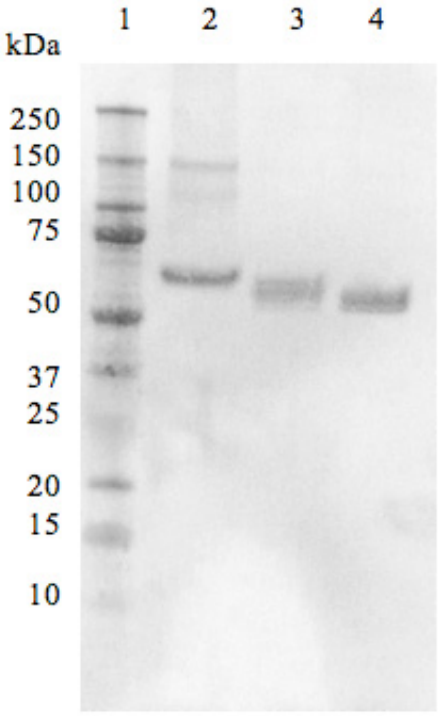

B)

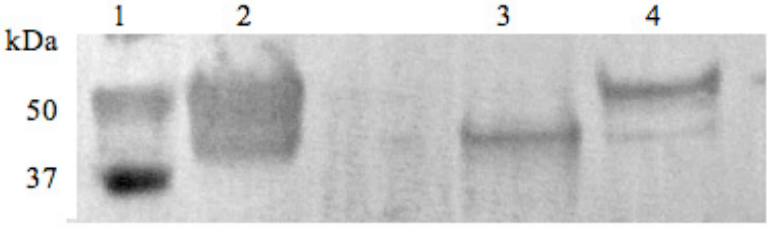

Figure 24. Western blot of hMPV FΔTM digested with N-glycosidase F. **A**) FΔTM is digested with increasing amount of N-glycosidase F. Lane 1: MW marker, lane 2: undigested FΔTM (bands corresponding to possible dimeric and trimeric forms of F are visible), lanes 3 and 4: FΔTM digested with 6 µl and 10 µl of N-glycosidase F, respectively. **B**) Mass difference between the fully aglycosylated and undigested protein. Lane 1: MW marker, lane 2: undigested FΔTM at 0.5 mg/ml concentration, lanes 3 and 4: fully digested, aglycosylated and undigested, diluted protein bands. Note that protein stored in PBS for 1-2 weeks undergoes degradation and looses some of the carbohydrate chains, as can be seen in lane 2 and 4. Anti-polyHistidine mouse monoclonal antibodies were used as primary antibody for Western blot.

Although Western blots of digested FΔTM proved that the protein is glycosylated and we could see the mass difference between the aglycosylated and the undigested forms, enzymatic analysis did not give us information about the glycosylation of the individual N-glycosylation sites and the lengths of the carbohydrate chains attached to the asparagine residues. Expression of mutated F proteins helped to answer these questions.

Plasmids containing N/Q single, double or triple mutations at the positions of N57, N172 and N353 were successfully transfected into 293-F mammalian cells, similarly to the wild type F protein. As a positive control, the original plasmid for FΔTM was used for transfection and protein expression and untransfected cells were the negative control. We used the same amount of plasmid, cell number, and conditions for each transfection. We analyzed the transfected cell lysates as well as the supernatant by gel electrophoresis and immunoblots for protein expression. **Figure 25** shows Western blot results of the supernatant removed from cells transfected with the original FΔTM and the mutated plasmids. All mutated proteins were successfully expressed in the culture media except double mutant N172/353Q and the triple mutant N57/172/353. This was a surprise, although not totally unexpected, since we knew from previous reports that mutations at N-glycosylation sites of other paramyxovirus fusion proteins effect protein transport and expression. Both N172 and N353 residues are in the F1 subunit, so these findings might suggest that for correct protein folding and expression at least one of these glycosylation sites has to be glycosylated. Since both anti-polyHistidine and anti-hMPV antibodies recognized the other mutants, and they don't bind to the same epitope on the protein, lack of detection of these two mutants might be the result of failed protein expression. Interestingly, the analysis of cells lysates showed no difference for the

mutants, protein seemed to be present in the cell lysate by Western blots (data not shown). We also fixed and stained the transfected cells (along with untransfected ones as a negative control) on a slide to show the presence of mutated proteins inside the cell by immunofluorescence. All mutated samples were positive for staining with anti-hMPV polyclonal serum compared to the untransfected control, in which we detected only background fluorescence. The presence of the mutated proteins in the cytoplasm/cellular compartments suggests that protein expression failed somewhere at the transport-folding-secretion steps, since transcription and translation seem to be unaffected by the mutations. However, to prove that transcription is not affected by the mutations, studies using RT-PCR with hMPV F-specific primers would be helpful. In addition, further experiments can be designed to analyze the effects of mutations on protein transport inside the cell, protein translocation in the cellular compartments, folding and modifications of the nascent polypeptide chains and expression of the mutated proteins.

Based on the Western blot results on **Figure 25** one can also notice that the rate of glycosylation and the lengths of the carbohydrate chains are very similar at the individual sites. However, it has to be mentioned that proteins expressed by different cell lines may display completely different arrays of carbohydrates and the site heterogeneity and occupancy might also be affected. Selective labeling, partial digestion of carbohydrates or mass spectrometry analysis could give a more detailed picture about the oligosaccharide chains attached to the individual sites.

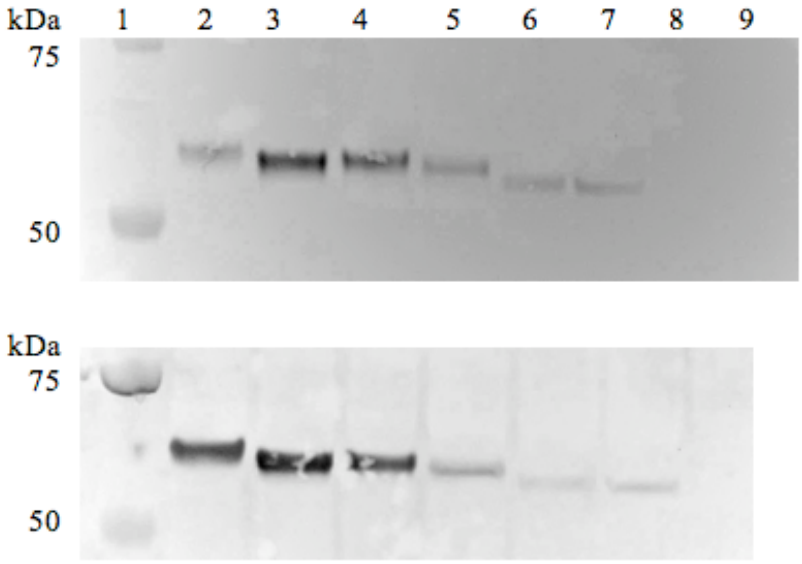

Figure 25. Western blots of FΔTM and mutated proteins. Lane 1: MW marker, 2: FΔTM, 3: N57Q, 4: N172Q, 5: N353Q, 6:N57/172Q, 7: N57/353Q, 8: (N172/353Q, not expressed in the medium), 9: (N57/172/353, not expressed in the medium). For the upper blot the primary antibody was anti-hMPV polyclonal guinea pig serum, the lower was done with anti-polyHistidine monoclonal antibodies.

3.4. Disulfide-mapping, computer models

To solve the structure of hMPV F protein without crystallizing it is a challenging task. There are many tools that one can use to map and characterize the secondary structure of subunits, antigenic sites and important epitopes. Computer models can also help by using the sequence homology, structural and chemical analogy between conserved residues of different viruses. Another useful approach is analytical proteomics. Protein identification is built around the fact that most peptide sequences of approximately six or more amino acids are largely unique in the proteome of an

organism. So, if we can obtain the sequence of the peptide or accurately measure its mass, we can identify the protein it came from[47].

The idea behind our disulfide-mapping experiment is, that if we are able identify and map the disulfide-bonding pattern in hMPV F, we can build a computer model based on previously reported paramyxovirus crystal structures (e.g. NDV, hPIV-3) and modify it according to the actual disulfide bond arrangement. With this approach we could simulate the secondary structure of hMPV F without crystallizing the protein itself.

Disulfide mapping by mass spectrometry is a difficult process, especially for large proteins. The greater the mass, the larger the absolute magnitude of error. Disulfide mapping is hard, but not only because of the size of the polypeptide chain, but also because of the folding and secondary structure of the native protein. We want to map the intact, native protein, without disturbing the original bonding pattern, but some residues might be inside the secondary structure hidden from alkylating and reducing agents and enzymes. Besides the protein secondary structure, post-translational modifications (e.g. cleavage, glycosylation) further complicate assignments based on mass.

Another approach that could be used to map the disulfide-bonding pattern instead of peptide analysis is site-directed mutagenesis experiment. Similar experiments were described previously, such as the mutation of cysteine residues in RSV F protein[48]. However, as we saw earlier in case of hMPV F N-glycosylation mutants, changing important residues in the wild type protein might have effect on protein transport, folding and expression, and some of the mutants could not be expressed at all.

So, we went on with the disulfide mapping process by labeling the cysteine residues with alkylating agents under non-reducing and reducing conditions to find free,

unbound sulfhydryls and disulfide-bonded cysteines. Peptide fragments were generated by enzymatic digestions. We needed peptide fragments, possibly between 6 to 20 amino acid residues, for ideal MS analysis. In order to map the entire sequence with short (but not too short) peptides, we had to use two different proteases: trypsin and chymotrypsin. These widely used enzymes have good activity both in solution and 'in gel' digestion. Trypsin has a characteristic autolysis fragmentation, which appears as by-product of tryptic-digestion protocols and it can serve as a calibration point. Trypsin cleaves proteins after lysine and arginine residues (cannot be followed by proline) and chymotrypsin cuts after tryptophane, tyrosine and phenylalanine residues (unless followed by proline).

Materials and Methods

Protein sample preparation for mass spec analysis, buffers, reagents. Protein stock with ~20 μM concentration was prepared, filtered through a 30 kDa MC regenerated cellulose filter (Millipore) and buffer was exchanged with 50-100 mM ammonium bicarbonate buffer, pH 8.0 To reduce disulfide bonds in the protein 1/10 volume of 50mM dithiothreitol (DTT) was added to the sample and incubated for 20 minutes at 60°C. To label free sulfhydryl groups and the reduced cysteines prior and after reduction by DTT alkylating agents, such as N-ethylmaleimide (NEM) and iodoacetamide (IAM) were used, respectively. Trypsin and chymotrypsin digest of reduced and unreduced sample was performed, as previously described by Manza et al[49].

LC-MS analysis of digested hMPV F ectodomain. LC-MS analysis of the resulting peptides was performed using a ThermoFinnigan LTQ ion trap mass spectrometer equipped with a Thermo MicroAS autosampler and Thermo Surveyor HPLC pump,

Nanospray source, and Xcalibur 1.4 instrument control. The peptides were separated on a packed capillary tip, 100 μm x 11 cm, with C18 resin (Jupiter C_{18}, 5 micron, 300 angstrom, Phenomonex, Torrance, CA) using an inline solid phase extraction column that was 100μm x 6cm packed with the same C18 resin (using a frit generated with from liquid silicate Kasil 1[50]) similar to that previously described by Licklider et al.[51], except the flow from the HPLC pump was split prior to the injection valve. The flow rate during the solid phase extraction phase of the gradient was 1 μL/min and during the separation phase was 700 nl/min. Mobile phase A was 0.1% formic acid, mobile phase B was acetonitrile with 0.1% formic acid. A 95 min gradient was performed with a 15 min washing period (100 % A for the first 10 min followed by a gradient to 98% A at 15 min) to allow for solid phase extraction and removal on any residual salts. After the initial washing period, a 60 minute gradient was performed where the first 35 min was perform a slow, linear gradient from 98% A to 75 % A, followed by a faster gradient to 10 % A at 65 min and an isocratic phase at 10 % A to 75 min. The MS/MS spectra of the peptides was performed using data-dependent scanning in which one full MS spectra was followed by 3 MS/MS spectra.

Data analysis. The data were searched with the Sequest algorithm using a human database created from the Uniref100. Protein matches were preliminarily filtered using the following criteria: if the charge state of the peptide is 1, the xcorr is greater than or equal to 1, the RSp is less than or equal to 5, and the Sp is greater than or equal to 350. If the charge state is 2, the xcorr is greater than or equal to 1.8, the RSp is less than or equal to 5, and the Sp is greater than or equal to 350. If the charge state is 3, the xcorr is greater than or equal to 2.5, the RSp is less than or equal to 5, and the Sp is greater than

or equal to 350. Once filtered based on these scores, all protein matches that had less than two peptide matches were eliminated from the search. Sample preparation, enzymatic digest and data analysis were performed in the Proteomics Laboratory within the Mass Spectrometry Research Center at Vanderbilt University under the supervision of Dr. Amy Ham.

Results

Both the hMPV F protein and the purified ectodomain have 14 cysteines (no Cys in the transmembrane domain and cytoplasmic tail), so in disulfide mapping experiments we could use the purified ectodomain in order to map all the disulfide bonds and cysteine residues that are present in the native protein. The protein was labeled by NEM alkylating agent prior reduction and digest to find the free sulfhydryl groups in the construct. Our results indicate that there are no free cysteines in the protein (although residues that were not accessible to alkylating agents prior reduction and digest because of protein folding and 3D structure would also fall in this category), so presumably all the cysteine residues that we found in the sequence, participate in disulfide bond formation.

Tryptic and chymotryptic digests were used to cover the almost the entire sequence of FΔTM and to get shorter overlapping peptides, since 6-20 amino acid-long peptide fragments are ideal for MS analysis. With the two-enzyme digestion we couldn't find one cysteine (Cys 60). All the other 13 cysteines are covered and identified after reduction and the enzymatic digests. **Figure 26** shows the coverage map following cleavage by trypsin and/or chymotrypsin. Overlapping peptides were identified both by tryptic and chymotryptic digests.

Figure 26. Coverage map of FΔTM digested with trypsin and chymotrypsin. Fragments identified by chymotryptic digestion are in red. Fragments identified by tryptic digestion are underlined. Cys60 (blue) is not covered by the peptides that were identified.

Further mass spectrometry analyses will determine the actual bonding pattern among cysteine residues. Once we know that we will use this information to modify our existing computer model. Previously, Scott Miller at Vanderbilt University generated a computational model of the hMPV F fusion core[39]. He examined the available hexameric crystal structures for similarity with hMPV F heptad repeat regions, and obtained a reasonably good homology model based on the sequence identity of hMPV F with the

RSV F fusion core (50% sequence homology in HR-1 and 35% I HR-2). The overall energy and probability function density values were calculated for each model to isolate the most stable final model (**Figure 27**). Overall, the hMPV fusion core model was consistent with other hexameric cores found in type I viral fusion proteins. Details about the cysteine-bonding pattern will make further refinements in this computer model and take us closer to the real protein structure.

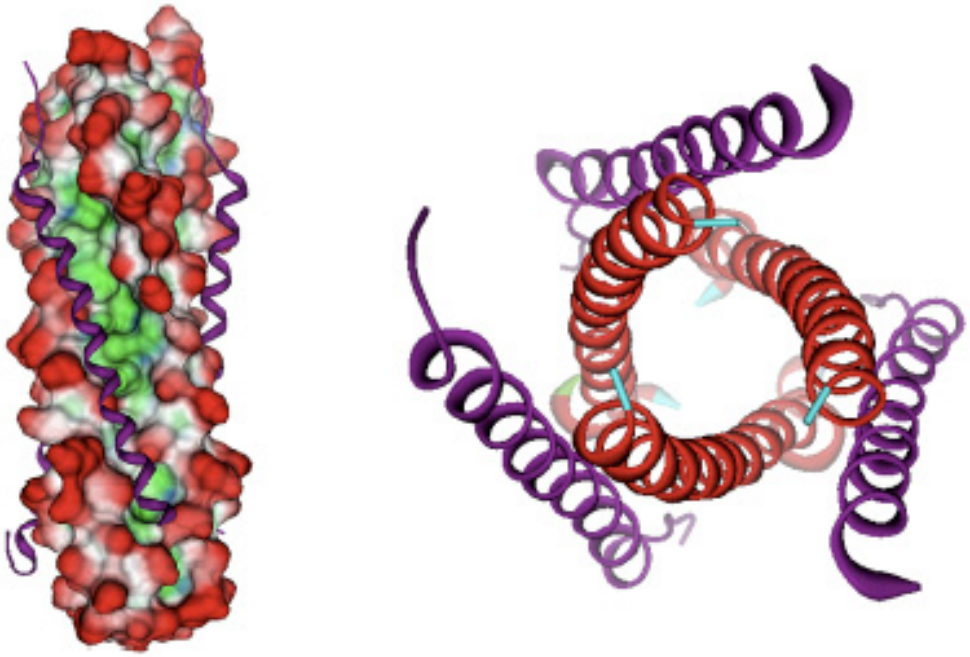

Figure 27. Hexameric fusion core of hMPV F model. The sequence of RSV F fusion core crystal was subjected to a strong local alignment with hMPV F sequence to determine appropriate homology sequences for the hMPV F fusion core model. (Left) The surface of HR-1 trimeric stalk (red: solvent exposed, blue: hydrophilic, green: hydrophobic) with the HR-s (purple ribbon) filling the hydrophobic grooves. (Right) Axial view of the hexameric coiled coil. Adapted from Miller[39].

3.5. Discussion

The results of our structural studies on purified hMPV ectodomain further proved that we successfully generated a recombinant protein by using mammalian expression system that was secreted in a soluble state and forms trimers under native conditions. CD spectroscopy studies showed that the protein retains a dominant α-helical secondary structure. Our results are consistent with the data of other fusion protein hexameric cores found in the literature[29, 31, 52] and also with our synthetic peptide studies[39], although it is the subject of further experiments to find out that this conformation belongs to the pre- or post-fusion form or an intermediate state[35]. According to the fusion model based on hPIV-3 and SV5 F crystal structure, after cellular docking the cleavage activated pre-fusion F protein undergoes a conformation change via a transient pre-hairpin structure, where the fusion peptide gets exposed toward the target membrane and inserts into it. Another series of conformational changes refolds the HR-2 region into an α-helical structure and the formation of the hexameric fusion core in the post-fusion state pulls the target membrane close to the viral membrane, resulting fusion[35]. In case of hMPV F the dominant α-helical structure can be either the pre- or the post-fusion state, although the fact that adding synthetic HR-1 or HR-2 peptides to the F ectodomain did not cause changes in the secondary structure (data not shown) suggests the post-fusion state.

If we talk about the fusion mechanism here, we have to mention the unusual behavior of synthetic hMPV HR-1 peptides in membrane fusion inhibition assays. The postulated mechanism for fusion inhibition by synthetic peptides is that binding of the individual HR-2 peptides to the hydrophobic grooves presented on the surface of HR-1 helical trimers in the pre-fusion or pre-hairpin intermediate inhibits fusion by blocking

the surface from the native HR-2 regions of the protein, so conformation change cannot occur. In case of hMPV F, while HR-2 peptides prevented fusion as predicted by the literature, HR-1 peptides inhibited fusion at least 1000 times more effectively than the previously reported HR-1 peptides from other paramyxoviruses. These findings might suggest that hMPV F protein has different structural properties than other paramyxoviruses or subtle, but distinct differences in the fusion core structure that cause different behavior in fusion inhibition. Although the overall protein structure is probably very similar to other paramyxovirus fusion proteins, we have to be critical in the fine details, because these might have major effects on protein function and its role in the fusion mechanism. Further structural studies on hMPV F probably will focus on the hexameric fusion core and give detailed information about the secondary structure of this important protein region, so it will help us to understand better the structural-functional connections.

Experiments using SPR methods confirmed that our recombinant protein construct presents at least some of the major antigenic epitopes on its surface that are recognized by hMPV-specific monoclonal antibodies and are important in viral neutralization. These findings suggest that the recombinant hMPV F ectodomain possesses native conformation. The fact that some neutralizing (and non-neutralizing) antibodies bind very strongly to the recombinant hMPV F gives new possibilities for epitope mapping studies, crystallization of the protein and also vaccine development.

With the mammalian expression system and codon-optimization strategy we were able to express a protein that is cleaved and glycosylated at all three potential N-glycosylation sites. We also showed that glycosylation of the F1 subunit is necessary for

correct protein transport, folding and expression. Changing the glycosylation sites by mutagenesis had an effect on protein translocation and folding, since some of the mutated proteins containing changes in the F1 glycosylation sites could not be expressed in the culture medium. It would be interesting to study these mutagenesis constructs (e.g. in *in vivo* animal models) in order to determine the effect of glycosylation on immunogenicity and antigenic activity. Furthermore, enzymatic deglycosylation of the expressed protein might help in successful crystallization of the ectodomain, although glycosylation has important role in the formation of the correct secondary and tertiary structure.

We also proved that all fourteen cysteine residues that are present in the recombinant hMPV F ectodomain form disulfide bonds. The disulfide-bonding pattern will be further analyzed with proteomics methods and mass spectrometry analysis. Once we determine the actual bonding pattern in the sequence, we will be able to modify our computer model that was generated based on the known crystal structures of other paramyxovirus fusion cores.

CHAPTER IV

F PROTEIN BINDING TO RGD-SPECIFIC ADHESION MOLECULES

4.1. Introduction

Integrins are structurally, immunochemically and functionally related cell-surface heterodimeric receptors that are widely expressed on metazoan cell membranes and integrate the extracellular matrix with the intracellular cytoskeleton to mediate cell migration, and adhesion[53]. They activate intracellular signaling and play crucial role in development, immune responses, leukocyte trafficking and hemostasis[54, 55]. Integrins are heterodimeric molecules, comprising 18 α and 8 β subunits that are currently known to assemble into 24 distinct integrins. These subunits interact non-covalently in a restricted manner. The diversity of integrins is expanded further by alternative splicing, post-translational modifications and interactions with other cell-surface and intracellular molecules[53].

The members of the integrin family recognize multiple ligands. The list of such ligands includes a large numbers of extracellular matrix proteins (bone matrix proteins, collagens, fibronectins, fibrinogen, laminins, thrombospondins, vitronectins and von Willebrand factor), which reflects the primary function of integrins in cell adhesion to extracellular matrices. Integrins also mediate cell-cell interactions and many microorganisms utilize integrins to gain entry into the host cells. A group of integrins has RGD recognition specificity meaning that these types of integrins recognize Arg-Gly-Asp (RGD)-containing ligands. RGD sequence was originally identified as the sequence in

fibronectin that engages the fibronectin receptor, α5β1, but now it's known that it serves as a recognition motif in multiple ligands for several different integrins. A number of viruses have been shown to utilize RGD-recognizing integrins as receptors or co-receptors, including echovirus, adenovirus, human parechovirus, foot-and-mouth disease virus, rotavirus, hantavirus, West Nile virus, human herpes virus-8 and reovirus[56-61]. Virus binding to these integrin receptors can be inhibited with RGD containing peptides or function blocking anti-integrin antibodies.

Each integrin heterodimer contains 3-5 divalent cation (Ca^{2+}, Mg^{2+} or Mn^{2+}) binding sites and these bound cations can act as effectors, promoting ligand binding; as antagonists, inhibiting ligand binding; and as selectors, changing the ligand binding specificity[53]. Thus, ligand binding can be blocked using chelating agents that bind divalent cations, such as EDTA.

Integrin binding to viral proteins has been shown to mediate attachment or internalization, as well as intracellular signaling cascades. Virus-integrin binding triggers activation of focal adhesion kinase (FAK) in cells infected with HHV-8 and West Nile virus. In case of HHV-8 it has been reported that binding of recombinant viral glycoprotein gB alone activated FAK and paxillin. So, virus binding to RGD-specific integrins can be monitored by the detection of phosphorylation of FAK in the infected cell.

Sequence analysis of the F genes from over 78 clinical isolates collected over a 20-year period at Vanderbilt University along with the full-length F gene sequences deposited in Genbank showed that there is an Arg-Gly-Asp (RGD) motif that is absolutely conserved in all hMPV F sequences. This motif is unique to hMPV F among

human paramyxovirus fusion protein and it is in a region predicted to be surface exposed by antigenic and hydrophilicity plots. These findings let us to further investigate the possibility that integrin binding might be a function of hMPV F protein. Confirming that hMPV F binds to RGD-specific receptors will help to elucidate mechanism of pathogenesis, understand viral-cell receptor interactions and lead to develop targeted antivirals to treat severe hMPV disease in the high-risk population, such as infants, young children, elderly and immunocompromized people.

We identified permissive and poorly permissive cell lines for hMPV infection and probably found that there is a correlation between permissivity for hMPV and the types of surface expressed integrins. LLC-MK2 cells, a monkey renal epithelial cell line, are equally permissive for RSV and hMPV ad both viruses grow to equivalent titers of 10^6 pfu/ml in hMPV growth medium. CHO cells (Chinese hamster ovary cells), however, are poorly permissive for hMPV infection, with yield of approximately 20% of that of LLC-MK2 cells. LLC-MK2 cells have several RGD-binding integrin expressed on the surface: αv, $\alpha 5$, $\beta 1$, $\beta 3$, $\beta 5$, while CHO cells express only some of the $\alpha 5$ and $\beta 3$ integrins. To show the correlation between integrin surface expression and hMPV infectivity we tried to block hMPV infection in LLC-MK2 cells with EDTA, which is a chelating reagent that binds divalent cations, linear RGD-containing oligopeptides and function blocking anti-integrin antibodies. To further confirm this correlation we planed loss-of-function studies on LLC cells and gain-of function permissivity experiments with CHO cells to specifically prove hMPV F binding to certain types of RGD-binding integrins.

4.2. Materials and Methods

Fluorescent-focus assay of hMPV infectivity. LLC-MK2 cell monolayers were pre-incubated with the putative inhibitor for 60 minutes, virus was adsorbed at 4 °C (at which cell entry does not occur) for 60 min and cells were incubated at 37 °C for one hour to allow membrane fusion and virus entry. Virus inoculum was removed by washing the monolayer with PBS three times. Cells were incubated for 24 hours (a single cycle for viral replication), fixed and stained by indirect immunofluorescence for hMPV or RSV. Infectious foci were counted in three replicate experiments. Infectivity is expressed as the percentage of fluorescent foci compared to control wells inoculated with virus alone in the absence of any inhibitor.

Detection of integrin receptors by flow cytometry. Human anti-αV integrin antibodies (MAB1219, mouse IgG1) were purchased from R&D Systems, human anti-β1 integrin antibodies (AIIB2, rat IgG) from DSHB at University of Iowa and anti-β3 integrin antibodies (MAB1957Z, mouse IgM) from Chemicon. LLC-MK2 and CHO cells were detached from culture plates by scraping and centrifuged at 2600 rpm for 5 min. Culture media was removed and 2-3x10^5/ml cells were resuspended in 1.2 ml of staining buffer (PBS with 1%FBS, 1% BSA and 1% goat serum). Cells were centrifuged and washed with staining buffer one more time then resuspended in 200 µl staining buffer containing anti-αV or -β1 or -β3 integrin primary antibodies. Cells were incubated for 30 min at 4 °C then centrifuged at 2600 rpm for 5 minutes, staining medium was removed and cells were resuspended in 1.2 ml staining buffer. Cells were washed one more time and resuspended in 200 µl staining buffer with FITC-conjugated goat anti-mouse or goat anti-rat IgG secondary antibodies (1:500 dilution). Cells were stained for 30 min at 4 °C,

centrifuged and resuspended in 1 ml staining buffer. Flow cytometric analysis was performed with a BD LSR II instrument at the VUMC Flow Cytometry Core at Vanderbilt University.

Integrin plasmid constructs. Plasmids with cDNA encoding for human integrins were kindly provided by Melissa Maginnis in Dr. Dermody's lab at Vanderbilt University. A cDNA encoding human integrin αv cloned into the BamHI and XbaI site of pcDNA-1neo was excised by digestion and subcloned into pcDNA3.1+ (Invitrogen) using complementary restriction enzyme sites. A cDNA encoding human β1 integrin cloned into the EcoRI and XhoI sites of pBluescript SK- was obtained from the ATCC (Manassas, VA) and was excised by digestion and subcloned into complementary restriction enzyme sites of pcDNA3.1+. A cDNA encoding human integrin β3 cloned into the XbaI site of pcDNA-1neo was excised by digestion subcloned into the XbaI site of pcDNA3.1. A cDNA encoding β5 cloned into the EcoRI site of pcDNA-1neo was excised by digestion and subcloned into the EcoRI site of pcDNA3.1+. Successful cloning was confirmed by automated sequencing at Vanderbilt DNA Sequencing Facility.

Transfection of integrin cDNA. One day before transfection CHO cells were seeded in Ham's F12K growth medium supplemented with 5% fetal bovine serum on 24-well plates, so they were 80-90% confluent on the day of transfection. Cells were transfected with human αV and β1 integrin cDNA in pcDNA 3.1+ expression vector by using 1 μg integrin cDNA and 1 μl TransFectin Lipid Reagent (Bio-Rad)/well. Transfection protocol was followed as recommended by the manufacturer. Cells were incubated 24-48 h at 37 °C and 5% CO_2 before further analyses.

HMPV F protein binding assay. Purified hMPV F ectodomain was prepared as described previously (hMPV vaccine paper). LLC-MK2 and CHO cells were detached from culture plate and pelleted by centrifugation. 2-3x10^5 cells/ml were resuspended in 1.2 ml staining buffer (PBS with 1% FBS, 1%BSA and 1% goat serum) in Eppendorf tubes. Cells were pelleted and washed again with staining buffer then resuspended in 200 µl staining buffer with 10 µg/tube of purified hMPV F ectodomain and incubated for 1 h at 4 °C. Cells were centrifuged, buffer was removed and after washing cells were incubated with 200 µl staining buffer with anti-hMPV polyclonal guinea pig serum for 30 min at 4 °C. Cells were pelleted, washed twice and stained with 200 µl staining buffer with Alexa Fluor 568-conjugated goat anti-guinea pig IgG secondary antibodies (Molecular Probes) for 30 min at 4 °C. After washing cells were resuspended in staining buffer and analyzed by flow cytometry.

Integrin gene knockdown with siRNA. LLC-MK2 cells were plated on 24-well plates in Opti-MEM growth medium supplemented with 2% fetal bovine serum. Cells were 90% confluent on the day of siRNA transfection. Human αV and β1 integrin siRNAs were ordered from Qiagen and reconstituted in our laboratory as recommended by the manufacturer. Cells were transfected with 5-10 nM siRNA and 3 µl HiPerFect Reagent (Qiagen) per well. 48 h post-transfection cells were harvested by scraping, integrin mRNA was quantitated by RT-PCR and integrin surface expression was analyzed by flow cytometry.

HMPV binding and infectivity assay. LLC cells in 48-well plates were washed twice with PBS. To three wells of 48-well plate a serial dilution of EDTA from 2.5 mM to 300 nM concentrations was added, this served as a positive control for the infectivity

assay. The appropriate dilutions of integrin antibodies were added to triplicate wells of the plate. To the virus control well 75 µl of 0% OptiMEM medium was added. Cells were incubated for 90 min at 37°C in a humidified incubator with 5% CO_2, then for 30 min at 4°C. 10 µl hMPV diluted to give approx. 60 virus particle/10 µl was added to each well. Plates were incubated for 60 min at RT, then for 60 min at 37°C with 5% CO_2. Cells were washed with PBS twice and 0.5 ml OptiMEM medium supplemented with 2% FBS was added to the wells. Cells were incubated for 24 h at 37°C with 5% CO_2. Cells were fixed with formalin and stained with anti-hMPV polyclonal guinea pig serum and with HRP-conjugated goat anti-guinea pig IgG at 1:1000 dilution in blotto. Plates were rinsed with water and 100 µl of TrueBlue peroxidase substrate was added to each plate and incubated for 10 min at RT to develop color. Plates were rinsed with water, dried and stained cells were counted.

4.3. Results

Blocking hMPV infectivity in LLC-MK2 cells. We tested the effects of EDTA, RGD-containing peptides and function blocking anti-integrin antibodies on hMPV infectivity in LLC-MK2 cells. Integrin function is divalent cation-dependent and the binding of other viruses to RGD-binding integrins can be blocked by the presence of the divalent cation chelator EDTA. We tested the ability of EDTA to inhibit hMPV binding and infection of cells *in vitro* in a quantitative fluorescent-focus based assay we developed. We included RSV as a control virus, because it is a closely related paramyxovirus, but RSV F protein lacks the RGD motif. We performed *in vitro* infectivity assays on LLC-MK2 cells with hMPV and RSV, in the presence or absence of increasing (0.3 mM - 2.5 mM) EDTA concentrations. These experiments demonstrated

that there is a titratable concentration-dependent effect of EDTA on hMPV infectivity in LLC cells, with complete inhibition at EDTA concentrations above 2.5 mM (**Figure 28**). EDTA had no effect on RSV infectivity at any concentration. These differences were highly statistically significant and these data suggest that EDTA exerts a specific inhibitory effect on hMPV and support a role for integrins in hMPV infection.

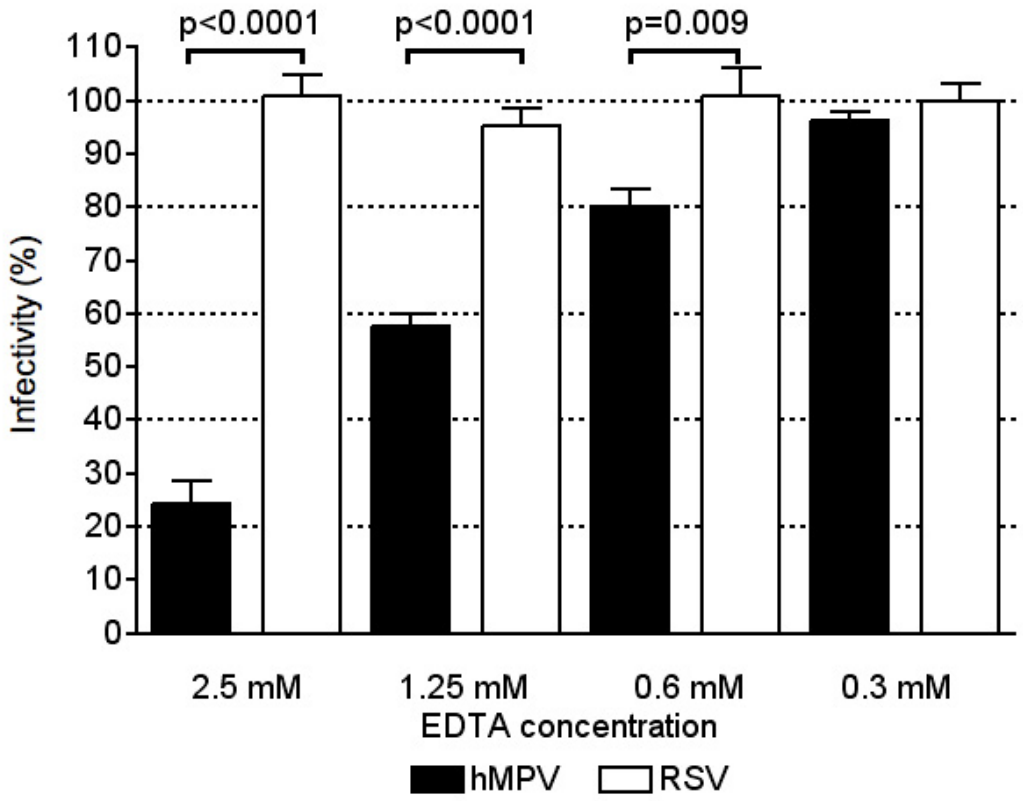

Figure 28. Effect of decreasing EDTA concentration on infectivity of hMPV and RSV. Mean percent infectivity was calculated as percentage of fluorescent foci compared to control wells inoculated with virus alone in the absence of any inhibitor. Data represents three separate experiments, and means were compared with student's t test, 2-tailed assuming unequal variance. White bars are RSV infected controls, black bars represent hMPV infected cells.

We also tested specific oligopeptide (GRGDSP) inhibitors as well as a control (GRGESP) peptide in the same quantitative assay. Increasing concentrations of GRGDSP had increasing inhibitory effect on hMPV infectivity (**Figure 29**), while the control GRGESP peptide had no effect (data not shown). Neither peptide exhibited any inhibitory effect on RSV, suggesting a specific effect on RGD-binding by hMPV. The inhibitory effect of linear GRGDSP peptides was modest, consistent with the results reported by other investigators in similar studies of virus-integrin binding.

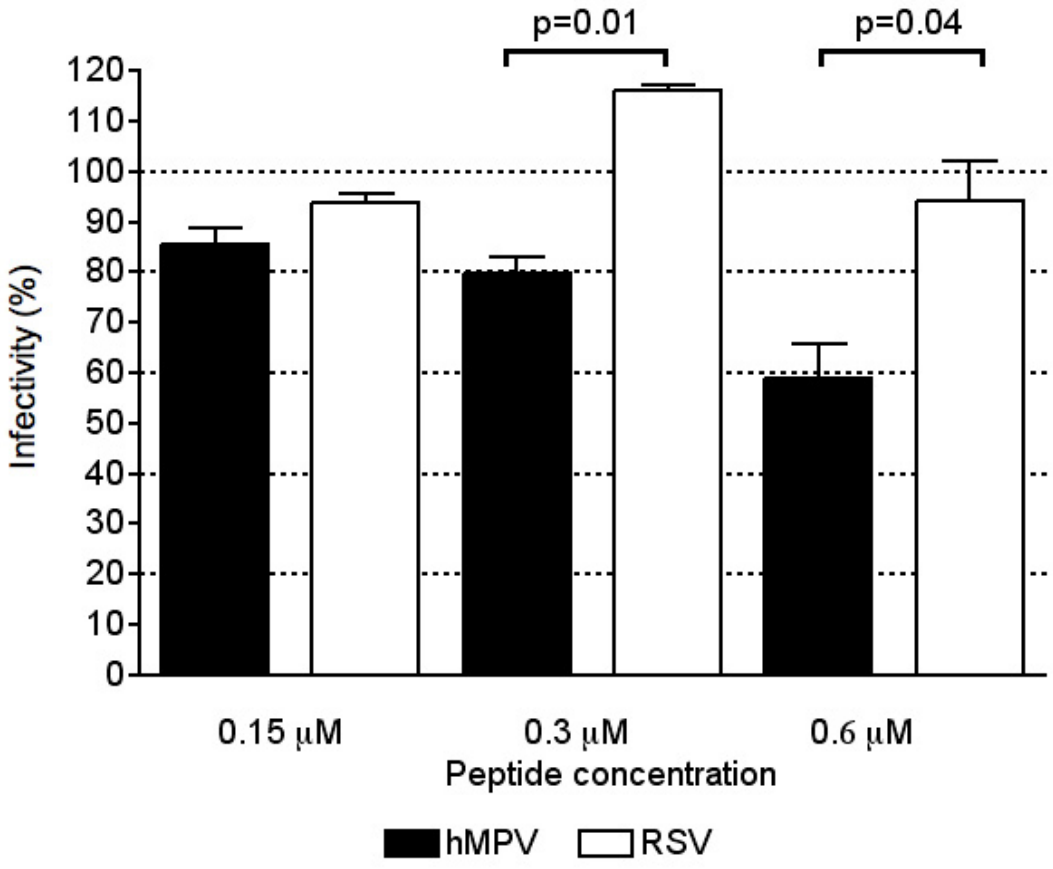

Figure 29. Effect of decreasing GRGDSP linear peptide concentration on hMPV and RSV infectivity. White bars are RSV infected controls, black bars represent hMPV infected cells.

Previously, it has been reported that function-blocking monoclonal antibodies directed against specific RGD-binding integrins inhibited viral infectivity. We performed experiments using commercially available anti-integrin monoclonal antibodies that were previously determined to possess function-blocking activity by the supplier or other investigators. Cell monolayers were pre-incubated with the antibodies, then infected with hMPV or RSV by the same method described in the experiments with EDTA or RGD-containing peptides. We found that antibodies against αv and β1 integrin exhibited the greatest inhibition of hMPV infectivity, while no inhibition of RSV (**Figure 30**). Anti-αv and anti-β1 antibodies combined together showed even greater inhibition than either alone, suggesting synergy for the combination. While anti-β3 antibodies showed modest effect, anti-αvβ3 and anti-αv alone had a greater inhibition, which suggests that αv is more important for infectivity. Antibodies against α5 and β5 integrins had no effect (data not shown). All of these data suggest that αvβ1 heterodimers might be required for hMPV infection and further support the hypothesis that this interaction occurs at the site of integrin expression on the cells surface, where viral attachment and entry occur.

hMPV F binding to LLC-MK2 cells. To test whether or not our purified hMPV F ectodomain (which also contains the RGD-motif) binds to αvβ1 integrins, LLC-MK2 cells were incubated with hMPV FΔTM at 4 °C for 45 minutes with agitation and washed with staining buffer for flow cytometry (PBS with 1% goat serum, 1% HI-FBS and 1% BSA). Cells then were stained for hMPV F using anti-hMPV polyclonal guinea pig serum as primary antibody and Alexa Fluor 568-conjugated goat anti-guinea pig secondary antibody. Cells were analyzed on a BD LSRII flow cytometer. Cells stained with primary and secondary antibodies without FΔTM were used as controls.

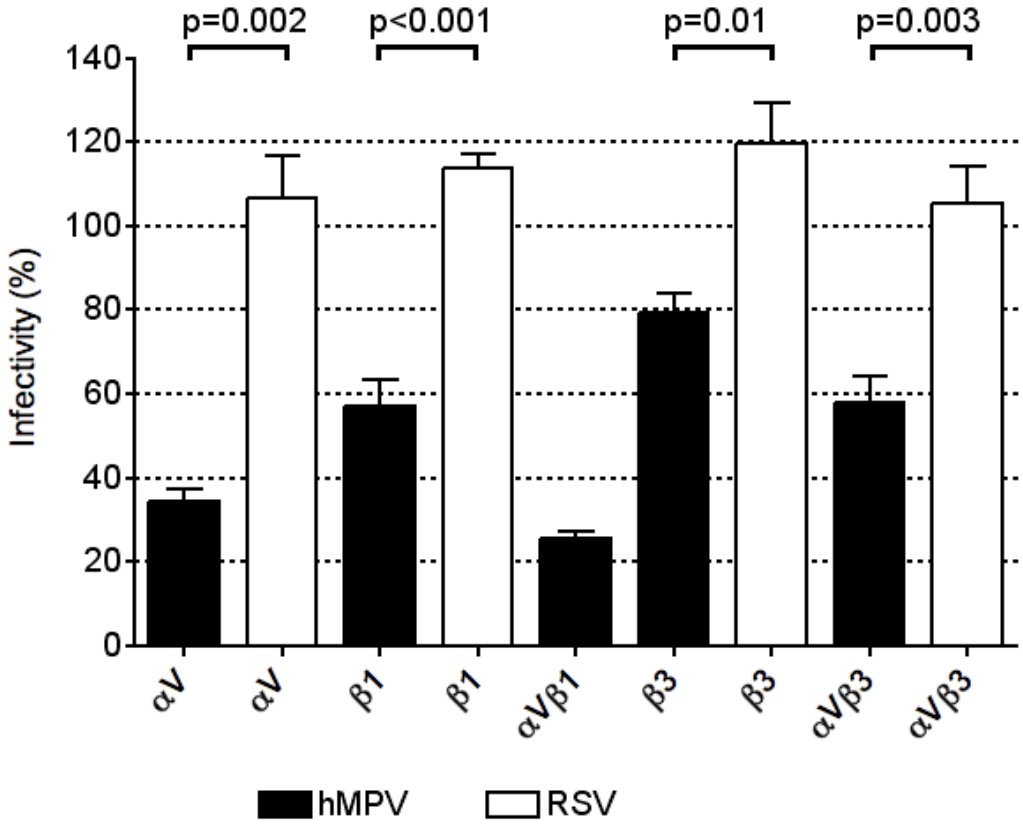

Figure 30. Effect of integrin-function blocking antibodies on hMPV and RSV infectivity. Data represent three separate experiments, mean % was calculated as percentage of fluorescent foci compared to control wells with virus alone in the absence of any inhibitor. Means were compared with student's t test, 2-tailed assuming unequal variance. White bars are RSV infected controls, black bars represent hMPV infected cells.

The control LLC-MK2 cells had very low background fluorescence, showing that there was little non-specific binding of guinea pig anti-hMPV serum or goat anti-guinea pig secondary Ab to LLC-MK2 cells (**Figure 31, upper panel**). In contrast, cells incubated with hMPV FΔTM protein followed by anti-hMPV antibodies showed significant increase in fluorescence, indicating FΔTM binding to the cells (**Figure 31, histogram in the second row**). Pre-incubation of LLC cells with function blocking anti-

αv or anti-β1 antibodies decreased FΔTM binding (**Figure 31, two histograms in the third row**). We also utilized site-directed mutagenesis to produce an RGE-mutant FΔTM protein, by changing aspartic acid in the native FΔTM to glutamic acid (RGD to RGE). Cells were incubated with the RGE mutant protein then stained similarly to FΔTM incubation and staining. We did not detect a significant increase in the fluorescence signal, which suggests that RGE mutant protein did not bind to LLC-MK2 cells (**Figure 31, bottom left histogram**). These experiments need to be confirmed by replicate assays and control experiments with irrelevant proteins (e.g. RSV F) and with other anti-integrin antibodies are needed to further confirm the results that we have so far. Nonetheless, these data provide strong evidence that hMPV F protein mediates viral binding to cell surface integrins.

siRNA knockdown of αv and β1 integrin expression on LLC-MK2 cells. We used an RNAi approach to block integrin gene expression in LLC-MK2 cells. We obtained synthetic αV and β1 integrin-specific siRNA oligos (Qiagen) and transfected them into LLC-MK2 cells using cationic lipid-mediated transfection. We have optimized this protocol and successfully transfected LLC-MK2 cells with siRNA directed against αV and β1 integrins, separately and together, and have shown by flow cytometry that cell surface expression is decreased (**Figure 32**). We have also confirmed by quantitative RT-PCR that amount of αV and β1 integrin mRNAs are decreased (data not shown). These cells were then infected with hMPV and infectivity determined using the fluorescent focus assay we previously described. Knockdown of αV and β1 integrins substantially decreased the infectivity of hMPV in LLC-MK2 cells (**Figure 33**).

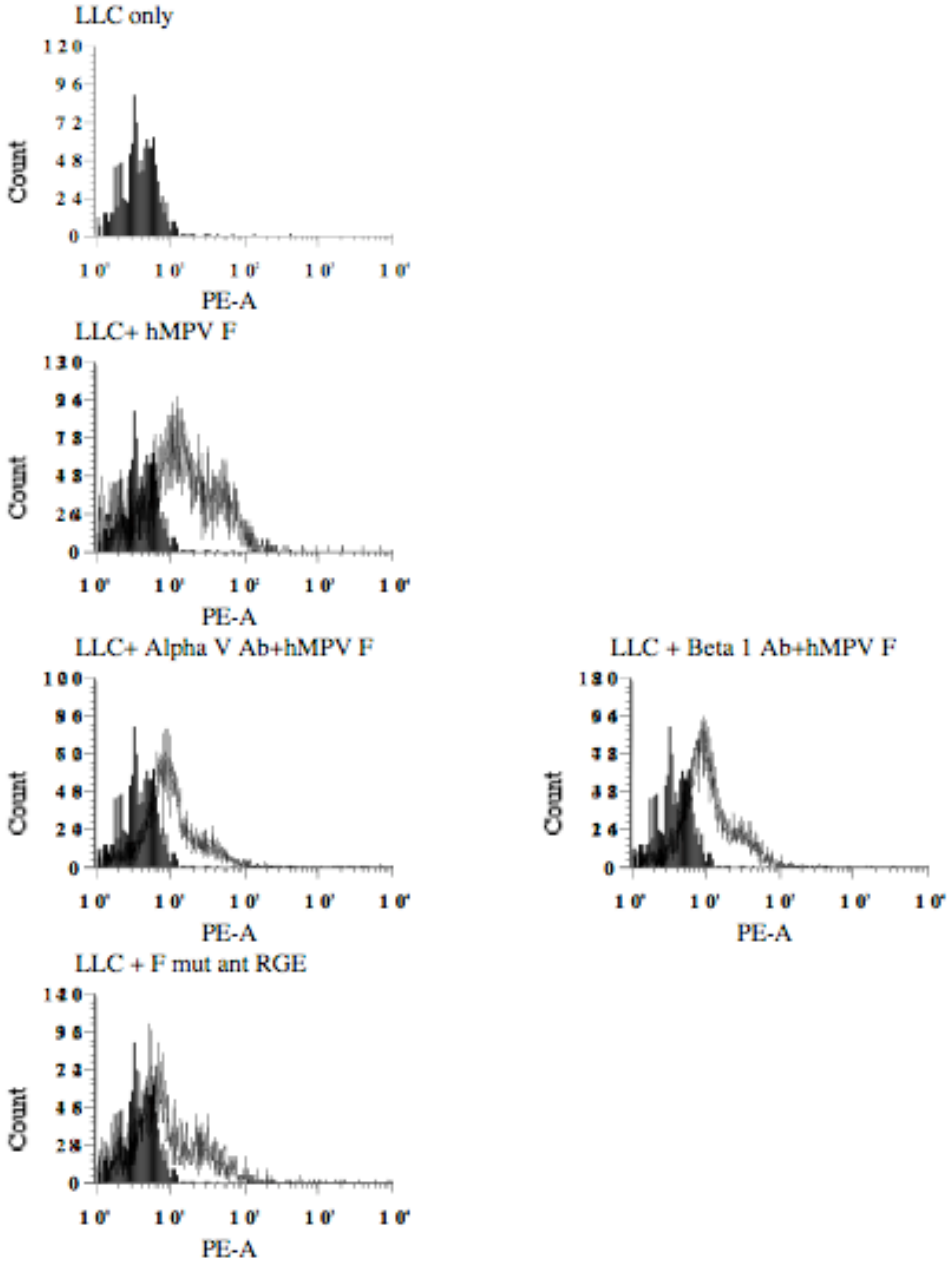

Figure 31. Histograms of flow cytometric analysis of LLC-MK2 cells stained for cell surface binding of hMPV F protein. Solid histogram in each panel represents LLC-MK2 control cells, incubated only with anti-hMPV primary and goat anti-guinea pig, Alexa Fluor 568-conjugate secondary antibodies. White histograms show cells incubated with FΔTM, anti-αv or anti-β1 antibodies followed by FΔTM and RGE mutant protein, respectively, then stained with primary and secondary antibodies against hMPV, as the control. Mean fluorescent intensity of events is shown on the y-axis, decades of fluorescence are on the x-axis.

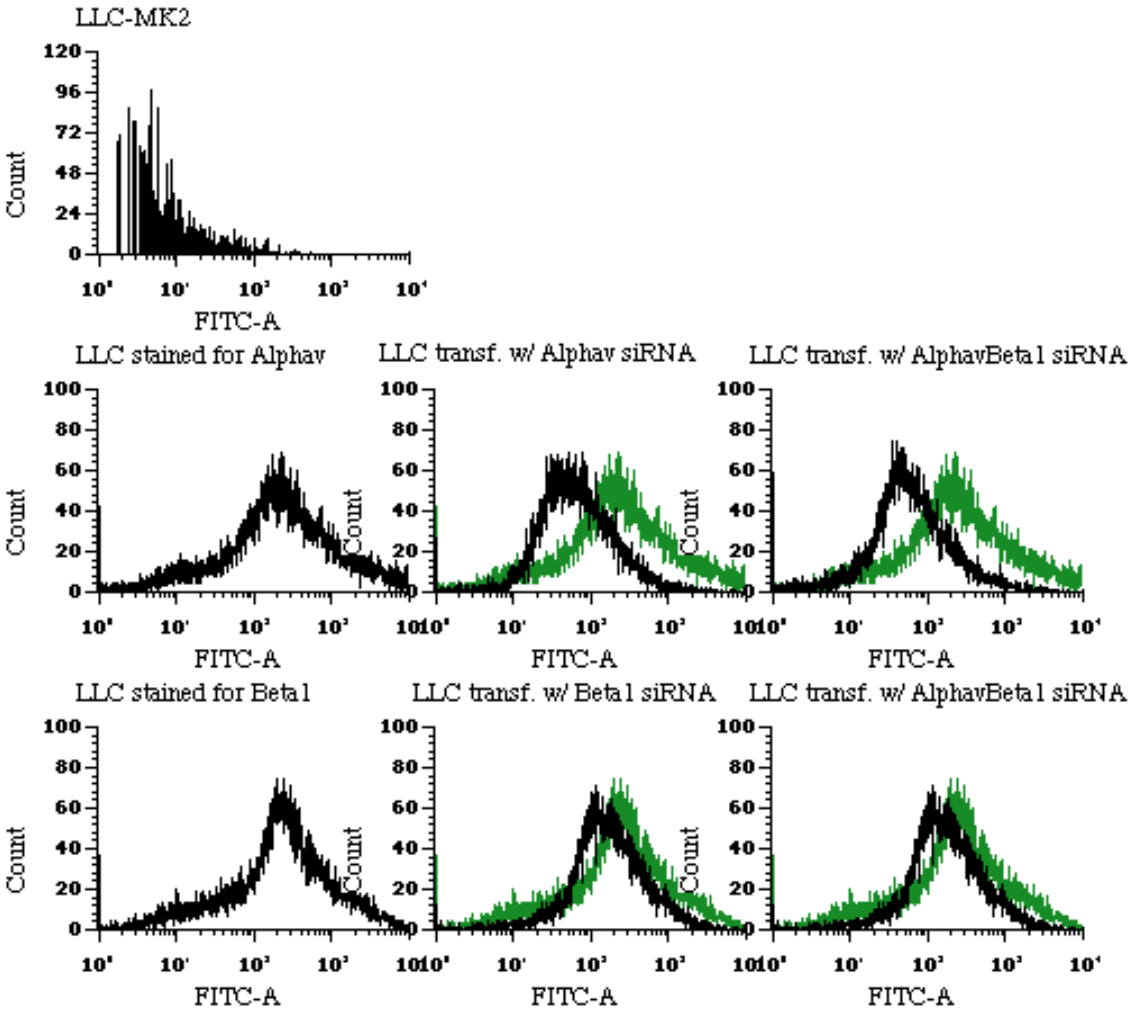

Figure 32. Flow cytometric analysis of siRNA transfected LLC-MK2 cells. Solid panel shows background fluorescence of LLC-MK2 cells stained alone with secondary antibody. Wild type LLC cells (first panels in second and third rows) and siRNA-transfected ones (panels with two histograms) were stained for αv (second row) and β1 (third row) integrins. Green histograms represent the wild type control for siRNA-transfected cells. Anti-αv mouse IgG1 and anti-β1 rat IgG were used as primary antibodies and goat anti-mouse or goat anti-rat FITC-conjugated antibodies as secondary Abs for flow cytometric staining.

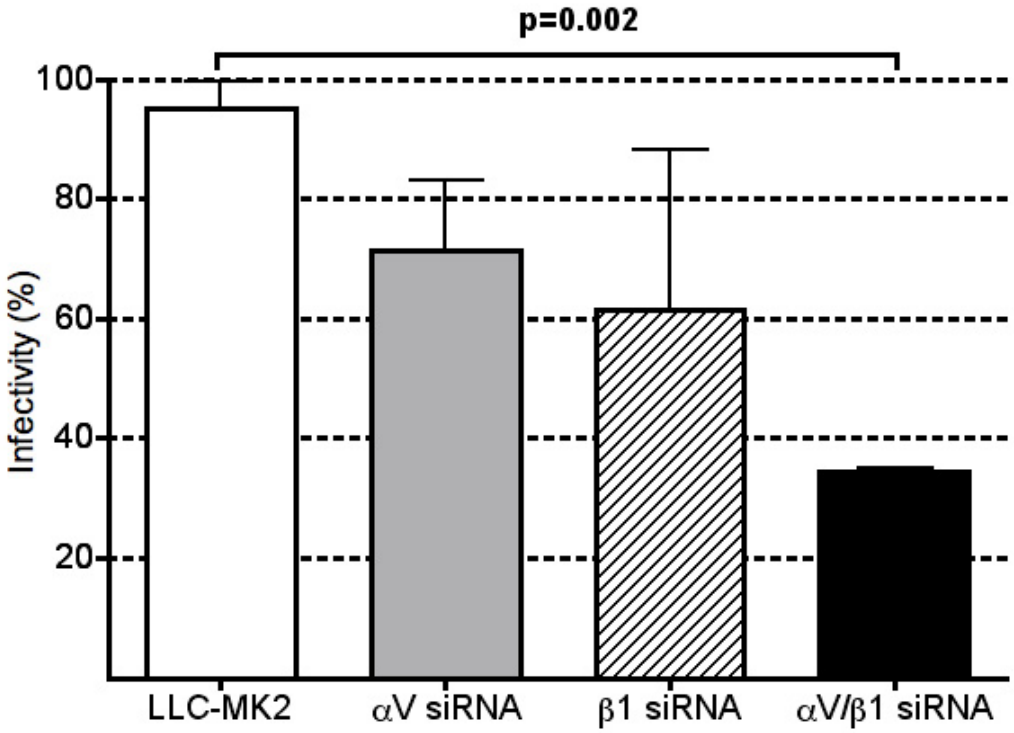

Figure 33. Infectivity of LLC-MK2 cells transfected with siRNA for αV and/or β1 integrins. Mean % infectivity was calculated as percentage of fluorescent foci compared to control wells inoculated with virus alone in the absence of any inhibitor. Means were compared with student's t test, 2-tailed assuming unequal variance. Data represent three separate experiments.

The greatest inhibition was achieved by transfecting LLC-MK2 cells together with both αV and β1 integrin siRNAs. These data confirm that blocking the αV and β1 integrin interactions with hMPV by inhibiting integrin surface expression significantly decreases hMPV infectivity. However, further experiments are necessary to prove that hMPV F binding can be also blocked by integrin siRNA-transfection.

Integrin expression in CHO cells. CHO cells are poorly permissive for hMPV infection. They express some α5 and β3 on their surfaces, but lack αv and β1 integrins,

which are present in LLC cells and thought to be important in hMPV binding to host cell surface based on our previous experimental data. In order to further confirm a specific role for αvβ1 integrins in hMPV infection, we performed transient transfection of CHO cells with cDNAs encoding either human αv or β1 integrin contained in a mammalian expression vector (from Melissa Maginnis in Dr. Dermody's lab at Vanderbilt University). We confirmed successful cDNA transfection and the surface expression of integrins on CHO cells by flow cytometry as shown in **Figure 34** and the presence of integrin mRNA by RT-PCR (data not shown). We also performed the hMPV infection by using fluorescent focus assay to detect hMPV infectivity in integrin cDNA-transfected CHO cells. Our results showed that expression of either αv or β1 integrin substantially increased the permissivity of CHO cells for hMPV (data not shown). Expression of αv integrin in CHO cells increased the permissivity by almost 200% (compared to wild type CHO-s), and expression of β1 integrin increased the permissivity by over 300%. Furthermore, we also proved that this increase in permissivity can be blocked by function-blocking anti-integrin antibodies, similarly to the permissivity of LLC-MK2 cells. Both anti-αV and anti-β1 inhibited hMPV infectivity significantly, and both together exhibited additive inhibition (**Figure 35**). These data strongly suggest that the increased permissivity of transfected CHO cells is due to αV and β1 integrins. The next experiments planned will use flow cytometry to determine the effect of integrin transfection and antibody-mediated blockade on hMPV F protein binding to CHO cells.

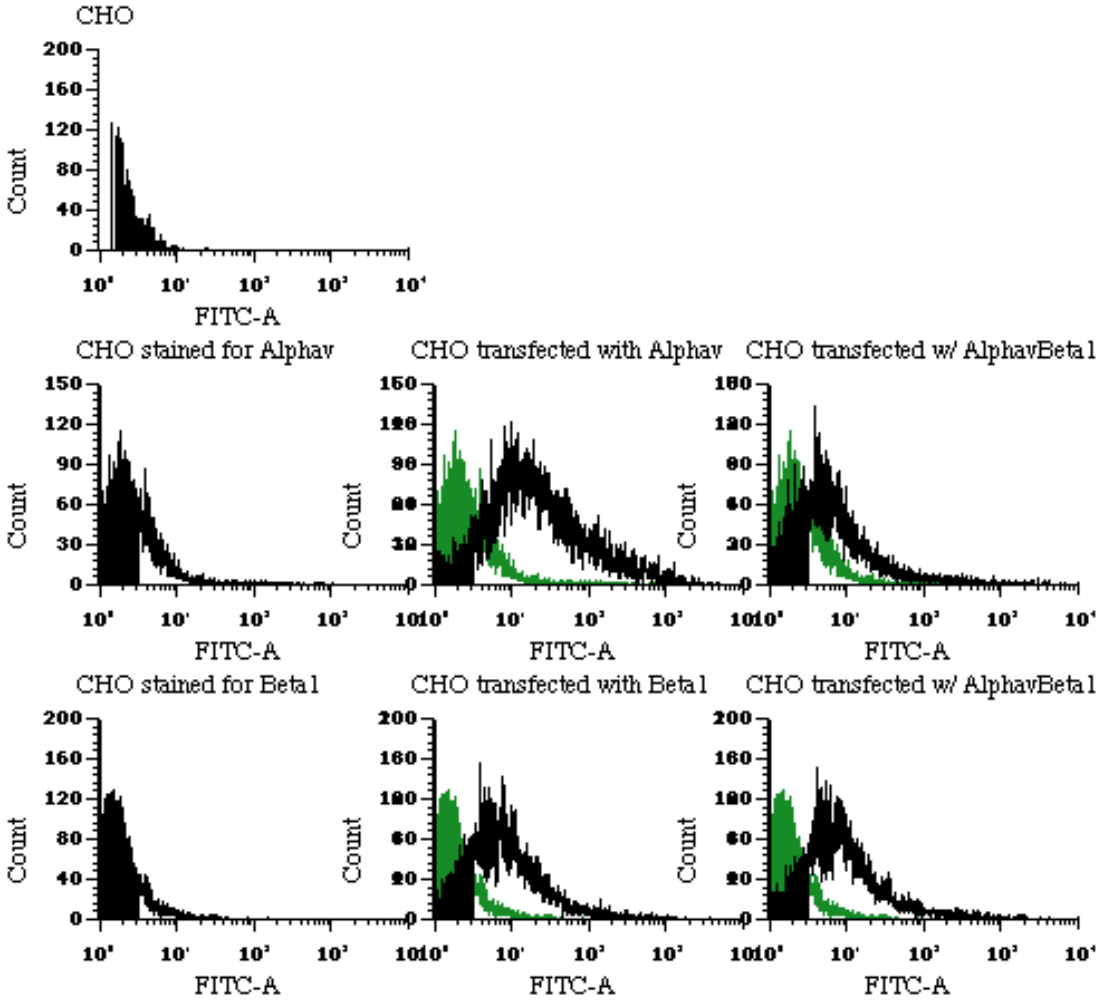

Figure 34. Histograms of flow cytometric analysis of integrin surface expression in transiently transfected CHO cells. Top panel shows background fluorescence of CHO cells stained with secondary antibody alone, as a negative control. Wild type (first panels on the left) and transfected (middle and right panels) CHO cells stained for αv (second row) or β1 (third row) are shown. Green histograms are the same as wild types, for comparison of fluorescent signals in transfected cells. Anti-αv mouse IgG1 and anti-β1 rat IgG were used as primary antibodies and goat anti-mouse or goat anti-rat FITC-conjugated antibodies as secondary Abs for flow cytometric staining.

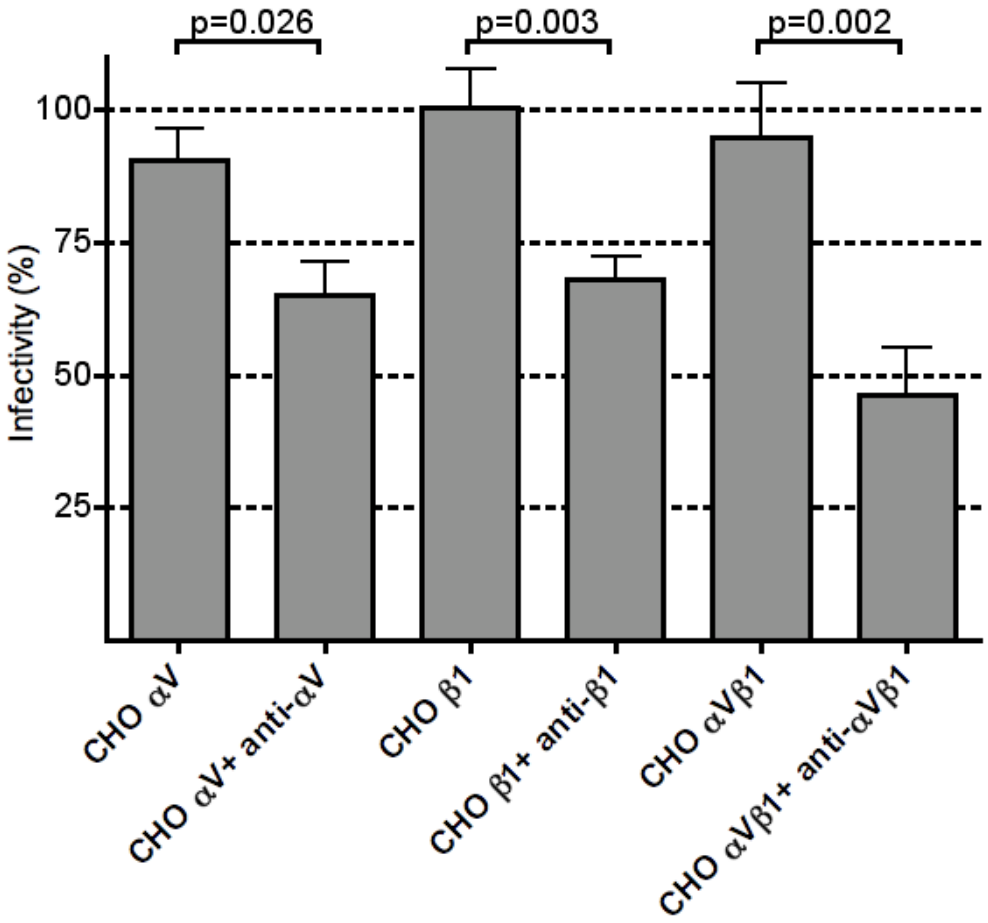

Figure 35. Effect of integrin function-blocking antibodies on infectivity of hMPV in integrin-transfected CHO cells. Mean % infectivity was calculated as percentage of fluorescent foci compared to control wells inoculated with virus alone in the absence of any inhibitor. Means were compared with 2-tailed t test assuming unequal variance. Data represent three separate experiments.

4.4. Discussion

Our hypothesis was that cell surface receptors, specifically RGD-binding integrins serve as receptor for hMPV and that αvβ1 integrin binding and cell entry is mediated by the hMPV fusion protein. The RGD motif is highly conserved in all previously reported hMPV F sequences and we also found a correlation between permissivity for hMPV infection and surface integrin expression different cell lines.

We found that LLC-MK2 cells are permissive for hMPV infection and they express αvβ1 integrins on the surface along with other RGD-binding receptors. In contrast, CHO cells are poorly permissive for hMPV infection and they don't express αvβ1 integrin heterodimers, but the permissivity can be increased by transfecting αv and β1 integrin cDNA-s into the cells. We showed that hMPV infectivity could be increased by over 300% with integrin expression in CHO cells. Furthermore, we showed that this increase could be blocked back with function-blocking anti-integrin antibodies.

Experiments were performed to prove that the permissivity of LLC-MK2 cells for hMPV infection can be inhibited in several ways, and these methods targeted αv and β1 integrins on the cell surface. We used divalent cation chelator, EDTA, RGD-containing linear peptides, and function-blocking anti-integrin antibodies; all of which inhibited hMPV infectivity in LLC cells. We also used the technique of RNA interference and knocked down αv and β1 integrin mRNA expressions in the cells. These experiments further confirmed that hMPV infectivity is related to the presence (or absence) of αv and β1 integrins on the cell surface.

These 'gain-of-function' and 'loss-of-function' experiments provided starting points for further investigations of hMPV F-integrin binding, cell signaling and possible

cytoskeletal rearrangement mediated by hMPV F-integrin binding. To prove that hMPV F binds to αv and β1 integrins, we will design flow cytometric experiments to monitor hMPV F ectodomain binding to siRNA transfected LLC-MK2 cells, and also to integrin cDNA-transfected CHO cells. We will use anti-αv and anti-β1 function-blocking antibodies, to block binding and irrelevant integrin antibodies to show lack of blockade. To confirm RGD-containing F ectodomain binding to integrins, co-purification of hMPV F and LLC cell lysate over Histrap column, immunoprecipitation and immunoblots of integrins and hMPV F could be performed.

It has been reported that virus-integrin binding triggers activation of focal adhesion kinase (FAK) in infected cells, so we could follow hMPV binding to surface receptors by detecting phosphorylation of FAK at the time of virus binding to infected cells. Lack of phosphorylation probably would mean no binding to integrins.

And finally, we could generate RGE-mutant virus in order to directly test the infectivity of non-RGD motif F protein mutants in vitro and in vivo in a small animal model. It is possible that such a mutant virus will be difficult to recover, if it is less able to bind and/or internalize. Future experiments will be necessary to determine which specific steps of viral entry are mediated by integrin engagement. Furthermore, it is possible that additional cellular receptors for hMPV exist. The results of these experiments will advance our understanding of the pathogenesis of a novel emerging human virus. The findings will likely have broader implications for the paramyxovirus family, which includes a number of important human pathogens.

CHAPTER V

ANIMAL MODEL AND VACCINE DEVELOPMENT

5.1. Introduction

Infectious diseases are responsible for one-fifth of all deaths worldwide, killing at least 11 million people per year. Beyond this high death toll millions more children and adults suffer disability and illness because they were not immunized. Vaccines are the keystones fighting against deadly pathogens. The eradication of smallpox and polio and decreasing the global numbers of deaths due to measles all illustrate the benefits of vaccination[62]. Today over 50% of the 10.6 million deaths of young children are due to acute respiratory infections, diarrhoeas, malaria, measles and AIDS. HIV pandemic affects around 40 million people with more than 14,000 new infections every day. Acute respiratory infections (ARIs) are the most important cause of infant and young children mortality being responsible nearly 4 million deaths every year mostly in developing countries. The main agents causing ARIs include influenza virus, respiratory syncytial virus (RSV), parainfluenza virus type 3 (PIV-3), Streptococcus pneumoniae and Haemophilus influenzae. Vaccines have been developed against influenza virus, S. pneumoniae and H. influenzae, but to date no vaccines are available against RSV, hPIV-3, metapneumovirus (hMPV) or the new coronavirus strains[63].

Several approaches have been used to develop effective vaccines against respiratory viruses. In case of influenza virus the currently available vaccines are the

inactivated vaccines made from inactivated, detergent-split influenza virus grown in the allantoic cavity of embrionated chicken eggs. Another approach to influenza vaccines has been the live-attenuated vaccines by using cold-adapted (*ca*) virus strains. The *ca* strains grow well in chicken eggs at 25-33°C and have reduced replication titer at 37°C. Subunit, synthetic peptide and DNA vaccines are also under development for influenza. Subunit vaccines use recombinant HA protein[64] produced in serum-free cultures with baculovirus expression systems. Synthetic peptides for nasal administration showed protective efficacy in mice and clinical trials are planned. An epidermal DNA vaccine was found to be safe and immunogenic in subjects with prevaccinnation antibodies to influenza, other DNA vaccines are at the early stage of development.

Several strategies have recently been used for RSV vaccine development, including generation of peptide, subunit and live attenuated vaccines. Of these, only inactivated, subunit and live attenuated RSV vaccines have been evaluated in clinical trials. Early studies in the 1960s showed that children vaccinated with formalin-inactivated RSV vaccines suffered from more severe disease on subsequent exposure to virus as compared to the unvaccinated control group. These early studies resulted hospitalization of the 80% of vaccinees and two deaths. The enhanced severity of disease was reproducible in animal models and it was thought to result from lack of local immunity, inadequate serum neutralizing antibody level and an elevated type 2 helper T-cell-like (Th2) immune response. Purified fusion protein (PFP) subunit vaccines for RSV have been shown to be immunogenic and safe in seropositive children and adults. However, in rodent studies, Th2-type responses have been observed following inoculation with purified F protein, leading to concern that this could occur in

seronegative infants and produce enhanced disease with natural infection. An immature or non-native conformation of F protein in these preparations may account for the phenomenon of immune-mediated enhanced disease.

Human metapneumovirus shares substantial homology with RSV and its glycoproteins. To develop a vaccine against hMPV many issues of the RSV vaccine development studies need to be considered. Previously, Williams et al. showed that cotton rat is a good animal model for hMPV infection and protective immunity[38] and anti-hMPV polyclonal serum was produced in our laboratory by vaccination of guinea pigs with DNA-F construct (pcDNA3.1+-F). We wanted to test the hypothesis that F protein is a major protective antigen for hMPV and it is immunogenic in cotton rats. We immunized cotton rats twice, at two-week interval (0 and 14 days) with either control vector (pcDNA3.1), DNA-F alone, DNA-F followed by FΔTM protein, or FΔTM protein alone. Animals were bled on day 27 to measure serum antibodies to hMPV. All groups were challenged intranasally on day 28 with live hMPV. Four days post-infection, the animals were sacrificed and nasal and lung tissue titers for virus were measured by plaque assay. Lung tissue sections from animals were also examined by a pathologist and scored in a group-blinded fashion.

5.2. Materials and Methods

Immunization of animals. Animals were purchased at 5-6 weeks of age from a commercial breeder (Harlan, Indianapolis, IN), fed standard diet and water ad libitum and kept in microisolator cages. Animals were anesthetized by methoxyflurane (Metofane) inhalation prior to immunization, blood sampling or virus inoculation. In initial

experiments, guinea pigs were immunized at monthly intervals with 100 μg of DNA-F intramuscularly (i.m.) and 10 μg of DNA-F intradermally. Cotton rats immunized with DNA received 100 μg i.m. of either control vector pcDNA3.1 or pcDNA3.1-F (DNA-F). Protein immunizations consisted of 25 μg FΔTM adjuvanted with TiterMax Gold (Sigma). Serum was collected from cotton rats by retro-orbital bleed. Serum hMPV-neutralizing titers were determined by a plaque reduction assay.

hMPV challenge. The virus strain used was hMPV strain TN/96-12, a genotype group A1 virus, according the proposed nomenclature. Virus was grown in LLC-MK2 cells and purified over a 20%/60% discontinuous sucrose gradient. This virus stock was determined to have a titer of 1×10^6 plaque-forming units (pfu)/ml by plaque titration in LLC-MK2 cell monolayer cultures. Cotton rats were inoculated on day 28 intranasally with 1×10^5 pfu in a volume of 100 μl. Four days later, the animals were sacrificed by CO_2 asphyxiation, and exsanguinated. Nasal and right lung tissues were harvested and immediately homogenized, while the left lungs were inflation-fixed with 4% paraformaldehyde. The right lungs were pulverized in ice-cold glass homogenizers and nasal turbinates were ground with sterile sand in a cold porcelain mortar and pestle in 3 ml of ice-cold Hanks' balanced salt solution. Tissue homogenates were centrifuged at 4 ºC for 10 minutes at 300 x g and the supernatants were collected, and snap-frozen in liquid nitrogen. Virus yields were measured by plaque titration. Comparisons between groups were made using a 2-tailed Student's t test that assumed unequal variance. The Vanderbilt Institutional Animal Care and Use Committee approved the study.

Pathological examination. Specimens for histological examination were embedded in paraffin, processed and slides prepared in the Vanderbilt

Immunohistochemistry Core. All lobes of the right lung were examined, including 2 sections per lung. Sections were reviewed by a pathologist experienced in small animal studies of RSV and hMPV without knowledge of the immunization status of the specimens. Slides were examined in their entirety in a group-blinded fashion. The following compartments of the lung were assessed: alveolar spaces, airways at all levels, interstitium, and vessels (both arteries and veins). Inflammatory infiltrates were evaluated for location, severity, and composition (cell types: small mononuclear cells, transformed lymphocytes, histiocytes, neutrophils, eosinophils). The perivascular 'cuff thickness' was assessed semiquantitatively as a measure of severity of inflammation and was evaluated at the point of minimal diameter of the structure. The degrees of inflammation were graded as follows: 0 = no infiltrate; 1+ = most vessels had an infiltrate up to 4 cells thick; 2+ = most vessels had an infiltrate 5–7 cells thick; 3+ = most vessels had an infiltrate greater than 7 cells thick. Interstitial alveolar cellularity was graded as follows: 0 = no infiltrate; 1+ = minimal increased cellularity without widening of septa; 2+ = obvious increased cellularity with widening of septa; and 3+ = markedly increased cellularity with thickened septa; this score also included blood or edema fluid in the tissue space. Lung sections were also stained with Periodic Acid-Schiff (PAS) to quantitate mucus.

5.3. Results

We immunized cotton rats intramuscularly twice, at 2-week intervals, with pcDNA3.1 alone (vector control), DNA-F, FΔTM protein adjuvanted with TiterMax Gold (Sigma), or DNA-F followed by FΔTM (**Table 3.**). Animals were bled on day 27 for measurement of serum antibodies to hMPV. All groups except the vector control

group had elevated immunofluorescent antibody titers to hMPV-infected LLC-MK2 cells (range 1:320 to 1:1280) (**Figure 36 C**).

Animals were challenged with hMPV virus on day 28 and sacrificed four days post-infection. Animals immunized twice with FΔTM showed a modest, but highly significant level of protection against shedding in nasal tissues compared to control animals (mean 2.5×10^3 pfu/g vs. 5.3×10^4 pfu/g, p=0.008, **Figure 36 A**), while DNA-F/FΔTM and DNA-F/DNA-F groups showed reductions in nasal virus shedding that did not reach significance (mean 2.2×10^4 pfu/g and 3×10^4 pfu/g, respectively, **Figure 36 A**). Conversely, 2 doses of FΔTM protein alone were highly protective against lung virus shedding, giving a >1,500-fold reduction in mean lung hMPV titer compared to controls (mean 1.9×10^1 pfu/g vs. 2.9×10^4 pfu/g, p=0.02, **Figure 36 B**). DNA-F/FΔTM and DNA-F/DNA-F groups showed modest but highly significant reduction of virus replication in the lungs (mean 2.2×10^3 pfu/g and 7×10^2 pfu/g, respectively, **Figure 36 B**). Cotton rats immunized with the vector control exhibited nasal and lung tissue virus replication similar to naïve cotton rats during primary hMPV infection, as described by Williams et al.[38].

We measured *in vitro* serum neutralizing titers in all groups prior to challenge. The FΔTM/ FΔTM immunized animals developed a significant rise in hMPV-neutralizing titers (mean 1:570, range 1:250-1:984, **Figure 36 C**). This titer was markedly higher than the mean serum neutralizing titer of 1:180 we previously observed in cotton rats following primary infection with hMPV[38]. The DNA-F/DNA-F group exhibited a rise in serum neutralizing titer that approached significance (mean 1:132, range 1:33 to 1:250, **Figure 36 C**), while only one animal in the DNA-F/FΔTM group

showed a significant neutralizing antibody titer (mean 1:86, range 1:10 to 1:282, **Figure 36 C**), despite this group exhibiting a significant reduction in lung virus shedding (**Figure 36 B**).

Lung sections from the animals were studied by a pathologist in a group blinded fashion. There were no major differences in pathological changes seen in the lungs of any groups. However, subtle differences between groups were noted in **Table 3**. The animals that were immunized with vector control had mild (1+) mononuclear cell interstitial infiltrates, with pronounced (1-2+) peri-bronchiolar lymphocytic cuffing (**Figure 37**). This is similar to changes in cotton rats with primary hMPV infection previously described by Williams et al.[38]. All animals in the vector control group had copious (3+) mucous plugs present in the large airways (**Figure 37 E**). Animals immunized with DNA-F/FΔTM exhibited mild to moderate (1-2+) interstitial and circumferential peri-bronchiolar mononuclear cell infiltrates (**Figure 37 B**), with mucous plugs present in only 1 of 4 animals. Lungs from cotton rats immunized with DNA-F/DNA-F exhibited mild to moderate (1-2+) interstitial infiltrates with thickening of the interstitium, and moderate (2+) circumferential peri-bronchiolar lymphoid cuffs (**Figure 37 C**). Animals immunized with FΔTM/FΔTM showed mild (1+) interstitial mononuclear infiltrates and an absence of peri-bronchiolar mononuclear cuffs (**Figure 37 D**). Mild (1+) airway mucus was detected in 2 of 4 animals (**Figure 37 F**).

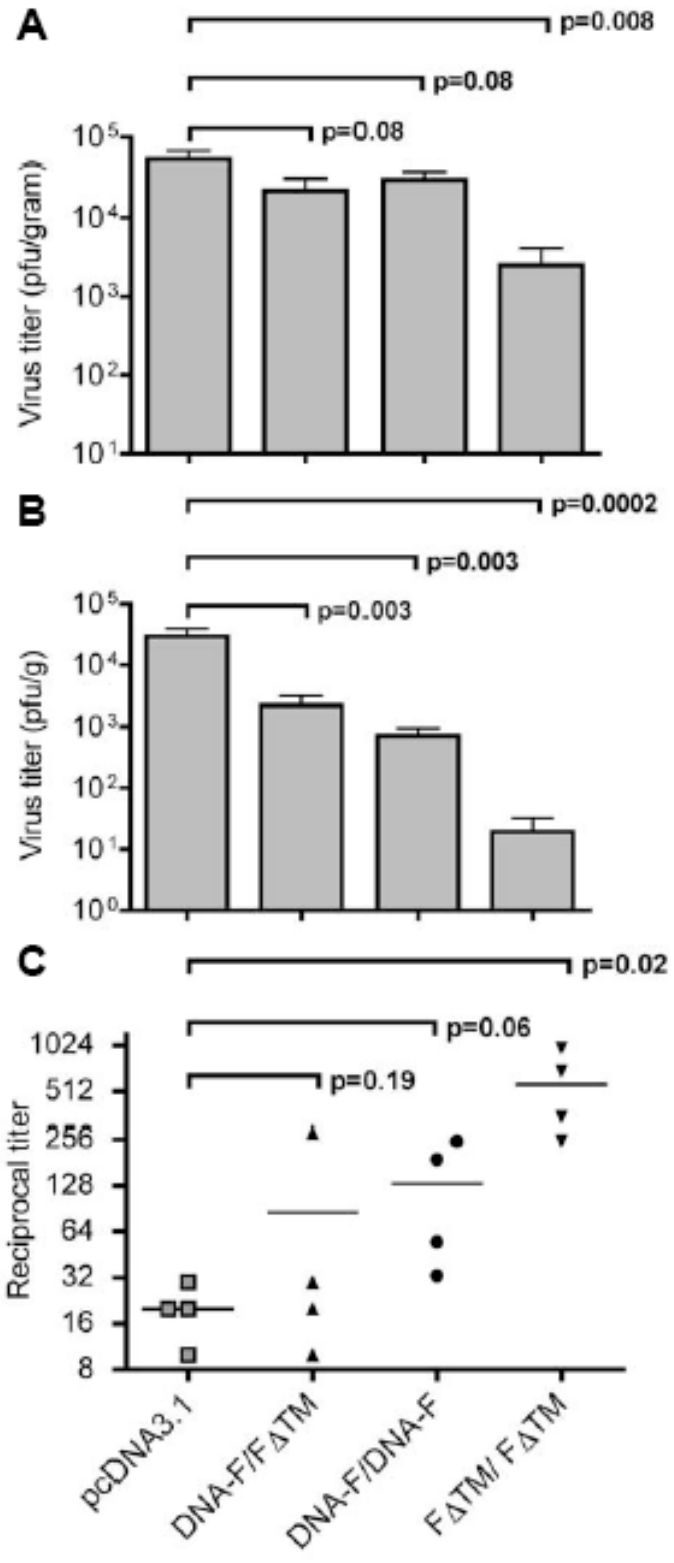

Figure 36. Nasal (A) and lung (B) hMPV titer and reciprocal serum antibody titer (C) in cotton rats. See explanation in the text above.

Table 3. Histopathological scoring of lung sections from immunized groups of cotton rats after hMPV challenge. Lung sections were examined in a group-blinded fashion. Scoring ranged from 0 (absent) to 3+ (severe), as described in text.

	pcDNA3.1/pcDNA3.1	DNA-F/FΔTM	DNA-F/DNA-F	FΔTM/ FΔTM
Interstitial infiltrates	1+	1-2+	1-2+	1+
Peri-bronchiolar infiltrates	1-2+	1+	2+	0
PAS+ (mucus plugs)	3+ (all animals)	1+ (1 of 4)	0	1+ (2 of 4)

5.4. Discussion

Our results indicate that both DNA-F and FΔTM, alone or in combination, were immunogenic in cotton rats and induced partial protection against virus shedding. Virus titer results in the nasal turbinates showed that animals immunized with FΔTM twice had >20-fold reduction in nasal virus titer, while the DNA-F/DNA-F and DNA-F/FΔTM groups had modest decrease in the nasal virus titer after hMPV challenge. In the lungs, however, we found more significant reductions of viral titers. The highest protection in the lower respiratory tract was detected in animals immunized twice with FΔTM protein, with a >1,500-fold reduction in the lung virus titer. DNA-F/DNA-F and DNA-F/FΔTM immunized animals also exhibited significant virus titer reductions in the lung compared to the control group, which was immunized with vector alone.

The serum neutralizing antibody titer results showed that all three groups (FΔTM/FΔTM, DNA-F/DNA-F and DNA-F/FΔTM) had hMPV-specific antibody response after two vaccinations. The highest antibody titer (mean: 1:570) was detected in the FΔTM/FΔTM group correlating with the greater degree of protection in the lungs.

DNA-F/DNA-F and DNA-F/FΔTM groups had less robust neutralizing titer, as they showed less protection against virus shedding in the nose and lung.

Pathological examination of the lung tissues can give information about enhanced lung histopathology following virus challenge. As it was observed in case of the formalin-inactivated RSV vaccine, upon challenge enhanced disease and Th2 type immune response occurred in children, who were vaccinated. In our vaccination study the highest histopathological scores were observed in the vector control group. In fact, animals that were immunized with FΔTM/FΔTM had the lowest scores in peri-bronchiolar infiltrates, which likely reflects decreased viral replication due to the high serum neutralizing antibody titer.

These data all suggest that our purified FΔTM protein construct offers potential as a subunit vaccine, as we demonstrated that DNA-F and FΔTM, alone or in combination, are immunogenic and induce protective immune response in cotton rats. Although further studies are necessary to prove that no enhance disease and type 2 helper T-cell response occurs following FΔTM vaccination, these findings have important implications in hMPV vaccine and prophylactic antibody development.

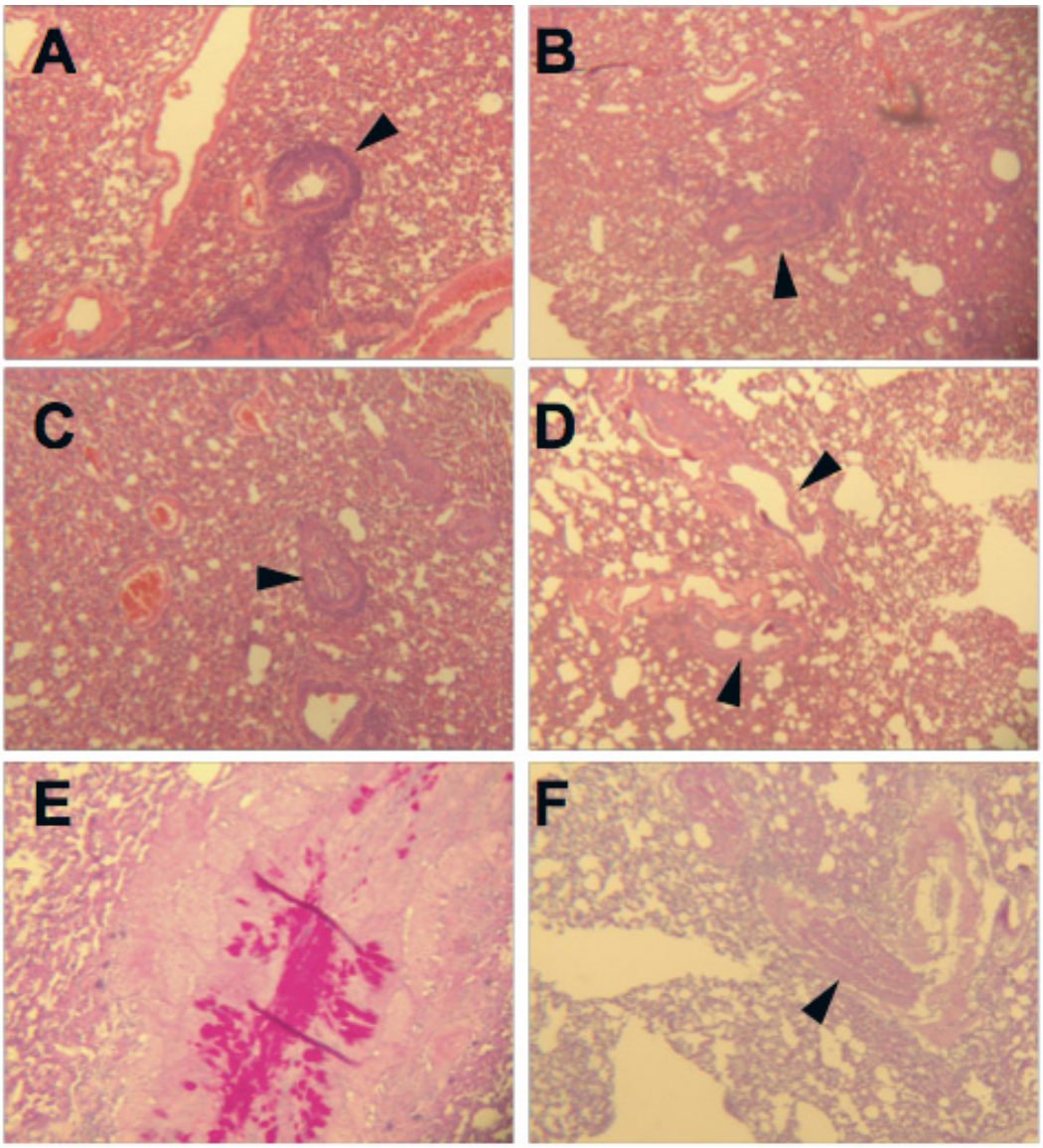

Figure 37. Representative sections demonstrating histopathology of hMPV infection in lungs of immunized cotton rats. A. Lung of control vector immunized (pcDNA3.1/pcDNA3.1) animal exhibits mild to moderate interstitial and significant peri-bronchiolar infiltrates (arrow). B. Lung section of DNA-F/FΔTM immunized animal exhibits moderate interstitial and moderate peri-bronchiolar mononuclear infiltrates (arrow). C. The lung of DNA-F/DNA-F immunized cotton rats exhibit moderate interstitial and mild peri-bronchiolar infiltrates (arrow). D. Lung section of FΔTM/FΔTM immunized cotton rat exhibits minimal interstitial mononuclear infiltrates, no peri-bronchiolar infiltrates, no alveolitis (arrows). E. Periodic acid-Schiff (PAS) staining reveals copious mucus in the large airways of control vector immunized animals. F. PAS staining of FΔTM/FΔTM immunized cotton rat lung shows minimal mucus in airway lumen (arrow). A-D, H&E staining. All sections original magnification x25.

CHAPTER VI

CONCLUSION

HMPV is a recently discovered Paramyxovirus, which causes serious upper and lower respiratory tract infections in infants, young children, elderly and immunocompromized people. Based on sequence homology with other paramyxoviruses, hMPV F gene encodes for the fusion protein, which mediates virus-cell membrane fusion and it is thought to form characteristic hexameric coiled coil conformation in its fusion active state.

To confirm that F protein has a hexameric α-helical structure, we generated a sequence-optimized clone of the hMPV F gene and modified it by removing the transmembrane domain- and cytoplasmic tail-encoding regions. The gene has been cloned into pcDNA3.1/*myc*-His mammalian expression vector, which has been transfected into 293-F suspension adapted cell line. We successfully expressed and affinity purified the soluble hMPV F ectodomain with C-terminal c-*myc*-epitope and 6xHistidine tag, and this recombinant protein served as subject for further structural, biochemical and immunogenic characterizations.

The native F ectodomain formed trimers, which fell apart into stable monomers under denaturing conditions. Our results showed that the protein has a dominant α-helical secondary structure, probably due to the hexameric HR-1/HR-2 fusion core formation in the F1 subunit, although it is not known whether this represents the pre-fusion, the post-fusion or the pre-hairpin intermediate state. The expressed protein underwent post-

translational modifications, and it is N-glycosylated at all three N-glycosylation sites. Glycosylation of the F1 subunit is important and necessary in proper protein folding and transport, since mutations at the F1 glycosylation sites affected expression of the mutated proteins. Our disulfide-mapping studies indicated that all fourteen cysteines in hMPV F participate in disulfide-bond formations, which have important role in stabilizing the structure of the protein.

Our hMPV FΔTM construct can be recognized by anti-hMPV polyclonal human and guinea pig sera and also by monoclonal antibodies generated against hMPV. Surface plasmon resonance studies showed that this antibody-antigen interaction is a strong, specific binding. These results suggest that the expressed ectodomain retains native conformation and presents some antigenic epitopes on its surface that are important in antigen recognition.

A subset of integrin receptors binds to the specific RGD recognition sequence and this motif can be found in all of the reported hMPV F sequences. A number of human viruses utilize RGD-recognizing integrins as receptors or co-receptors and our most recent data suggest that RGD-binding integrins serve as receptors for hMPV too.

We also tested the hypothesis that F is a major protective antigen for hMPV. We immunized cotton rats with the purified F ectodomain and found that it induced robust neutralizing antibody responses and protected animals against virus shedding in the lungs following wild-type virus challenge. Our findings indicate that FΔTM retains several important characteristics of native hMPV F protein, suggesting that it is a promising vaccine candidate and a valuable reagent for functional and structural studies of this important hMPV protein.

Future work

The future studies of hMPV F protein will probably concentrate on two major fields: 1) biochemical and structural characterizations and crystallization of the protein and 2) immunogenic studies with antibody and vaccine development strategies.

The ultimate goal in structural studies is to generate stable crystals of the properly folded, native protein and determine its crystal structure. However, only three paramyxovirus F protein crystal structures[28, 34, 35] are known to date, and all of them are from modified polypeptides, not from the actual native fusion protein. Solving the atomic structure of a native paramyxovirus F protein in its pre-and post-fusion and metastable state will be a major achievement and give us information to understand the structural and biochemical bases of viral entry, fusion and pathogenesis.

Data from structural and biochemical experiments will also help the immunogenic studies and vaccine development. Acute respiratory infections are the most important cause of infant and young children mortality being responsible nearly 4 million deaths every year, and to date there is no effective vaccine available. In order to develop novel vaccines, either based on protein antigens or prophylactic monoclonal antibodies, it is necessary to know the biochemical properties and structural details of the targeted antigen or the antigenic binding site of the antibody, so for this reason hMPV vaccine development will utilize the structural information on hMPV fusion protein.

REFERENCES

1. Fields, B. N.; Howley, P. M.; Griffin, D. E.; Lamb, R. A.; Martin, M. A.; Roizman, B.; Straus, S. E.; Knipe, D. M., *Fields-Virology*. 4th Edition ed.; Lippincott Williams and Wilkins Publishers: 2001; Vol. 1.

2. Easton, A. J.; Domachowske, J. B.; Rosenberg, H. F., Animal Pneumoviruses: Molecular Genetics and Patogenesis. *Clinical Microbiology Reviews* **2004,** 17, (2), 390-412.

3. Barik, S., Control of nonsegmented negtaive-strand RNA virus replication by siRNA *Virus Research* **2004,** 102, 27-35.

4. Barik, S., Transcription of Human Respiratory Syncytial Virus Genome RNA In Vitro: Requirement of Cellular Factor(s). *Journal of Virology* **1992,** 66, (11), 6813-6818.

5. van den Hoogen, B. G.; de Jong, J. C.; Groen, J.; Kuiken, T.; de Groot, R.; Fouchier, R. A.; Osterhaus, A. D., A newly discovered human pneumovirus isolated from young children with respiratory tract disease. *Nat. Med.* **2001,** 7, (6), 719-724.

6. Cook, J. K., Avian Pneumovirus Infections of Turkeys and Chickens. *The Veterinary Journal* **2000,** 160, 118-125.

7. van den Hoogen, B. G.; Bestebroer, T. M.; Osterhaus, A. D. M. E.; Fouchier, R. A. M., Analysis of the Genomic Sequence of a Human Metapneumovirus. *Virology* **2002,** 295, 119-132.

8. Kahn, J. S., Epidemiology of Human Metapneumovirus. *Clinical Microbiology Reviews* **2006,** 19, (3), 546-557.

9. Williams, J. V.; Tollefson, S. J.; Nair, S.; Chonmaitree, T., Association of Human Metapneumovirus with Acute Otitis Media. *Int. J. Pediatr. Otorhinolaryngol.* **2006**.

10. Williams, J. V.; Harris, P. A.; Tollefson, S. J.; Halburnt-Rush, L. L.; Pingsterhaus, J. M.; Edwards, K. M.; Wright, P. F.; James E. Crowe, J., Human Metapneumovirus and Lower Respiratory Tract Disease in Otherwise Healthy Infants and Children. *The New England Journal of Medicine* **2004,** 350, (5), 443-450.

11. Blumenthal, R.; Clague, M. J.; Durell, S. R.; Epand, R. M., Membrane Fusion. *Chem. Rev.* **2003,** 103, 53-69.

12. Peisajovich, S. G.; Shai, Y., Viral fusion proteins: multiple regions contribute to membrane fusion. *Biochimica et Biophysica Acta* **2003,** 1614, 122-129.

13. Gruenke, J. A.; Armstrong, R. T.; Newcomb, W. W.; Brown, J. C.; White, J. M., New Insights into the Spring-Loaded Conformational Change of Influenza Virus Hemagglutinin. *Journal of Virology* **2002,** 76, 4456-4466.

14. Morrison, T. G., Structure and function of a paramyxovirus fusion protein. *Biochimica et Biophysica Acta* **2003,** 1614, 73-84.

15. Yin, H.-S.; Wen, X.; Paterson, R. G.; Lamb, R. A., Structure of the parainfluenza virus 5 F protein in its metastable, prefusion conformation. *Nature* **2006,** 439, (38-44).

16. Li, Y., Han, X.; Tamm, L. K., Thermodynamics of Fusion Peptide-Membrane Interactions. *Biochemistry* **2003,** 42, 7245-7251.

17. Skehel, J. J.; Wiley, D. C., Influenza haemagglutinin. *Vaccine* **2002,** 20, S51-S54.

18. Armstrong, R. T.; Kushnir, A. S.; White, J. M., The Transmembrane Domain of Influenza Hemagglutinin Exhibits a Stringent Length Requirement to Support the Hemifusion to Fusion Transition. *The Journal of Cell Biology* **2000,** 151, (2), 425-437.

19. Carr, C. M.; Kim, P. S., A Spring-Loaded Mechanism for the Conformational Change of Influenza Hemagglutinin. *Cell* **1993,** 73, 823-832.

20. Burton, D. R.; Stanfield, R. L.; Wilson, I. A., Antibody vs. HIV in a clash of evolutionary titans. *PNAS* **2005,** 102, (42), 14943-14948.

21. Chan, D. C.; Fass, D.; Berger, J. M.; Kim, P. S., Core structure of gp41 from the HIV Envelope Glycoprotein. *Cell* **1997,** 89, 263-273.

22. Yang, X.; Florin, L.; Farzan, M.; Kolchinsky, P.; Kwong, P. D.; Sodroski, J.; Wyatt, R., Modification That Stabilize Human immunodeficiency Virus Envelope Glycoprotein Trimers in Solution. *Journal of Virology* **2000,** 74, (10), 4746-4754.

23. Yang, X.; Farzan, M.; Wyatt, R.; Sodroski, J., Characterization of Stable Soluble Trimers Containing Complete Ectodomains of Human Immunodeficiency Virus Type 1 Envelope Glycoproteins. *Journal of Virology* **2000,** 74, (12), 5716-5725.

24. Pancera, M.; Lebowitz, J.; Schön, A.; Zhu, P.; Freire, E.; Kwong, P. D.; Roux, K. H.; Sodroski, J.; Wyatt, R., Soluble Mimetics of Human Immunodeficiency Virus Type 1 Viral Spikes Produced by Replacement of the Native Trimerization Domain with a Heterologous Trimerization Motif: Characterization and Ligand Binding Analysis *Journal of Virology* **2005,** 79, (15), 9954-9969.

25. Yang, X.; Lee, J.; Mahony, E. M.; Kwong, P. D.; Wyatt, R.; Sodroski, J., Highly Stable Trimers Formed by Human Immunodeficiency Virus Type 1 Envelope Glycoproteins Fused with the Trimeric Motif of T4 Bacteriophage Fibritin. *Journal of Virology* **2002,** 76, (9), 4634-4642.

26. Copeland, K. M.; Elliot, A. J.; Daniels, R. S., Functional Chimeras of Human Immunodeficiency Virus Type 1 gp120 and Influenza A Virus (H3) Hemagglutinin. *Journal of Virology* **2005,** 79, (10), 6459-6471.

27. Chen, L.; Gorman, J. J.; McKimm-Breschkin, J.; Lawrence, L. J.; Tulloch, P. A.; Smith, B. J.; Colman, P. M.; Lawrence, M. C., The Structure of the Fusion Glycoprotein of Newcastle Disease Virus Suggests a Novel Paradigm for the Molecular Mechanism of Membrane Fusion. *Structure* **2001,** 9, 255-266.

28. Yin, H.-S.; Paterson, R. G.; Wen, X.; Lamb, R. A.; Jardetzky, T. S., Structure of the uncleaved ectodomain of the paramyxovirus (hPIV3) fusion protein. *PNAS* **2005,** 102, (26), 9288-9293.

29. Lawless-Delmedico, M. K.; Sista, P.; Sen, R.; Moore, N. C.; Antczak, J. B.; White, J. M.; Greene, R. J.; Leanza, K. C.; Matthews, T. J.; Lambert, D. M., Heptad-Repeat Regions of Respiratory Syncytial Virus F1 Protein Form a Six-Membered Coiled-Coil Complex *Biochemistry* **2000,** 39, 11689-11695.

30. Gonzàlez-Reyes, L.; Ruiz-Argüello, M. B.; Garcia-Barreno, B.; Calder, L.; López, J. A.; Albar, J. P.; Skehel, J. J.; Wiley, D. C.; Melero, J. A., Cleavage of the human respiratory syncytial virus fusion protein at two distinct sites is required for activation of membrane fusion. *PNAS* **2001,** 98, (17), 9859-9864.

31. Matthews, J. M.; Young, T. F.; Tucker, S. P.; Mackay, J. P., The Core of the Respiratory Syncytial Virus Fusion Protein is a Trimeric Coiled Coil. *Journal of Virology* **2000,** 74, (13), 5911-5920.

32. Lamb, R. A.; Paterson, G. R.; Jardetzky, T. S., Paramyxovirus membrane fusion: Lessons from the F and HN atomic structures. *Virology* **2006,** 344, 30-37.

33. Baker, K. A.; Dutch, R. E.; Lamb, R. A.; Jardetzky, T. S., Structural Basis for Paramyxovirus-Mediated Membrane Fusion. *Molecular Cell* **1999,** 3, 309-319.

34. Chen, L.; Colman, P. M.; Cosgrove, L. J.; Lawrence, M. C.; Lawrence, L. J.; Tulloch, P. A.; Gorman, J. J., Cloning, Expression and Crystallization of the Fusion Protein of Newcastle Disease Virus. *Virology* **2001,** 290, 290-299.

35. Yin, H.-S.; Wen, X.; Paterson, R. G.; Lamb, R. A.; Jardetzky, T. S., Structure of the parainfluenza virus 5 F protein in its metastable, prefusion conformation. *Nature* **2006,** 439, (5), 38-44.

36. Kim, D. R.; McHenry, C. S., Biotin Tagging Deletion Analysis of Domain Limits Involved in Protein-Macromolecular Interactions. *The Journal of Biological Chemistry* **1996,** 271, (34), 20690-20698.

37. Ward, G. A.; Stover, C. K.; Moss, B.; Fuerst, T. R., Stringent chemical and thermal regulation of recombinant gene expression by vaccinia virus vectors in mammalian cells. *PNAS* **1995,** 92, 6773-6777.

38. Williams, J. V.; Tollefson, S. J.; Johnson, J. E.; James E. Crowe, J., The Cotton Rat (Sigmodon hispidus) Is a Permissive Small Animal Model of Human Metapneumovirus Infection, Pathogenesis and Protective Immunity. *Journal of Virology* **2005,** 79, (17), 10944-10951.

39. Miller, S. A. Peptides and Proteins: Anti-Virals and Novel Materials. Vanderbilt University, Nashville, 2006.

40. Medzihradszky, K. F., Characterization of Protein N-Glycosylatio. *Methods in Enzymology* **2005,** 405, 116-138.

41. Chavan, M.; Lennarz, W., The molecular basis of coupling of translocation and N-glycosylation. *TRENDS in Biochemical Sciences* **2006,** 31, (1), 17-20.

42. Klink, H. A.; Brady, R. P.; Topliff, C. L.; Eskridge, K. M.; Srikumaran, S.; Kelling, C. L., Influence of bovine respiratory syncytial virus F glycoprotein N-linked glycans on in vitro expression and on antibody responses in BALB/c mice *Vaccine* **2006,** 24, 3388-3395.

43. Moll, M.; Kaufmann, A.; Masiner, A., Influence of N-Glycans on Processing and Biological Activity of the Nipah Virus Fusion Protein. *Journal of Virology* **2004,** 78, (13), 7274-7278.

44. Zimmer, G.; Trotz, I.; Herrler, G., N-Glycans of F Protein Differentially Affect Fusion Activity of Human Respiratory Syncytial Virus. *Journal of Virology* **2001,** 75, (10), 4744-4751.

45. Carter, J. R.; Paer, C. T.; Fowler, S. D.; Dutch, R. E., Role of N-Linked Glycosylation of Hendra Virus Fusion Protein. *Journal of Virology* **2005,** 79, (12), 7922-7925.

46. Quinones-Kochs, M. I.; Buonocore, L.; Rose, J. K., Role of N-linked Glycans in a Human Immunodeficiency Virus Envelope Glycoprotein: Effects on Protein Function and the Neutralizing Antibody Response. *Journal of Virology* **2002,** 76, (9), 4199-4211.

47. Liebler, D. C., *Introduction to Proteomics*. Humana Press Inc.: Totowa, New Jersey, 2002; p 198.

48. Day, N. D.; Branigan, P. J.; Liu, C.; Gutshall, L. L.; Luo, J.; Melero, J. A.; Sarisky, R. T.; Vecchio, A. M. D., Contribution of cysteine residues in the extracellular domain of the F protein of human respiratory syncytial virus to its function. *Virology Journal* **2006,** 3, 34.

49. Manza, L. L.; Stamer, S. L.; Ham, A.-J. L.; Codreanu, S. G.; Liebler, D. C., Sample preparation and digestion for proteomic analyses using spin filters. *Proteomics* **2005,** 5, 1742-1746.

50. Cortes, H. J.; Pfeiffer, C. D.; Richter, B. E.; Stevens, T. S., Porous Ceramic Bed supports for Fused Silica Packed Capillary Columns Used in Luquid Chromatography. *Journal of High Resolution Chromatography* **1987,** 10, (8), 446-448.

51. Licklider, L. J.; Thoreen, C. C.; Peng, J.; Gygi, S. P., Automation of Nanoscale Microcapillary Liquid Chromatography-Tandem Mass Spectrometry with a Vented Column. *Analytical Chemistry* **2002,** 74, 3076-3083.

52. Zhu, J.; Li, P.; Wu, T.; Gao, F.; Ding, Y.; Zhang, C. W.-H.; Rao, Z.; Gao, G. F.; Tien, P., Design and analysis of post-fusion 6-helix bundle of heptad repeat regions from Newcastle disease virus F protein. *Protein Engineering* **2003,** 16, (5), 373-379.

53. Plow, E. F.; Haas, T. A.; Zhang, L.; Loftus, J.; Smith, J. W., Ligand Binding to Interins. *The Journal of Biological Chemistry* **2000,** 275, (29), 21785-21788.

54. Hynes, R. O., Integrins: Bidirectional, Allosteric Signaling Machines. *Cell* **2002,** 110, 673-687.

55. Dickerson, S. K.; Mathis, N. L.; Rahman, M.; Bergelson, J. M.; Santoro, S. A., Determinant of Ligand Binding Specficity of the α1β1 and α2β1 Integrins. *The Journal of Biological Chemistry* **1999,** 274, (45), 32182-32191.

56. Maginnis, M. S.; Forrest, J. C.; Kopecky-Bromberg, S. A.; Dickerson, S. K.; Santoro, S. A.; Zutter, M. M.; Nemerow, G. R.; Bergelson, J. M.; Dermody, T. S., ß1 Integrin Mediated Internalization of Mammalian Reovirus. *Journal of Virology* **2006,** 80, (6), 2760-2770.

57. Bergelson, J. M.; Shepley, M. P.; Chan, B. M.; Hemler, M. E.; Finberg, R. W., Identification of the integrin VLA-2 as a receptor for echovirus. *Science* **1992,** 255, 1718-1720.

58. Wickham, T. J.; P.Mathias; Cheresh, D. A.; Nemerow, G. R., Integrins alpha v beta 3 and alpha v beta 5 promote adenovirus internalization but not virus attachment. *Cell* **1993,** 73, 309-319.

59. Berinstein, A.; Roivainen, M.; Hovi, T.; Mason, P. W.; Baxt, B., Antibodies to the vitronectin receptor (integrin alpha v beta 3) inhibit binding and infection of foot-and-mouth disease virus to cultured cells. *Journal of Virology* **1995,** 69, 2664-2666.

60. Guerrero, C. A.; Mendez, E.; Zarate, S.; Isa, P.; Lopez, S.; Arias, C. F., Integrin alpha(v)beta(3) mediates rotavirus cell entry. *PNAS* **2000,** 97, 14644-14649.

61. Chu, J. J.; Ng, M. L., Interaction of West Nile virus with alpha v beta 3 integrin mediates virus entry into cells. *J. Biol. Chem* **2004,** 279, 54533-54541.

62. Kieny, M. P.; Girard, M. P., Human vaccine research and development: An overview. *Vaccine* **2005,** 23, 5705-5707.

63. Girard, M. P.; Cherian, T.; Pervikov, Y.; Kieny, M. P., A review of vaccine research and development: Human acute respiratory infections. *Vaccine* **2005,** 23, 5708-5724.

64. Wang, K.; Holtz, K. M.; Anderson, K.; Chubet, R.; Mahmoud, W.; Cox, M. M. J., Expression and purification of an influenza hemagglutinin-one step closer to a recombinant protein-based influenza vaccine. *Vaccine* **2006,** 24, 2176-2185.

APPENDIX A

FPLC PURIFICATION OF HMPV F ECTODOMAIN USING HISTRAP COLUMN AND ÄKTA-FPLC SYSTEM

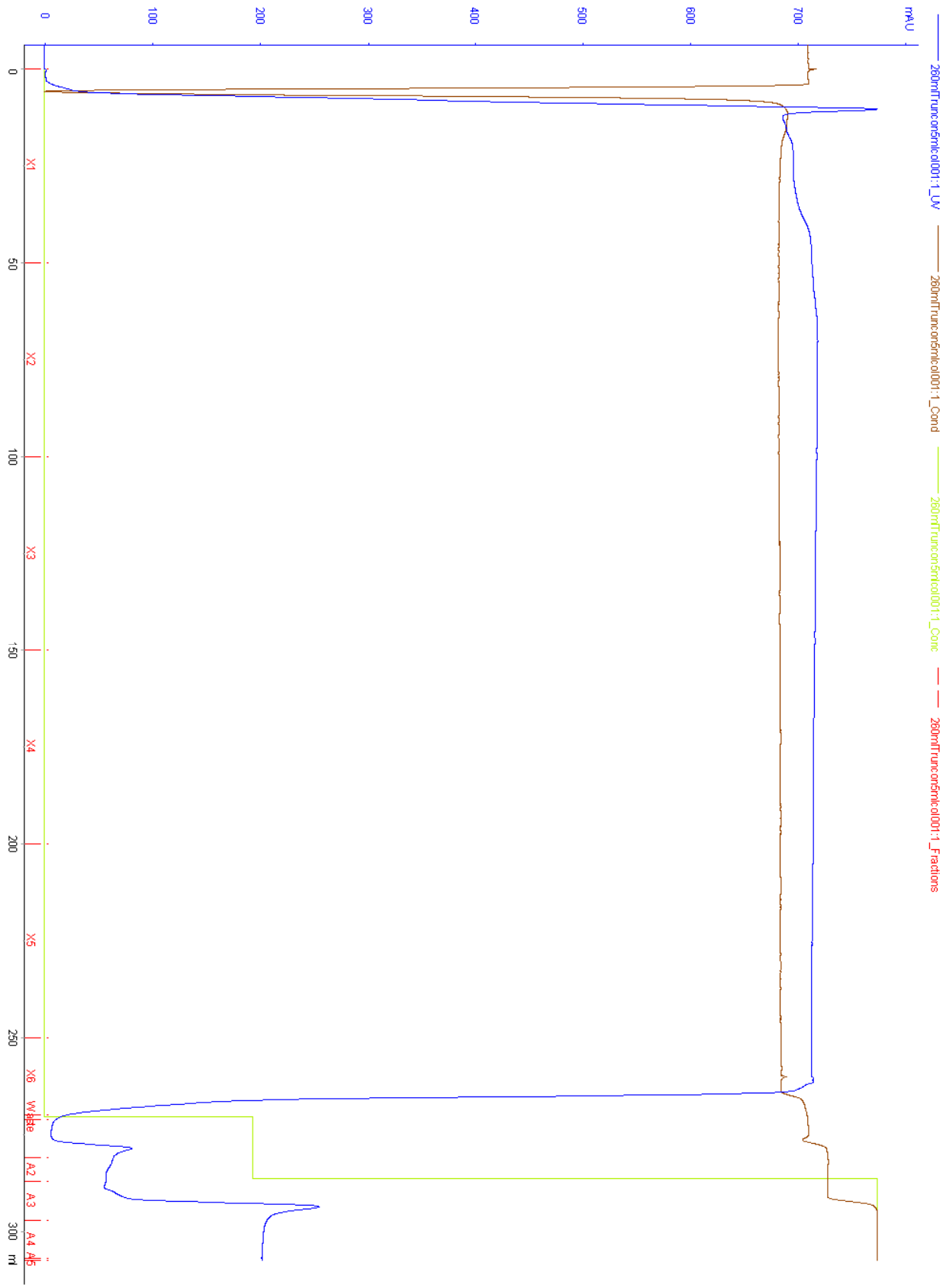
mAU
0
100
200
300
400
500
600
700
260nmTruncon5mlcol001:1_UV
260nmTruncon5mlcol001:1_Cond
260nmTruncon5mlcol001:1_Conc
260nmTruncon5mlcol001:1_Fractions
0
50
100
150
200
250
300
ml
X1
X2
X3
X4
X5
X6
Waste
A2
A3
A4
A5

Table 4. Parameters for purification protocol of hMPV F ectodomain using ÄKTA-FPLC system and 5 ml HisTrap column.

Block	Variable	Value	Range
Main	Column	HisTrap_5_ml	
Start_with_PumpWash	Wash_InletA	ON	
	Wash_InletB	Off	
Flow_Rate	Flow_Rate {ml/min}	5	0.00 - 20.00
Column_Pressure_Limit	Column_PressureLimit {MPa}	0.3	0.000 - 5.000
Averaging_Time_UV	Averaging_Time_UV	5.1	
Alarm_Sample_PressureLimit	Sample_PressureLimit {MPa}	0.3	0.00 - 2.00
Eluent_A_Inlet	Eluent_A_Inlet	A1	
Start_Conc_B	Start_ConcB {%B}	0	0.0 - 100.0
Column_Equilibration	Equilibrate_with {CV}	5	0.00 - 999999.00
Aut_PressureFlow_Regulation	System_Pump	PressFlowControl	
	System_PressLevel {MPa}	3	0.000 - 5.000
	System_MinFlow {ml/min}	0.1	0.000 - 20.000
Direct_Sample_Loading	Injection_Flowrate {ml/min}	5	0.0 - 50.0
	Volume_of_Sample {ml}	600	0.0 - 20000.0
PressureReg_Sample_Pump	Sample_Pump	Normal	
	Sample_Min_Flow {ml/min}	0.1	0.1 - 49.9
Wash_Out_Unbound_Sample	Wash_column_with {CV}	2	0.00 - 999999.00
Buffer_Inlet_A_Segment_1	1_Buffer_Inlet_A	A1	
ConcB_Step_1	1_ConcB_Step {%B}	6	0.0 - 100.0
Wash_1	1_Wash_Inlet_A	OFF	
	1_Wash_Inlet_B	OFF	
Fractionation_Segment_1	1_Tube_Type	18mm	
	1_Fraction_Size {ml}	11	0.000 - 99999.000
	1_Start_at	FirstTube	
	1_PeakFrac_TubeType	18mm	
	1_PeakFraction_Size {ml}	0	0.000 - 99999.000
	1_PeakFrac_Start_at	NextTube	
Step_1	1_Length_of_Step {CV}	4	0.00 - 999999.00
Buffer_Inlet_A_Segment_2	2_Buffer_Inlet_A	A1	
ConcB_Step_2	2_ConcB_Step {%B}	25	0.0 - 100.0
Wash_2	2_Wash_Inlet_A	OFF	
	2_Wash_Inlet_B	OFF	
Fractionation_Segment_2	2_Tube_Type	18mm	
	2_Fraction_Size {ml}	11	0.000 - 99999.000
	2_Start_at	NextTube	
	2_PeakFrac_TubeType	18mm	
	2_PeakFraction_Size {ml}	0	0.000 - 99999.000
	2_PeakFrac_Start_at	NextTube	
Step_2	2_Length_of_Step {CV}	4	0.00 - 999999.00
Gradient_Delay	Gradient_Delay {ml}	10	0.00 - 999999.00

APPENDIX B

SPR-BIACORE ANALYSIS OF HMPV F BINDING TO HMPV-SPECIFIC HUMAN MONOCLONAL ANTIBODY

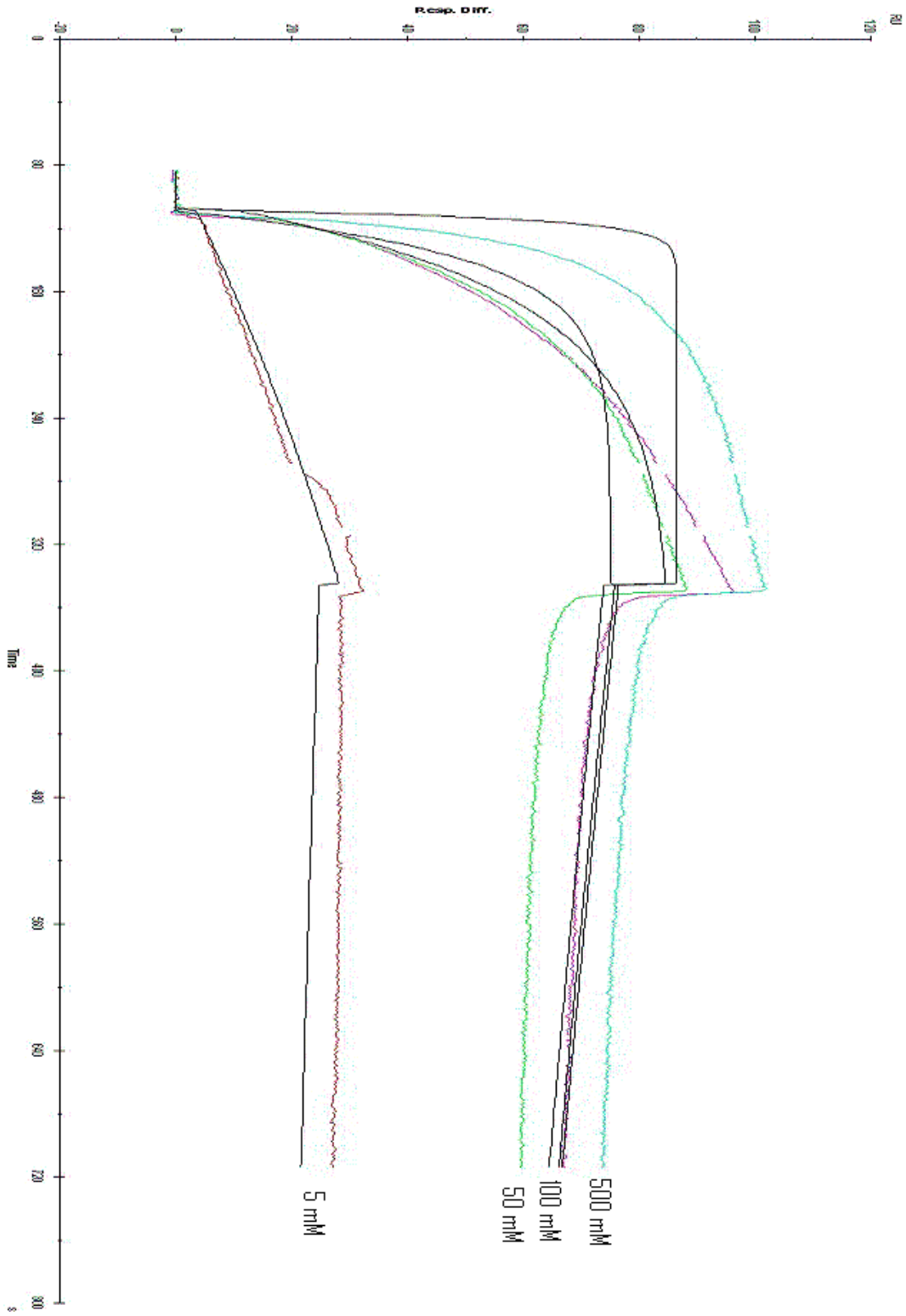

Figure 38. Kinetic analysis of hMPV F binding to anti-HMPV human monoclonal Fab. Binding curves (colored) for different Fab concentrations are fitted with a 1:1 Langmuir binding model (black curves).